TRANSIENT LIQUID PHASE BONDING OF FERRITIC OXIDE DISPERSION STRENGTHENED ALLOYS

Except where reference is made to the work of others, the work described in this dissertation is my own or was done in collaboration with my advisory committee. This dissertation does not include proprietary or classified information.

Venu Gopal Krishnardula

Certificate of Approval:

Jeffrey W. Fergus
Associate Professor
Materials Engineering

William F. Gale, Chair
Alumni Professor
Materials Engineering

Dr. Terry C. Totemeier
Staff Metallurgist
Materials Sciences
Idaho National Laboratory

Stephen L. McFarland
Acting Dean
Graduate School

TRANSIENT LIQUID PHASE BONDING OF FERRITIC OXIDE DISPERSION STRENGTHENED ALLOYS

Venu Gopal Krishnardula

A Dissertation

Submitted to

the Graduate Faculty of

Auburn University

in Partial Fulfillment of the

Requirements for the

Degree of

Doctor of Philosophy

Auburn, Alabama
May 11, 2006

TRANSIENT LIQUID PHASE BONDING OF FERRITIC OXIDE DISPERSION STRENGTHENED ALLOYS

Venu Gopal Krishnardula

____
Signature of Author

____
Date of Graduation

VITA

Venu Gopal Krishnardula, son of late Sri. Krishnardula Rama Mohan Rao and Smt. Krishnardula Satya Veni, was born on April 2, 1979, in Visakhapatnam, India. He graduated from Vikas college in May 1996. He joined Andhra University College of Engineering, Visakhapatnam in August 1996 and graduated with a Bachelor of Engineering in Metallurgical Engineering with distinction in May 2000. He joined the graduate program in Materials Engineering at Auburn University in August of 2001.

DISSERTATION ABSTRACT

TRANSIENT LIQUID PHASE BONDING OF FERRITIC OXIDE DISPERSION STRENGTHENED ALLOYS

Venu Gopal Krishnardula

Doctor of Philosophy, May 11, 2006
(B.E., Andhra University, India, 2000)

200 Typed Pages

Directed by Dr. William F. Gale

Oxide dispersion strengthened (ODS) alloys possess excellent properties including resistance to oxidation, corrosion, creep and thermal fatigue. In addition, ferritic ODS alloys exhibit resistance to void swelling and are of particular interest to the nuclear industry. The present study involves the joining of fuel cans to end caps that will be utilized in the nuclear industry.

Mechanically alloyed (MA) ODS alloys possess coarse columnar grain structure strengthened with nanosize yttria dispersoids. In that past, fusion welding techniques resulted in microstructural disruption leading to poor joints. This work investigated joining of two ferritic MA ODS alloys, MA956 and PM2000, using; (a) Transient liquid phase (TLP) bonding and (b) Solid-state diffusion bonding.

TLP bonds were prepared with MA956 and PM2000 in the unrecrystallized and recrystallized conditions using electron beam physical vapor deposited (EBPVD) boron thin films as interlayers. The use of thin interlayers reduced the amount of substrate dissolution and minimized the bondline microstructural disruption. Different bond orientations were also investigated. Successful bonds with better microstructural continuity were obtained when substrates were joined in the unrecrystallized condition followed by post bond recrystallization heat treatment with the substrate faying surface aligned along the working (extrusion or rolling) direction than when substrates were aligned perpendicular to the working direction. This was attributed to the number of yttria stringers cut by the bondline, which is less when the substrate faying surface is lying parallel to the working direction than when the substrate faying surface is lying perpendicular to the working direction.

Solid-state diffusion bonding was conducted using MA956 and PM2000 in the unrecrystallized and recrystallized conditions. Bonding occurred only when an unrecrystallized substrate was involved. Bonding occurred at unusually low stresses. This may be attributed to the grain boundary diffusion, owing to submicron grain size of the unrecrystallized substrates. Post bond heat treatment was conducted in order to induce recrystallization in the bonds. Room temperature mechanical testing was conducted on the bonds and the bulk. Bond shear strengths and tensile strengths of up to 80% and 110% of bulk, respectively, were obtained.

Defects in the bulk material such as porosity and unwanted fine grain formation were observed. Pore formation at the bondline during post bond heat treatment seems to decrease the bond strength. These defects were attributed to prior thermomechanical history of the materials.

ACKNOWLEDGEMENTS

I came to know many people through the course my education, who have helped me and encouraged me to achieve this milestone, to whom I am always grateful. It is not possible to list all of them. However, I would like to thank few by their names.

I am indebted to Dr. William F. Gale for his guidance and encouragement throughout the course of this research. His constant support and enthusiasm have been a source of inspiration. Being a member of your group, I learned much beyond the classroom. I am also grateful to Dr. Jeffrey W. Fergus for his invaluable advice and great discussions. I have always enjoyed learning new concepts.

I am thankful to Dr. Terry C. Totemeier, Idaho National Laboratory, for providing me this opportunity to work on this project, his valuable advice and financial assistance for the completion of my Ph.D. My sincere appreciation to Dr. Curtis Shannon for acting as an external reader.

I am thankful to Mr. Charles Ellis for providing boron thin film depositions for this research, Dave Lindahl for all the help with the experimental setup, Roy Howard and Shirley Lyles for all their help. It is my pleasure to acknowledge my research group Jon Sofyan, Rajeev Aluru, Robert Love, Subhadra Chitti, Courtney Guasti, Raghu Viswanathan, Chad Callender, Daniel Butts and Jimmy Messick for their support, importantly their help and bearing with my questions in the group meetings.

I am grateful to my professors from Andhra University Dr. G.S. Murty, Dr. N.B.R. Mohan Rao, Dr. D. Narasimha Rao, Dr. Devaki Rani and Late Dr. Balusubramaniam for their encouragement during my undergraduate studies to pursue higher education.

I appreciate the company of my friends who made my stay at Auburn memorable and help me remain sane during the period of my qualifiers. They are Vamshi, Kalyan, Vivek, Sashil, Muthu, Sourabh, Partha, Phani, Amit, Subbu, Nikhil, Rajesh, Kalla, Ramji, Kashyap, Deepika, Sameera, Lisa, Gayatri, Priyanka, Seema and many more. Thank you.

Finally and importantly, I am deeply indebted to my family. Their continual encouragement and support helped me achieve this degree. My elder brother, Vasu, sister-in-law, Aruna, and neice, Sarayu, have always been cheering me from thousands of miles away. I dedicate this dissertation to my father Late Sri K. R. Mohan Rao and mother Smt. K. Satyaveni, who always were and will be my heroes. I love you folks.

Style Manual or journal used: Metallurgical Transactions A

Computer software used: Microsoft Office

TABLE OF CONTENTS

LIST OF TABLES

LIST OF FIGURES

1. INTRODUCTION

1.1. Necessity for the Project

The increase in energy consumption in various sectors, such as transportation, commercial, residential, and industrial, has raised the world's demand for energy [1]. This has led to the development of advanced designs for more efficient power plants, which operate at elevated temperatures.

A major consequence is the need for materials with high-temperature properties that are capable of operating at these elevated temperatures. Many superalloys were originally developed during 1950s and 1960s to meet the requirements of the new gas turbine aerospace applications [2]. These alloys attain their high temperature strength by gamma prime (γ') hardening and carbide strengthening [3, 4]. For example, coherent phase strengthening in nickel-base alloys is obtained by varying the γ content in the microstructure, where γ is the face-centered cubic (fcc) matrix of the Ni-base alloy and γ' is the intermetallic which is the ordered phase $Ni_3(Al,Ti)$ and has a lattice spacing similar to the fcc matrix. Changes in the relative lattice spacing between the γ - γ' results in a boundary misfit and induces additional strain. The lattice spacing can be changed by varying the ratio of Al:Ti in the γ', or by the introduction of solid solution elements. Increasing the total Al + Ti content of the alloy increases the phase boundary area, resulting in higher strength due to coherent phase strengthening. Long exposures of the alloy to temperatures below the solvus temperature results in coarsening of the second-phase particles, termed ‘gamma-prime coarsening’. This coarsening leads to a decrease in the alloy strength. The γ/γ′ solvus temperature is very important as dissolution of the second-phase (γ′) occurs at temperatures above the solvus temperature resulting in loss of strength. As the temperature decreases below the solvus, reprecipitation of γ′ occurs. However, the distribution of the γ′ particles is not effective for strengthening. Liquid phase formation also occurs at temperatures above the solidus temperature. These three mechanisms (γ′ coarsening, γ′ dissolution and reprecipitation, and liquid formation) result in the decrease of the strength of the alloy, Ni-base superalloys may be used up to around 1100 °C without degrading the alloy strength. Carbide strengthening was also developed to improve high temperature strength. Carbide particles precipitate at the grain boundaries and restrict the grain boundary motion leading to increased creep resistance. However, the formation of a continuous carbide film at the grain boundaries results in embrittlement and coarse carbide particles reduce the strength of the alloy.

In contrast, mechanically alloyed (MA) oxide dispersion strengthened (ODS) alloys, have a stable microstructure even at elevated temperatures (higher than 1000 °C) and in severe working environments due to the stability of yttria particles [5, 6]. MA ODS alloys possess excellent resistance to oxidation, corrosion, thermal fatigue and creep [7]. These alloys are widely used in the aerospace, marine, and land-based power generation industries [8, 9]. Some of their applications include vanes and honeycomb seals for gas turbines, burner nozzles, and furnace components [10]. In addition to the above-mentioned properties, MA ODS alloys also possess superior resistance to radiation-induced swelling and irradiation embrittlement compared to conventional superalloys [11]. Most commercially available MA ODS alloys include iron-based and nickel-based alloys. In general, ferritic alloys have higher radiation-induced swelling resistance and strength/weight ratios than austenitic alloys due to differences in their respective face-centered cubic (fcc) and body-centered cubic (bcc) structures [12]. Hence, ferritic ODS alloys are of particular interest in the nuclear industry for applications such as fuel cladding and fuel cans.

The application of various alloys in the industry requires the joining of the alloys to themselves or to dissimilar metals in order to fabricate and repair parts. The current research involves the joining of fuel cans that will be used in the nuclear industry. The advantages of using ferritic ODS alloys as a fuel can material are [5 - 7, 11 - 15];

a) High melting temperature
b) Creep resistance
c) Resistance to thermal fatigue
d) Microstructural stability at elevated temperatures and severe operating conditions
e) Radiation-induced swelling resistance
f) Resistance to irradiation embrittlement

Fuel cans made of ferritic ODS alloys need to be metallurgically bonded to end caps, ideally made of ferritic ODS alloys, although conventional ferritic alloys are being considered. Applications of these ODS alloys are currently limited by the joining techniques that are available.

1.2. Key Issues in Joining of ODS Alloys

Joining of ODS alloys is especially crucial [16] and is discussed in section 2. However, conventional joining techniques such as conventional fusion welding [17, 18] and solid-state friction welding [19] cannot be used successfully with ODS alloys to produce a strong joint.

Key issues involved in the joining of MA ODS alloys include:

- Oxide agglomeration
- Bondline porosity
- Formation of unwanted secondary recrystallized fine grains at the bondline
- Brittle secondary phase precipitation

All of these problems can cause premature failure of the component. It is thus very important to develop a joining technique that overcomes the above-mentioned defects. Hence, this current project investigates joining methods that can be used to develop a successful bond using ferritic ODS alloys for nuclear industry applications.

2. LITERATURE REVIEW

2.1. Demand for High Temperature Materials

A primary reason to develop heat-resistant materials is to increase the thermal efficiency of energy conversion systems [20, 21]. Carnot's efficiency of a system can be defined as:

$$\text{Efficiency } (\eta)\ \% = \frac{(T_{mx} - T_{mn})}{T_{mn}} \qquad \text{Equation 2-1}$$

Where, T_{mx} and T_{mn} are the maximum and minimum operating (absolute) temperatures, respectively. Overall efficiency of the system can be increased by increasing the maximum operating temperatures.

Oxide dispersion strengthened (ODS) alloys have the ability to perform at high homologous temperatures (> 0.5 absolute melting temperature), beyond the capabilities of conventional superalloys [22]. Use of dispersion strengthening mechanisms can be traced to the early 20th century (1913), when they were used to produce "ductile tungsten" for incandescent lamp filaments [23]. Oxide dispersion provided ductility at room temperature to tungsten, which otherwise is brittle, and also improved the high temperature life of tungsten filaments i.e., improved creep resistance, by retarding failure due to grain boundary sliding and/or dislocation motion. Dispersion strengthening can be effective almost up to the melting temperature of the matrix [24]. Fine inert oxide dispersions with a dispersoid spacing of less than 1 μm are required for effective strengthening.

2.2. ODS Superalloys

2.2.1. ODS Alloy Production

2.2.1.1. Conventional Techniques

ODS alloys can be produced by various techniques, including mechanical mixing, internal oxidation, selective reduction, rapid solidification and mechanical alloying [5,25]. Benjamin [5] reviewed and compared conventional techniques to mechanical alloying. All these techniques provide dispersion strengthening, but all suffer from certain drawbacks. In mechanical mixing, the interparticle spacing is limited by the starting metal grain size. Hence, it requires very fine powders to produce a dispersoid spacing of less than 1 μm. The internal oxidation technique involves the oxidation of a reactive element to form dispersoids. However, the thickness of the oxides varies with the depth of penetration of oxygen into the metal and it is difficult to obtain uniform oxide size. In the selective reduction method, the oxides of the alloying metals are mixed and exposed to reducing atmospheres. Some oxides, such as TiO_2 and Al_2O_3, are very stable and are thus hard to reduce, which often makes it difficult to obtain alloy with the required composition. The rapid solidification process (RSP) is a non-equilibrium processing technique by which extended solid-solubility has been achieved [25]. However, due to solid solubility limits, alloying of normally immiscible elements is not possible using RSP. The mechanical alloying (MA) technique circumvents the above-mentioned disadvantages, and the uniform oxide size and dispersoid spacing required for high temperature applications can be obtained by mechanical alloying.

2.2.1.2.Mechanical Alloying

The mechanical alloying (MA) process was developed to combine the advantages of precipitate strengthening and oxide dispersion strengthening in order to attain intermediate and high temperature strengths, respectively, in composite metal powders [26]. Conventional alloying techniques cannot be used to produce such an alloy [27]. Mechanical alloying is a solid-state process in which a mixture of alloying metal powders undergoes repeated welding, fracturing, and rewelding in a dry, high energy ball mill to produce metal powders with controlled microstructures [28]. This is clearly differentiated from conventional ball milling, which is a low energy technique in which cold welding is inhibited by the use of surfactants or liquids.

The important aspects of mechanical alloying are listed below [29]:

- Non-equilibrium processing technique
- Produces very fine second phase particle dispersion
- Produces alloys containing immiscible phases and amorphous materials
- Superior homogeneity

- Metastable crystal structures
- Nanosize grain refinement
- Extended solid solubility limits
- No use of liquid surfactants

2.2.1.3.Equipment

Mechanical Alloying is conducted in high-energy mills. The milling is carried out in order to reduce the particle size, and enable mixing, blending and shaping of the particles [30]. High energy mills include Szegvari attritor grinding mills, planetary ball mills, centrifugal ball mills, vibratory ball mills, and the Spex Shaker Mill. Conventional ball mills used under high energy, specific conditions can also be used for MA.

2.2.1.4.Materials

Commercial powders that are available in the form of pure metals, master alloys, and refractory compounds are used as starting materials for the MA process. The average powder particle size of these powders ranges from 1 to 200 μm. Although the particle size is not critical, the alloying particles are required to be smaller than the grinding ball size as the powder particles undergo deformation and exponential reduction of size to a very small value [31]. Pure metals used in the mechanical alloying include iron, nickel, cobalt, niobium, molybdenum and tungsten. Master alloys used in the mechanical alloying include nickel-based alloys with combinations of other metals. Commercially available pure metals and master alloys have oxygen contents ranging from 0.054 to 0.2

wt%. Carbides, nitrides and oxides can be used for dispersion strengthening. Thermodynamically stable oxides include yttria, alumina and thoria. These oxides are prepared by the thermal decomposition of less stable compounds of the reactive metals, which consist of crystallites of about 10 to 50 nm that are agglomerated into particles of about 1 μm. In the past, at least 15% of the powder particles used in mechanical alloying consisted of a ductile material that acts as a host or a binder. This requirement is no longer necessary since mechanically alloyed products using brittle powders have been produced since the 1990s [29]. The effects of various alloying elements on the properties of the alloys produced are shown in table 2.1.

2.2.1.5.Mechanical Alloying Process

There are three main stages involved in mechanical alloying [28]. A schematic of the process and microstructural development is shown in figure 2.1.

Initial stage: The particles at this stage may not be in the cold welded condition, and the particles may vary in size. The metal powders are soft and are able to cold weld under collision with balls in the mill, forming particles larger than the original powders. Uniform composition among the powders has not yet been achieved. The starting constituents are identifiable and form composite layers. The cold welded interfaces are widely spaced and the dispersoids are closely spaced along the weld interface.

Intermediate stage: Cold welding, fracture and re-welding of the powders continues, leading to further refinement of the material. Intimate mixing, cold working and slight heating of the powders due to the impact of balls in the mill facilitate the dissolution of solute elements and solid solution formation that begins at this stage. With increased time of processing, the distance between the welds decreases and the spacing between dispersoids along the welds increases. A logarithmic relation can be observed between the rate of internal structure refinement and the processing time. The formation of second phase constituents and the precipitation of other phases may also occur at this stage. For example, yttria aluminum garnets (YAG), alumina, and titanium carbides may form.

Final stage: At this stage, the composition of individual powder particle becomes uniform and reaches the overall composition of the starting powder blend, and optimum spacing between the dispersoids is approached. Large amounts of strain energy are created in the material during the alloying process resulting in an increase in the hardness in the material. The linear increase in the hardness that was observed during the initial stages finally reaches saturation hardness with increasing processing time. However, some regions with higher concentrations in the powders may be present. As the mixing of the powders is nearly complete, it becomes possible for the equilibrium phases to precipitate.

Consolidation: Once the process is complete, the powders have a very fine grain size of the order of subμm ranging up to a few microns. The constituents are well refined and uniformly distributed. Any contaminants from the mill or from the initial powders are also uniformly distributed and are not in the form of large defects. These powders can then be consolidated by hot compaction in steel cans using hot isostatic pressing or extrusion processes combined with a final heat treatment at a high temperature ($> 0.5\ T_m$) to result in desired grain structures. The compositions of some of the mechanically alloyed alloys are shown in table 2.2. It is to be noted that the material compositions are given in wt%, unless otherwise stated.

2.2.1.6.Mechanical Alloying Issues

Mechanical alloying is a complex process. It is a useful technique which allows producing a variety of alloys with compositions that cannot be obtained by conventional techniques. However, these advantages come with some drawbacks.

Powder Contamination: This is a major concern with mechanically alloyed products [31]. Powder contamination can occur due to the presence of fine particles (with a correspondingly large surface area) and the formation of fresh surfaces during milling. These surfaces, if exposed to air, can oxidize resulting in a change in the chemistry of the alloys. In the initial stages of milling, the alloying powders stick to the surfaces of the milling balls and form a coating. Spalling of these coatings from the surfaces of the balls during the later stages of milling can leave lumps of particles with a composition different from that of the alloy as a whole. Another source of contamination is air leakage in to the chamber. The oxygen and/or water vapor in the atmosphere react with alloying powders, especially when reactive elements such as titanium and zirconium are present.

Purging with argon is not successful in removing the nitrogen and oxygen trapped in the internal surfaces of the material. The starting compositions of the alloying material also directly relate to the final composition of the product, so high quality starting materials are required.

Porosity: Inert atmospheres are employed in the ball mills in order to avoid contamination from any leaks or reaction with air. Various researchers have observed the formation of porosity in ODS alloys during annealing [32, 33, 34, 35]. During mechanical alloying, the powder particles undergo cold-welding. However, when brittle-brittle components are mechanically alloyed, due to the difficulty in cold-welding some welds will not undergo complete closure. The presence of some voids (unbonded regions) can thus be expected. These pores remain throughout the process. Another source of porosity in mechanically alloyed products is the gas dissolved in the material during milling. Abnormally high amounts of gases can be dissolved due to the non-equilibrium nature of this alloying technique. Also, the type of shielding gas used during milling affects the volume fraction of the pores formed. For example, pore formation in MA956 was reported to be higher than in PM2000. Argon is used in alloy milling the former, while hydrogen is used for the latter. Hydrogen can diffuse faster than argon due to the smaller size of hydrogen as compared to argon. Hydrogen might be trapped in both atomic and molecular forms. During consolidation, it will be more difficult for the molecular hydrogen to diffuse away than atomic hydrogen and hence, leading to porosity [33]. In addition to the incomplete cold-welding and trapped gases, rapid secondary recrystallization in the ODS alloys is also responsible for pore formation [32,33]. Void growth during high temperature exposure has been observed to be time-temperature dependent, with void sizes of up to 25 μm produced. The size and volume fraction of the voids increased initially with time to reach a maximum; with prolonged exposure the volume fraction decreased [34,35].

2.2.1.7.MA ODS Alloys – Strengthening Mechanism

Nanosize yttria dispersoids in the MA ODS alloys act as obstacles and help to pin the dislocations [36]. The oxide dispersion and the very fine grain size of the alloys inhibit the recovery and recrystallization process that results in a coarse grain formation. The MA ODS alloys undergo recrystallization at very high homologous temperature on the order of 0.9 of the absolute melting temperature [37, 38]. In addition, the stored energy and columnar structure of the grains lead to high temperature strength [28]. The low temperature strengthening mechanism has been attributed to the classical Orowan looping of the dislocation around the hard particle. However, various explanations can be found in the literature and have been discussed by Herrick [39], who classified the theories into two categories; the Srolovitz et al. theories, based on dislocation-particle attachment model, and the Artz et al. theories, based on dislocations that undergo local climbs at the particle sites. In the Srolovitz et al. model, the dislocation is attracted to the particle. A viscous environment is created at the incoherent particle and dislocation interface. Hydrostatic and deviatoric stresses which act as repulsive forces to the dislocations are relieved by surface and volume diffusion. The relaxation of stresses at the particle-dislocation interface leads to dislocation attraction. The dislocation then reaches the particle and “smears” over the interface, releasing line tension. The dislocation attaches at the departing end of the particle. The Artz et al. model is based on the Srolovitz et al.’s work but proposes a local climb of the dislocation at the particle interface. Due to the local climb mechanism in the latter model, the dislocations are undisturbed. An illustration of both the models is given in figure 2.2.

2.2.2. MA ODS Alloys – Properties

2.2.2.1.Microstructure

The initial microstructure of the MA ODS alloys in the consolidated and as-extruded condition consists of very fine grains. In a nickel-based ODS alloy, grain sizes on the order of 300 nm and 400 nm were observed for MA754 in the transverse and longitudinal directions with respect to the extrusion direction, respectively [40]. In iron-based ODS alloys, grain sizes varying from 200 – 800 nm, and 400 nm– 1.0 µm were observed for PM2000 in the transverse direction and longitudinal direction, respectively, with respect to the extrusion direction [41, 42]. The yttria particles are generally aligned along the extrusion direction, which might lead to the formation of coarse columnar grain structures in PM2000 during isothermal recrystallization. However, such yttria alignment was not observed by Kelly [43] and Martin [44]. Typically, recrystallized MA956 material grains are 200 – 500 µm thick and 20 mm long [45]. Very high grain aspect ratios of higher than 30 were observed in the ODS alloys that are important for high temperature strength [46]. MA956 and PM2000 materials exhibited <111> and <100> grain textures, respectively. An average dispersoid size of 24 nm and 20 nm, with a mean interparticle spacing of 149 nm and 137 nm, have been observed in MA956 and PM2000, respectively. An average dislocation density of 1 x 10^{13} m^{-2} was also observed. In general, particles with different size ranges varying from 5 to 100 nm and larger particles above 100 nm were observed [41, 47, 48, 49]. The larger particles were identified as various combinations of yttrium aluminum oxides, such as yttrium-aluminum monoclinic (YAM, $Y_4Al_2O_9$), YAH (hexagonal, $YAlO_3$), YAP (pervoskite, $YAlO_3$), YAG (garnet, $Y_3Al_5O_{12}$), orthorhombic ($AlYO_3$) and titanium carbides. Although the dispersoids are very stable, some coarsening of the dispersoids was observed [48], which was attributed to the uptake of aluminum to form garnets.

2.2.2.2.Recrystallization

Mechanical alloying imparts true strains of the order of 9 to the alloyed powders, resulting in a very fine grain size in the submicron range. Bhadeshia [37] emphasized that these submicron fine grains are not merely deformation induced dislocation cell structures, but are true grains with large misorientations. These powders are then consolidated. However, some dynamic recrystallization may occur during consolidation due to the high temperatures involved (900 °C – 1050 °C), with some accompanying deformation. The extent of dynamic recrystallization depends on the temperature and deformation during consolidation. A fine grain structure is not favorable for high temperature applications, so a final heat treatment is given to induce complete recrystallization in the material. Recrystallization occurs in MA ODS alloys at very high homologous temperatures on the order of 0.9 T_m (melting temperature), compared to ~0.6

T_m for conventional alloys. Haussler et al. observed the impediment of dislocation motion by dispersoid pinning [36]. According to a model by Bhadeshia [37], in general, recrystallization initiates by bulging of a grain boundary and the influence of neighboring grains is not significant. However, when the grain size is very small, the grains cannot be considered to be independent and the grain boundary junctions themselves will act as pinning points retarding the grain growth, irrespective of the alloy system. During recrystallization of the ODS alloys, grain size increases by over three orders of magnitude, from submicron to millimeters. Recrystallized products have a very coarse columnar grain structure.

In Baloch's [50] recrystallization experiments on mechanically alloyed ODS alloys, he found the yttria dispersoids to be aligned in the working direction in both nickel-based (MA6000) and iron-based (MA956 and MA957) ODS alloys. Directional recrystallization resulting in coarse columnar grains was obtained in both types of alloy systems. The directionality of the grains along and perpendicular to the extrusion direction was obtained by zone annealing. Isothermal annealing of MA6000 produced equiaxed grains. However, in MA956 columnar grains were produced irrespective of the zone annealing direction or isothermal annealing. The anisotropic growth of MA956 was favored by the oxide dispersoid alignment in the "hot" working direction. In MA957, directionally recrystallized grains were observed when heated under a temperature gradient or with isothermal heat treatment at high temperatures. The amount of deformation prior to the heat treatment seemed to affect the directional recrystallization. Equiaxed grain formation was observed for low temperature isothermal heat treatments.

The difference in the behavior of MA956 and MA957 was attributed primarily to the reduced tendency of the oxide particles towards alignment along the working direction in MA957 compared to MA956.

2.2.2.3.Oxidation Resistance

High temperature materials are generally used in very hostile environments where they frequently encounter corrosion, sulphidation and oxidation atmospheres. Conventional high temperature alloys use special coatings for protection, but MA ODS alloys exhibit excellent resistance to such atmospheres due to their formation of protective scales [7]. MA956 surpasses many superalloys and other MA ODS alloys in oxidation resistance at elevated temperatures above 1000 °C. The slow growth of a well adhered alumina scale on the exposed surface of the alloy occurs as a result of its high alumina content [51’]. The inward diffusion of oxidant via the oxide grain boundaries controls the continuous scale growth. MA6000, with a relatively lower chromium content than MA956 also has good resistance to oxidation at 1000 °C. However, at higher temperatures MA6000 shows an increased loss of weight, although it still exhibits an oxidation resistance comparable to that of 713C and better than either IN 738 or IN792 [28]. Czyrska-Filemonowicz and coworkers [49, 52, 53], investigated the effect of dispersoid content on oxidation for two ferritic MA ODS alloys, PM2000 (0.5% Y_2O_3) and PM2002 (0.7% Y_2O_3). No significant change in the growth mechanisms was observed, but a higher oxide growth rate occurred in the higher yttria content alloy (PM2002) than in PM2000. Yttria-alumina garnets larger than bulk dispersoids precipitated at the grain boundaries affecting the diffusion paths. Higher cavity formation was observed in the oxide scale in the higher yttria content alloy. A yttria content of less than 0.5% was thus found to be favorable for higher oxidation resistance.

2.2.2.4.Corrosion Resistance

In turbine machinery, many critical components are subjected to aggressive environments that contain corrosive constituents like sulphur and chlorine salts [54]. Both iron-based and nickel-based ODS alloys, MA956 and MA754, respectively, exhibited good corrosion resistance in both H_2SO_4 and NaCl solutions. Both alloys showed no regular trend of corrosion with increasing H_2SO_4 concentration. However, in NaCl solution MA754 exhibited a better corrosion resistance than MA956 which was attributed to the reduced susceptibility of nickel (which has a higher pitting potential) to pitting than iron in a chloride environment [55]. MA6000 has a higher sulfidation resistance than 713C and is comparable to that of IN738 which was developed specifically for high corrosion resistance. This high corrosion resistance is due to an adequate amount of tantalum and/or titanium content in these alloys [28]. MA754, MA758 and MA956 also possess good resistance to attack by lime glass ($65SiO_2$-$4Al_2O_3$-$8.5Na_2O$-14CaO-3MgO-$5B_2O_3$ wt %) and C glass ($73SiO_2$-$1.7Al_2O_3$-$16.3Na_2O$-4.7CaO-3.1MgO-$0.4H_2O$-$0.15Li_2O$ wt %) [7]. MA ODS alloys thus exhibit superior corrosive properties compared to other superalloys.

2.2.2.5.Creep Resistance

One of the factors that affects the overall efficiency of a thermodynamic heat engine system is the operating temperature. With higher operating temperatures, higher efficiency can be achieved (see section 2.1). In general, however, the elevated temperature (> 700 °C) properties of the materials limit the operating temperatures. Conventional precipitation strengthened superalloys such as IN738 and IN939 undergo coarsening of the precipitates at elevated temperatures (800 °C – 1000 °C) and, hence, cannot be employed for applications with operating temperatures above 1000 °C [54, 56]. In contrast, MA ODS alloys exhibit superior creep resistance compared to conventional superalloys [57, 58, 59, 60]. For example, of two alloys with similar composition, the one with oxide dispersion developed by MA was able to maintain up to 126 MPa for 1000 h at 1100 °C, whereas the one with no oxide dispersion was able to maintain only up to 45 MPA for 1000 h at 1100 °C without failure [22]. A comparison of the stress rupture values for MA754 [57], MA758 [58], and MA956 [59] is shown in figure 2.3. Table 2.3 gives the stress rupture values for PM2000 [60].

A several orders of magnitude decrease in the minimum creep rate was observed by Wasilkowska et al. [46] in MA956 and PM2000 when compared to a nearly similar composition dispersoid free alloy, Kanthal. The strain rate decreased more gradually at very low stresses and high temperatures, suggesting a threshold stress below which significant deformation in the material would not be observed. MA956 exhibited a 30% higher tensile strength than PM2000 when tensile tested at 900 °C and strain rates above 10^{-5} s^{-1}. It was suggested that the variation in the tensile strength in these two alloys might be due to the difference in their Schmidt factors as a result of the <111> and <100> orientations in MA956 and PM2000, respectively. In addition, mechanically alloyed ODS alloys possess higher creep resistance than cast nickel-base alloys and conventional oxide dispersion strengthened alloys [27].

2.2.2.6.Void Swelling Resistance

In a nuclear reactor, the fast neutrons possess high energy, up to few hundred KeV. This energy is high enough that when a fast moving neutron collides with an atom, it displaces the atom from its lattice site. A cascade of such collisions and displacements can occur, leading to single or clustered vacant sites. Precipitation of these vacancies forms three dimensional "voids" [61]. Strong interaction exists between the interstitial and the dislocations due to relatively large distortion field as compared with a vacancy, which causes bias resulting in transfer of interstitial to the dislocations [62]. In contrast, neutral sinks (voids or incoherent precipitates) exist, which do not have any preference for interstitials or vacancies. Equal concentrations of vacancies and interstitials are caused due to irradiation [37]. Hence, biased sinks due to preference for interstitials cause an accumulation of vacancies at the voids (neutral sinks), leading to void growth. Irradiation induces both strongly biased and neutral dislocations in ferritic steels. Hence, both interstitials and vacancies can condense at these sites. Johnston et al. [12], observed a difference in the void swelling behavior in austenite and ferrite grains, irradiated under similar conditions. No swelling occurred in the body centered cubic (bcc) ferrite grains as compared to large swelling that occurred in the face centered cubic (fcc) austenite grains, although both grains were of the similar composition, and exposed to the same ion doses and temperature. Figure 2.4 shows that swelling in austenite regions decreased with decreasing Cr, and increased with increasing Ni with a constant Cr content. Johnston et al. concluded that void swelling is a structure-sensitive phenomenon and is affected by the alloy composition. The use of helium in the mechanical alloying process was more effective than argon in reducing the void swelling. The void swelling was also affected by the particle size and the density of the oxide particles [11]. The difference in the relaxation volume of the bcc and fcc structures was attributed to the higher resistance to swelling in ferritic steels compared to austenitic steels. ODS alloys enjoy better resistance to swelling than conventional alloys [63] because the matrix-dispersoid interface provides sites for recombination of point defects in addition to other sinks, such as dislocations and precipitates. Yttria dispersoids were stable and no dissolution of the dispersoids occurred under irradiation. Swelling may be minimized by the use of a fine dispersion of stable coherent precipitates as they act as recombination centers [62, 64]. Hence, the stable yttria dispersoids in MA ODS alloys results in excellent resistance to swelling.

2.2.3. Classification of MA ODS Alloys

The most common commercially available mechanically alloyed ODS alloys consist of (1) nickel-based and (2) iron-based alloys [54]. Various nickel-based and iron-based MA ODS alloys are given in table 2.2. MA956 is used in the industry for applications such as radiant heaters, hearth rollers, furnace fixtures and heat treatment equipment. Fe-based alloys find potential applications in the nuclear industry. Nickel-based MA ODS alloys may obtain their high strength, in addition to dispersion strengthening, through gamma-prime (γ') strengthening. MA760 and MA6000 possess both strengthening mechanisms, while MA754 and MA758 are Ni-based alloys that do not benefit from γ' strengthening. Ni-based MA ODS alloys find their applications in advanced aircraft gas turbine engines for nozzle guide vanes and many other high temperature industrial components. Other applications include furnace components, skid rails and hearth rollers. While both types of ODS alloys possess superior properties when compared to conventional superalloys, ferritic steels have certain advantages over austenitic steels.

Advantages of Fe-based over Ni-based MA ODS alloys: [6,65]

a) Better strength-to-weight ratio
b) Higher melting temperatures, leading to higher creep resistance at elevated temperatures
c) Lower thermal fatigue, as a result of their lower thermal expansion coefficient, that enables to better withstand cyclic thermal stresses
d) Higher resistance to void swelling under irradiation

2.3. Joining

2.3.1. Need for Joining

"As a process, joining lies at the interface between materials science and manufacturing science [66]." Applications of new materials developed to meet various demands of the industry may be limited by the lack of adequate joining technology. Joining is required for various reasons, as listed below:

a) Application of metals in the industry requires the ability to join the metals to similar metals or dissimilar metals. For example, MA ODS alloys exhibit good properties in various severe environments, such as those where oxidation, corrosion and elevated temperatures are present. ODS alloys can be used as materials for the vanes in aircraft engines, which requires the joining of ODS alloys to other superalloys. The current research is aimed at developing the ability to join fuel cans to end caps, where these end caps are made using ferritic ODS alloys or stainless steels.
b) It is difficult to manufacture large components with complex shapes. Hence, the ability to join several smaller components to build large components is required.
c) For cost-effectiveness and high thermal efficiency, some of the component designs need joints.
d) It is often necessary to conduct post-service repairs and to rectify any manufacturing defects, both of which require the ability to make effective joints.

In order to utilize the ODS alloys and benefit from their superior high temperature properties, it is necessary to be able to make ‘good’ joints between two parts made from the same alloy or dissimilar materials [40]. The joints must have the properties required to perform at elevated temperatures without degrading the ODS alloy properties, which must otherwise be compensated for by component design.

Joint Requirements

a) Stable and uniform oxide dispersion across the joint and the parent metal, i.e., no agglomeration of the oxide particles.

b) No formation of brittle phases in the joint.

c) No porosity.

d) No disruption of the elongated grains, preserving the high grain aspect ratio (GAR).

e) Uniform composition across the bond-line that is similar to the composition of the parent alloys.

ODS alloys, if subjected to sufficient thermal exposure to bring the material above the solidus temperature, may result in the formation of large Al-Ti-Y oxide particles, which are not effective in pinning the dislocations and hence, leading to deterioration of mechanical properties. Melting of the ODS alloys causes agglomeration of the dispersoids and creates a dispersoid-free zone which has inferior properties. Hence, joining of these alloys poses a challenge for engineers.

2.3.2. Overview of Joining Techniques for High Temperature Materials

2.3.2.1. Fusion Welding

This is the most widely used process. Fusion welding processes require melting of the base metal. Kelly [17] and Shoemaker [18] tested various techniques for joining ODS alloys. Gas tungsten arc welding (GTAW) was used to join MA956 sheet and following features were observed. The grains at the weldment were equiaxed as opposed to the elongated grain structure of the parent metal, grains normal to the original grain structure were observed and dispersoids seemed to be floating in the weldment while molten. The weldment also suffered from porosity. These defects caused the resulting bond to have very poor properties compared to the parent metal. In other experiments by Moilan et al. [67] using TIG welding, a loss of hardness was observed due to a loss of grain orientation and oxide agglomeration. Sulphidation resistance of the TIG weldment was low due to the discontinuous chromia scale that was present as a result of yttria agglomeration, micro-segregation of the alloying elements and a relatively coarse grain size compared to the bulk. Resistance spot welding is defined as ‘a process in which faying surfaces are joined in one or more spots by the heat generated by resistance to the flow of electric current through work pieces that are held together under force by electrodes’ [68]. Spot welding of MA956 and MA754 alloys resulted in crack free joints in both the alloys and yttria agglomeration did not occur in MA956, unlike in MA754. However, grain growth in the joint was perpendicular to the grain structure of the parent alloy. Flash butt welding of MA956 resulted in a grain boundary across the entire joint. Stress rupture values of 8.9 hours at 13.8 MPa, 1093 °C, and failure at 6.9 MPa, 1093 °C were measured for spot welded and flash butt-welded joints [17,18].

High-energy beam welding processes such as laser beam welding and electron beam (EBW) use a concentrated heat source. These processes provided joints with lower porosity and reduced agglomeration, but still with poorer strengths than the parent metal. Both these processes produced a microstructure with equiaxed grains at the weld centerline [17]. Porosity and agglomeration were not observed under optical microscopy. However, transmission electron microscopy (TEM) studies revealed porosity and dispersoid growth up to 190 nm. The large size particles observed were thought to be yttrium-aluminum-titanium oxides [48]. A 10 – 100 nm dispersoid size is known to be favorable for dispersion strengthening in ODS alloys. Although, oxide ripening occurred, the presence of adequate dispersoid distribution retained some of the high temperature strength. 1000 hour life at 34.5 MPa, 1093 °C was considered to be 100% joint strength. Fracture occurred at the transverse grain boundaries in all three of the laser and electron beam butt welds, and resistance spot welds. Seam welded lap joints provided up to 40% of the target joint strength. Weldment grain reorientation was observed by Molian et al. [67]. However, laser welded joints provided higher tensile and hot-corrosion properties than TIG welded joints.

2.3.2.2. Solid State Processes

Solid-state joining processes do not involve melting of the substrates, so an effectively undisturbed yttria dispersion can be retained in the joints using MA ODS alloys.

Explosion welding is achieved by detonating an explosive material and generating a shock wave between two metallic surfaces. However, adiabatic shear bands have been observed at the bondline when two ODS alloy substrates were explosion welded [18].

Friction welding is conducted by converting mechanical energy to heat energy by rotating one workpiece while pressing it against a non-rotating workpiece. Rotation of the workpiece is suddenly stopped after a specified time, and the pressure is increased and held for another length of time, producing a weld [68]. However, friction welding alters the chemistry, dimensions and shape of the particles [19] and the final forging force causes reorientation of some of the grains. Formation of large titanium-rich, aluminum-rich particles and yttria agglomeration has also been observed, which was attributed to the high strain rate deformation and oxidation inherent in the process.

Diffusion bonding is conducted by the application of pressure and heat between two faying surfaces, allowing the formation of intimate contact at the atomic level, and interdiffusion of the atoms across the interface and thus creating a bond. Only a limited literature is available on diffusion bonding of ODS alloys. Diffusion bonding will be explained in more detail in section 2.3.3.1. Diffusion bonding has been successfully achieved using unrecrystallized and recrystallized ODS materials in the working direction, although the resulting bond had a layer of fine grains at the bond-line [69, 70, 71], which degraded the properties of the joint. The need for a high bonding stress is a disadvantage for this process. Moore and Glasgow [69] successfully joined MA6000, a nickel-base ODS alloy, to itself in the unrecrystallized condition. Joints made between a recrystallized substrate and an unrecrystallized substrate showed lower stress rupture strength than for joints made between two unrecrystallized substrates and failure occurred in the bonds made between two recrystallized substrates. Bucklow [70] performed diffusion bonding primarily between unrecrystallized and recrystallized material. Here, specimen preparation was found to affect the epitaxial grain growth across the bondline. Electropolishing of substrates immediately prior to bonding resulted in epitaxial growth up to 50% and room temperature joint strengths comparable to the recrystallized material were obtained. However, the very high stresses (200 – 300 MPa) and special specimen preparation techniques required for this process are not economical. In other experiments conducted by Zhang et al. [71], recrystallized MA956 material was used. A thick layer of oxide was observed at the bondline at low bonding stresses. Bonding at stresses 56 MPa and 72 MPa resulted in bonds with tensile strengths comparable to that of the parent metal. However, circular voids were present at the bondline and a transverse grain boundary extended throughout the length of the joint. These defects can seriously degrade the mechanical properties of the joint strength. An increase in bond time and bonding stress was suggested to remove these voids, although this would significantly increase the cost of processing.

2.3.2.3.Brazing

Brazing comprises a group of welding processes which produces coalescence of materials by heating them to a suitable temperature above 450 °C, and by using a filler metal with a liquidus above 450 °C and below that of the solidus of the base metal [72]. The braze metal is placed between the faying surfaces and heated. The filler metal then melts and fills the joint by capillary action. Finally, the joint assembly is cooled to solidify the filler metal, resulting in a bond. The filler metals most commonly used for ODS alloys include nickel-, cobalt-, gold- and palladium-based alloys [73].

Iron- and nickel-based ODS readily form a protective oxide layer. However, the formation of such an oxide layer can inhibit the flow of the brazing filler metal. ODS alloys with no gamma-prime precipitates are easiest to braze. Brazed joints in some cases have considerable high temperature strength. For example, a more than 1000 hour rupture life at 26 MPa at 980 °C and 9 MPa at 1095 °C has been reported [73]. However, the brazing technique has certain disadvantages. The filler metal is generally very different from the base metal to allow melting below the melting point of the parent metal. This compositional inhomogeneity in the component imposes restrictions on high temperature applications. The cooling of the joint assembly is thus non-equilibrium cooling, resulting in the formation of brittle secondary phases leading to poor properties [74]. The main disadvantage with this technique is that the bond-line remains as a low-melting region. Hence, the joint limits the upper operating temperature of the component.

2.3.2.4.Transient Liquid-Phase (TLP) Bonding

TLP bonding is similar to the brazing technique, but here the joint is formed by the interdiffusion of the constituents of the interlayer (melting point depressant) and the base metal resulting in an increase of the melting temperature causing isothermal solidification, and a microstructure similar to that of the bulk material [74]. This technique is explained in more detail later, in section 2.3.3.2.

Markham [40] bonded MA754 and MA758 (both nickel-base alloys) using BNi1a and BNi5 as interlayers at 1100 °C. BNi1a is a nickel-based alloy using boron as primary melting point depressant (MPD) that was employed both in the form of a foil (25 µm) and as a sputter coating (1 – 25 µm). BNi5 is a nickel-based alloy using silicon as a primary MPD that was employed as a sputter coating. The foil and sputter coated interlayers behaved similarly at optimum heating rates. Porosity formation occurred with the use of both foils and interlayers for different reasons. Localized melting of the ODS alloy occurred, resulting in oxide agglomeration, and rapid diffusion of boron caused unwanted secondary recrystallization in the base metal. Melt-back could not be eliminated, which poses a major problem for high temperature applications. Markham recommended the use of high heating rates to avoid melt-back of the base metal, but noted that it is difficult to achieve reproducible and precise control of the process. Given enough time for diffusion of the MPD into the base metal, the braze microstructure was less sensitive to the brazing time and temperature. Secondary recrystallization was observed when using BNi1a as an interlayer, which was not observed when BNi5 was used. Hence, the secondary recrystallization was attributed to the diffusion of boron. Boron diffuses rapidly as an interstitial and hence allows short process times. However, boron is rather large for the available interstitial sites and hence imposes a significant strain on the solvent's lattice. The amount of boron and the rate of diffusion affect the initiation of the secondary grain growth. However, the mechanism controlling the process is not yet known.

Fe-9Si-13B wt% interlayers were used to join MA956, MA957 and PM2000, three ferritic ODS alloys by Khan [75]. Fe-9Si-13B wt% interlayers resulted in better bonds compared to bonds made using a BNi1a interlayer. However, problems such as excessive parent metal dissolution leading to oxide agglomeration and boron induced recrystallization occurred, similar to those observed while joining MA758 [40]. Use of an Fe-Si-B interlayer followed by isothermal recrystallization heat treatment resulted in grain growth across the bondline when joining MA956, although the bond microstructure was dissimilar to that of the bulk material when 25 μm Fe-Si-B foil was used. The use of a 2 μm Fe-Si-B sputter coating showed less parent metal dissolution and boron-induced recrystallization than that observed in the bonds prepared using foil interlayers. While, recrystallization occurred across the bondline using thin sputter coatings, the bonds failed at the bondline and exhibited only 17% of the tensile strength of the bulk. Non-uniform sputter coating or rapid isothermal solidification may be the cause of this failure.

Filler metals prepared by arc melting of MA956 base metal, 7% Si and 1% B wt% were used for TLP bonding of MA956 by Nakao and Shinozaki [76]. They observed a grain boundary between the joint and the base metal. The microstructure and grain orientations of the resulting joint were different from those of the base metal. Formation of yttria and alumina agglomerates at the bondline took place, which resulted in the formation of new grains in the joint and led to the fracture of the joints. It was suggested that this could be explained by the oxides entering the melt region during dissolution and isothermal solidification of the joint, causing yttria and alumina agglomeration. However, the present author would note that it is also possible that the oxide agglomeration that was observed in the joint occurred, at least in part, during the arc melting of MA956 material to prepare the filler metals. No melting occurs through out the mechanical alloying process. The melting of the base metal to form filler metal results in the formation large oxide agglomerates and defeats the purpose (to obtain fine oxide dispersion) of mechanical alloying technique.

Wei [77] attempted to join MA760 using two types of 45 μm amorphous thin foils; (1) boron-containing Ni-14Cr- 4.5Si- 3.2B wt %, and (2) P-containing Ni-14Cr-10.1P wt% interlayers, and MA956 using 1-2 μm thick Fe-13B-9Si wt% sputtered films. The presence of large amounts of boron and phosphorus in the interlayers caused melting of the base metal and formation of brittle second phase particles and a grain boundary line on each side of the bondline was observed. The grains recrystallized during bonding, and thus failed to grow into the bulk of the material. Fine metastable particles were observed on the bondline, which degraded the mechanical properties of the bonds.

2.3.3. Mechanism and Process Engineering of Selected Joining Techniques

Diffusion bonding (DB) and transient liquid phase (TLP) bonding share the potential to produce a joint with minimal disruption of the yttria dispersion and promote growth across the bondline. Hence, these techniques will be explained in detail.

2.3.3.1.Diffusion Bonding

The diffusion bonding technique is a solid state approach in which two faying surfaces are joined by the application of external pressures at elevated temperatures [78, 79, 80]. The applied pressure is low enough to avoid deforming the parent material macroscopically. When the mating surfaces are brought into contact, the heat allows local plastic deformation of the material both instantaneously and via rapid creep, bringing the two faying surfaces into intimate contact on atomic scale. Diffusion occurs across this atomic interface, developing a bond. Although the pressure applied is macroscopically low, the local stresses on the asperities at the faying surfaces are high enough to deform the material. Diffusion bonding can be applied to join metal-metal, ceramic-ceramic or metal-ceramic components. The components may either be joined directly to each other, or an interlayer may be used when joining two dissimilar materials in order to minimize the residual stresses that develop at the joint due to the difference in the thermal expansion characteristics [79]. In both the cases, the bonding temperature is below that of the melting point of the interlayer and the component to be joined. The interlayers are mostly metallic.

Diffusion bonding can be considered in terms of three different stages [78]. A schematic of the different stages of bonding is shown in figure 2.5.

Stage I: Initially, the true contact area between the two faying surfaces is very small. However, with the application of pressure and heat, plastic deformation of the asperities occurs, leading to a higher contact area. At this stage, a large number of pores are formed.

Stage II: This is a diffusion dominant stage, where application of pressure is no longer necessary. Most of the voids at the interface shrink in size and closure of the voids occurs. Migration of the interface out of planar orientation takes place simultaneously. Grains grow across the interface and the remaining pores are locked along the bondline.

Stage III: The closure of the remainder of the pores occurs in this stage, as volume diffusion permits the elimination of voids. It is very difficult to completely eliminate any pores present in the last stage. However, the combination of proper temperature and pressure can provide bonds comparable to those in the parent material.

Various mechanisms are involved in these stages of diffusion bonding. These mechanisms are analogous to those in pressure sintering. They are listed below and shown in figure 2.6:

(1) Plastic deformation resulting in original contact asperities at the bondline
(2) Power-law creep
(3) Surface diffusion from surface source to a neck
(4) Volume diffusion from a surface source to a neck
(5) Evaporation from a surface source to condensation at a neck
(6) Grain boundary diffusion from an interfacial source to a neck
(7) Volume diffusion from an interfacial source to a neck

2.3.3.1.1. Advantages of Diffusion Bonding

a) Requires no melting of the base metal, hence no disruption of the oxide particles.
b) Potentially results in a microstructure similar to that of the base metal.
c) Requires no additional material and so minimizes the cost of the process.
d) Dissimilar materials can be joined.

2.3.3.2.Transient Liquid-Phase Bonding

Transient liquid phase (TLP) bonding was first reported by Duvall, Owczarski and Paulonis in 1974 [74], although the process occurred in high temperature brazing as an unintended phenomenon before that time [81, 82]. TLP bonding is also sometimes termed 'Diffusion brazing' in the literature [40, 77]. The TLP bonding process involves a sandwich-like structure with an interlayer placed between two substrates, as shown in figure 2.7. This structure is heated to a temperature that is above the melting point of the interlayer but below that of the base metal. Diffusion of the interlayer components into the substrate at the bonding temperature and/or vice versa raises the melting temperature of the bond resulting in re-solidification of the bond. A number of nickel-base and cobalt-based alloys can be bonded using this technique, with various interlayers. The interlayer is chosen such that the interlayer melts at a temperature, below that of the base metal melting temperature, which does not deteriorate the properties of the base metal. The composition and amount of the interlayer should be homogeneous with the base metal and allow practical annealing temperature and times. The use of an interlayer with a composition close to that of the base metal can reduce the level of inhomogeneities.

In TLP bonding, the interlayer incorporates a melting point depressant (MPD) which lowers the melting temperature of the base metal. Melting point depressants that are commonly used include boron, silicon, manganese, niobium and titanium. However, unwanted second phases often form during the joining of nickel-base alloys with interlayers consisting of MPD other than boron. However, the primary consideration when selecting the MPD depends on the particular alloy system to be joined.

Process

A detailed study of the TLP bonding process using an Ag/Cu/Ag sandwich was conducted by Tuah-poku et al. [83]. The TLP process is generally classified into different stages based on the diffusion process involved as predicted by earlier theoretical approaches, and this was confirmed by their study. Several other models of TLP bonding have also been also developed [84 - 89]. Two substrates of material 'A' are sandwiched using an interlayer consisting of a melting point depressant (MPD) 'B'. When this assembly is heated above the melting point of the interlayer, the interlayer reacts with the substrate and melts. The heating rate is an important factor in this process as it governs the amount of MPD that diffuses into the base metal during the initial heating. This loss of the MPD affects the melting temperature of the interlayer and isothermal solidification stage. Following the melting of the interlayer, the process can be differentiated mainly into three stages; "substrate dissolution", "isothermal solidification" and "solid-state homogenization" [90].

Substrate Dissolution

The 'sandwich' is heated to the bonding temperature (T_B), during which the interlayer melts filling the gaps between the two substrate-surfaces. Dissolution of the substrate material occurs in order to attain equilibrium between the initial composition of the eutectic liquid (C_E) and the substrate (C_A). The liquidus (C_L) and solidus (C_S) at T_B are attained at the local equilibrium between the liquid and the substrate material. Dissolution does not require long range diffusion into the substrate. The activation energy for dissolution is also very low compared to interstitial diffusion. Hence, this stage occurs very rapidly, in the range of seconds to few minutes. This stage is complete once local equilibrium is attained at the solid-liquid interface [83, 90].

Isothermal Solidification

Isothermal (constant temperature) solidification commences after substrate dissolution. The diffusion of the MPD into the solid substrate material is dependent on the diffusion constant of the MPD in the bulk [83]. The width of the liquid gradually shrinks as the diffusion continues, maintaining the equilibrium solidus (C_S) and liquidus (C_L) compositions, till all the liquid is removed. Isothermal solidification requires long-range diffusion in the solid substrate material, unlike the dissolution stage. The isothermal solidification takes considerably longer than the dissolution stage, up to many hours depending on the interlayer composition, interlayer thickness, MPD diffusion coefficient in the substrate and the phase diagram of the constituents [90].

Solid-State Homogenization

Homogenization of the solute in the substrate material is achieved by continued holding at T_B. The homogenization time depends on the specific tolerance requirements. This process, similar to other homogenization processes, is also a solid-state diffusion process.

2.3.3.2.1. Advantages of TLP Bonding

The advantages of TLP Bonding include [74]:

a) The use of tailored interlayers and optimum bonding conditions can result in a microstructure that is similar to that of the parent metal. The mechanical properties of the joint can also be comparable to that of the bulk, and in some cases can even be higher.

b) Complex shapes can be joined economically as this technique requires very low stresses.

c) Joining of dissimilar metals (for example: nickel-base to cobalt-base alloys) is possible.

d) The flexibility of the interlayer and bonding parameters allows adaptability of the process to the manufacturing sequence.

e) The absence of unwanted second phase particles, agglomerated particles and minimal disruption of the base metal results in better mechanical properties compared to other joining techniques.

f) High yield (> 99.8%) and reliability of production can be achieved using this technique.

g) The joining process is highly tolerant of the presence of an oxide layer on the faying surface.

Table 2.1 Effect of Alloying Elements on the Product Properties [6]

Alloying Element	**Effect of alloying element**
Chromium (Cr)	Acts as a ferrite stabilizer. Improves oxidation resistance and high temperature strength.
Aluminum (Al)	Improves oxidation resistance.
Titanium (Ti)	Interstitial impurity (C, O, N) scavenger. Improves oxidation resistance and ductility. At least 0.2 wt% is required to provide oxidation resistance and to avoid Cr loss by oxidation during high temperature annealing.
Yttria (Y_2O_3)	Thermodynamically very stable oxide. Nanosize yttria dispersoids are very effective in pinning dislocations. Provides high temperature strength, retards grain growth.
Molybdenum (Mo)	Acts as a ferrite stabilizer and for solid solution strengthening. Improves high temperature strength, ductility and fabricability.
Tungsten (W)	Acts as a ferrite stabilizer and solid solution strengthener in ferrite.
Carbon (C)	Should be kept as low as possible to avoid any deteriorating effects by martensite formation.

Table 2.2 Nominal Compositions of Mechanically Alloyed Alloys [73, 91, 92]

Alloy	Ni	Fe	Cr	Al	Ti	Y_2O_3	Mo	W	Ta	C	B	Zr
MA754	Bal	-	20	0.3	0.5	0.6	-	-	-	0.05	-	-
MA758	Bal	-	30	0.3	0.5	0.6	-	-	-	0.05	-	-
MA760	Bal	-	20	6.0	-	0.95	2.0	3.5	-	0.05	0.01	0.15
MA6000	Bal	-	15	4.5	2.5	1.1	2.0	4.0	2.0	0.05	0.01	0.15
MA956	-	bal	20	4.5	0.5	0.5	-	-	-	0.05	-	-
MA957	-	bal	14	-	0.9	0.25	0.3	-	-	-	-	-
PM1000	Bal	-	20	0.3	0.3	0.6	-	-	-	-	-	-
PM2000	-	bal	20	5.5	0.5	0.5	-	-	-	-	-	-

Table 2.3 Stress Rupture Values of PM2000 Bar in Longitudinal Direction (based on [60])

Temperature	**Stress to produce rupture**			
° C (° F) (K)	10 h	100 h	1000 h	10000h
900 (1652) (1173)	112	97	94	87
1100 (2012) (1373)	71	63	62	58

(10 < bar diameter < 30 mm)

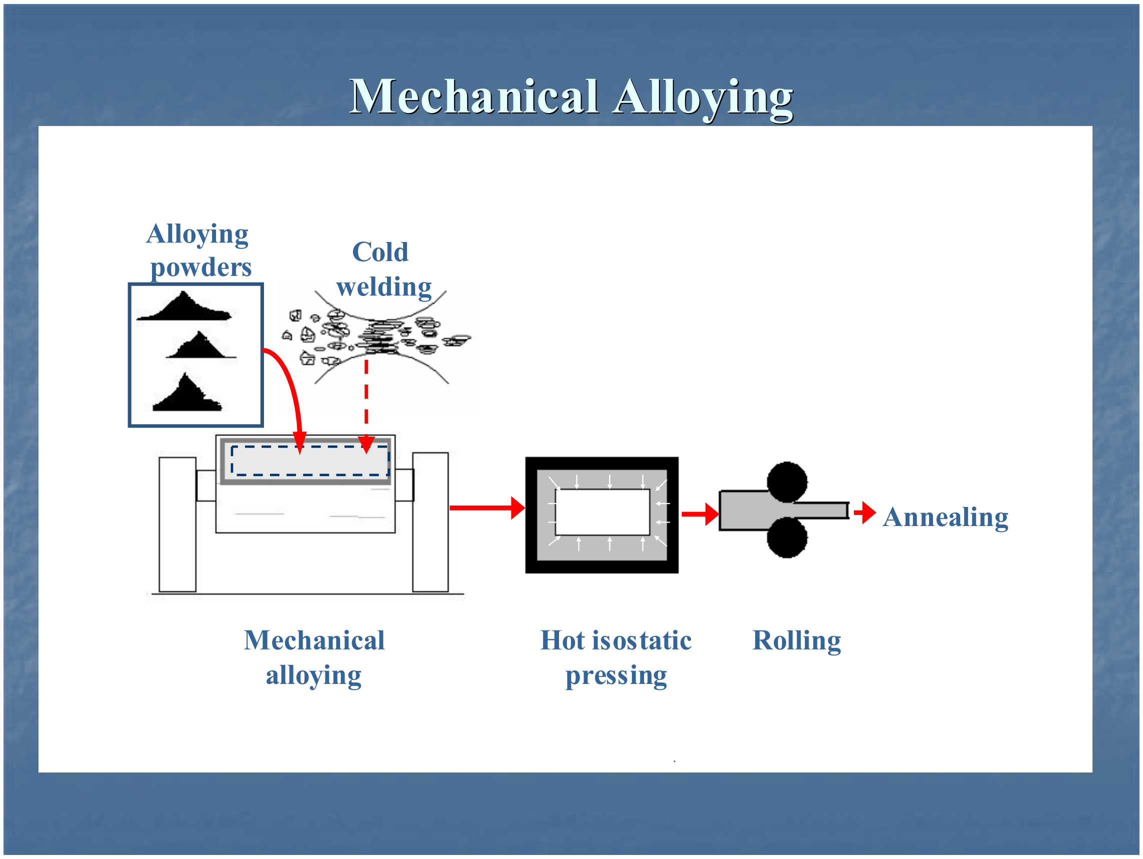

Mechanical Alloying

Alloying powders

Cold welding

Mechanical alloying

Hot isostatic pressing

Rolling

Annealing

Figure 2.1a Schematic of Mechanical Alloying Process based on [10]

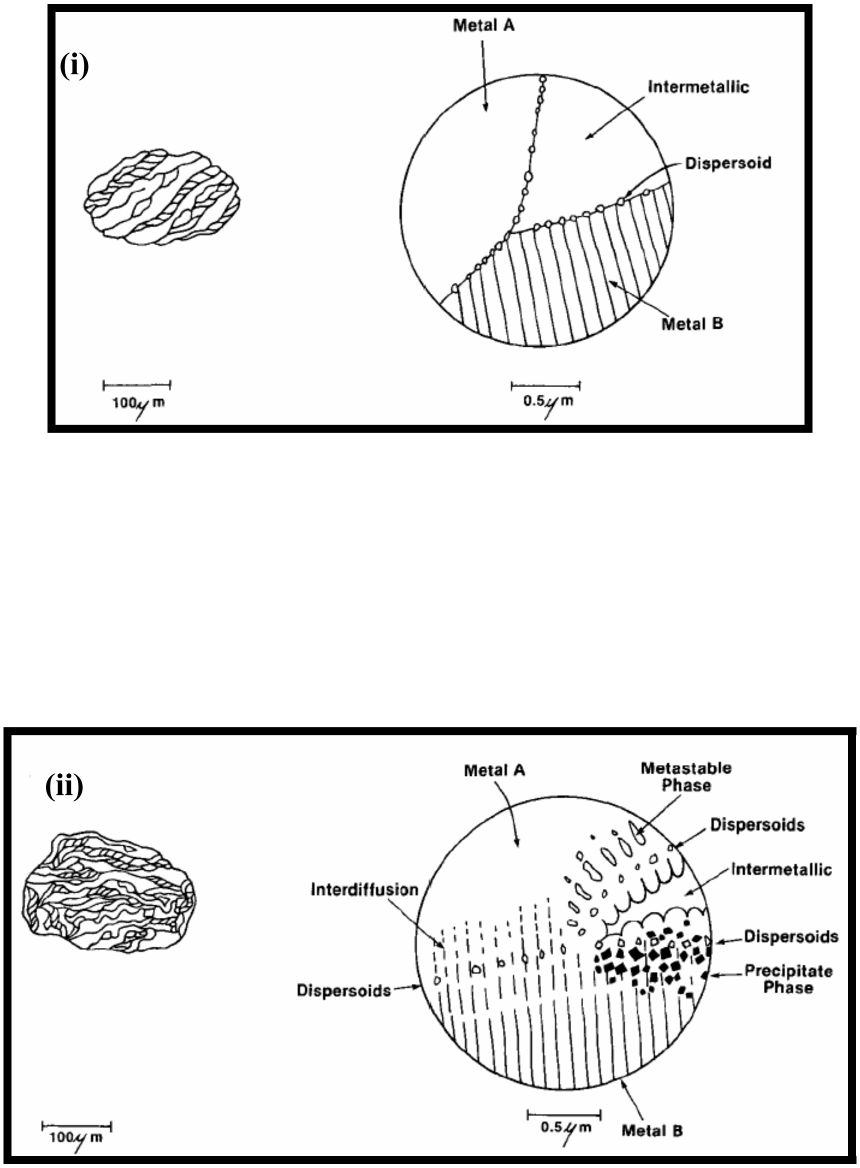

Figure 2.1b The different stages of mechanical alloying showing the developments in the particle size and dispersion of oxides. (i) Initial and (ii) Intermediate stages. Gilman and Benjamin [22].

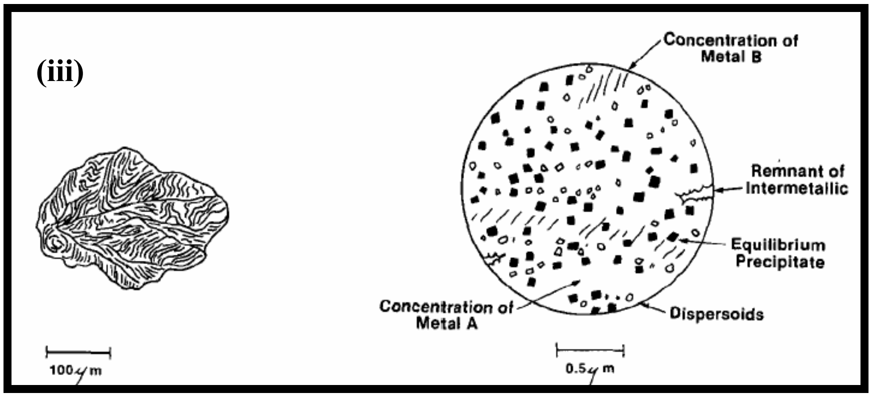

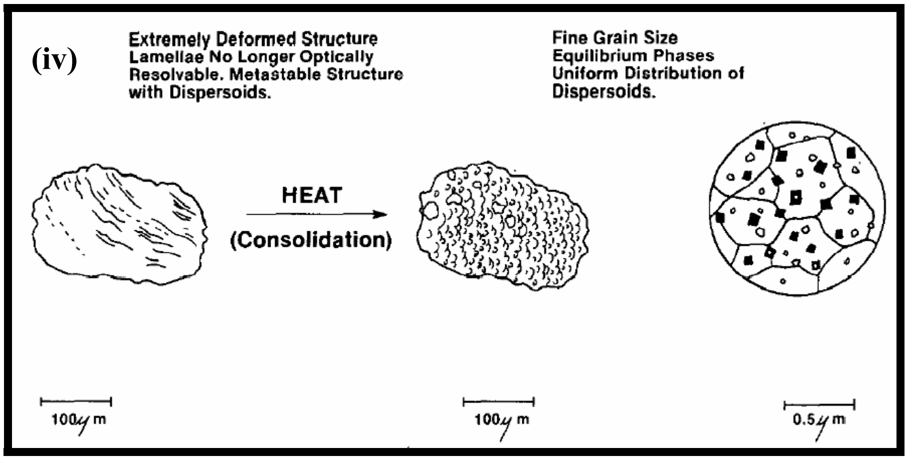

Figure 2.1c The different stages of mechanical alloying, showing the developments in the particle size and dispersion of oxides. (iii) Final stages and (iv) Completion of processing. Gilman and Benjamin [22].

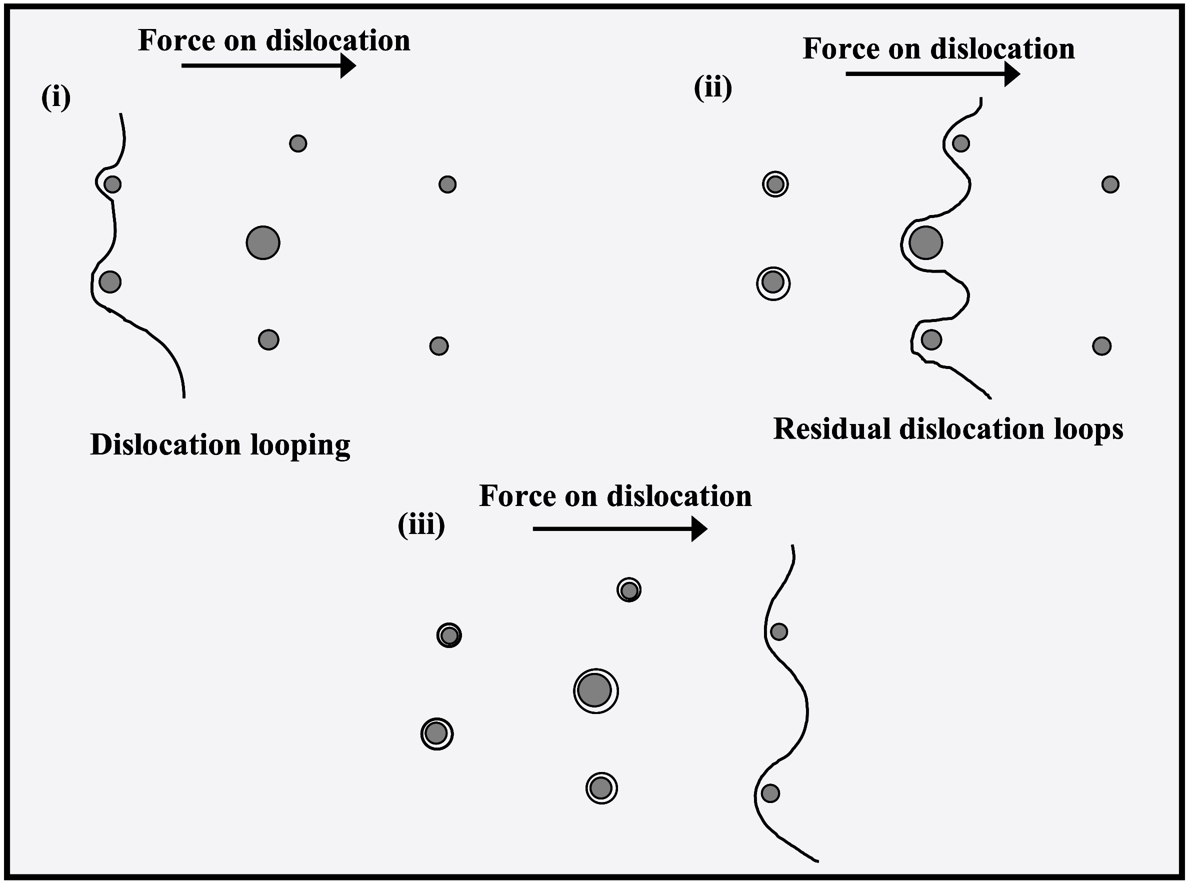

Figure 2.2a Strengthening mechanisms; dislocation/ particle interaction at low temperatures [39].

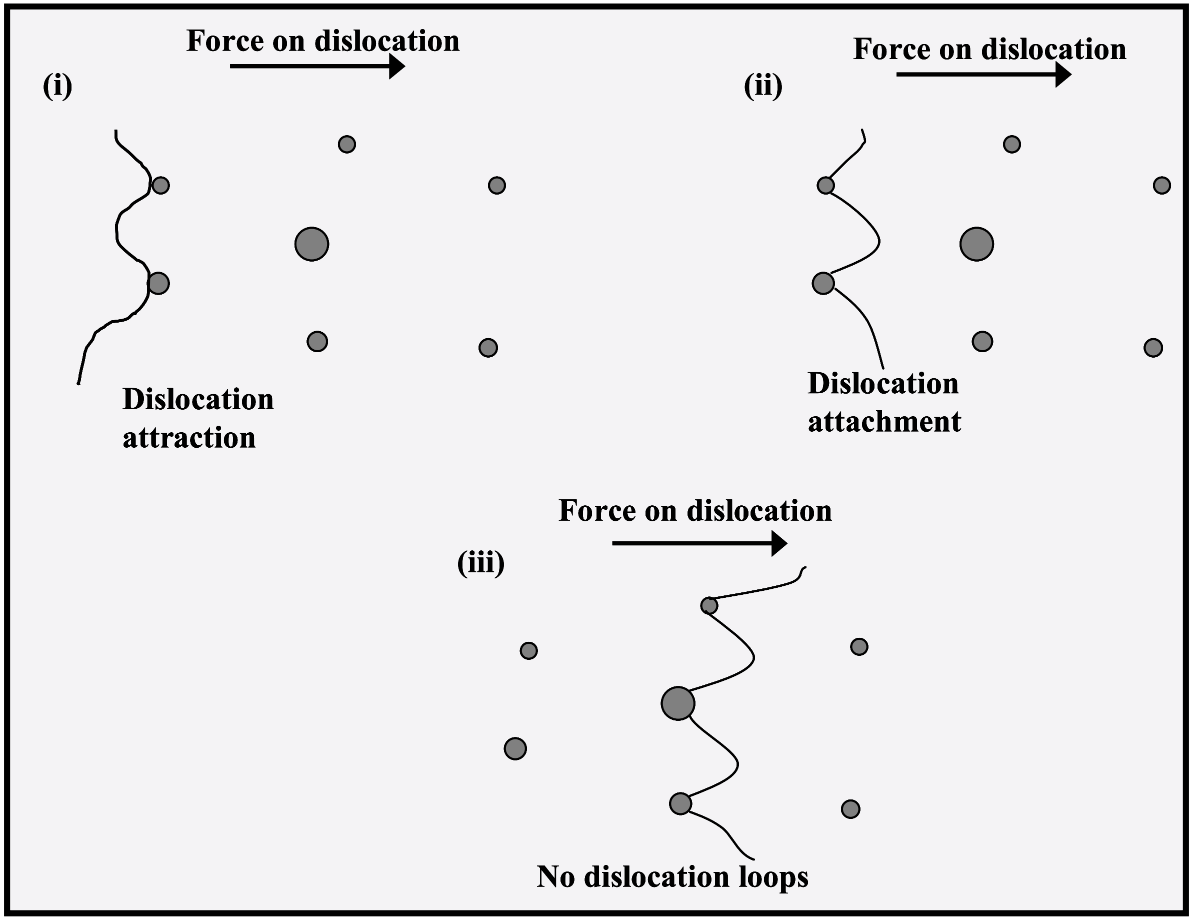

Figure 2.2b Strengthening mechanisms; dislocation/ particle interaction at high temperatures [39].

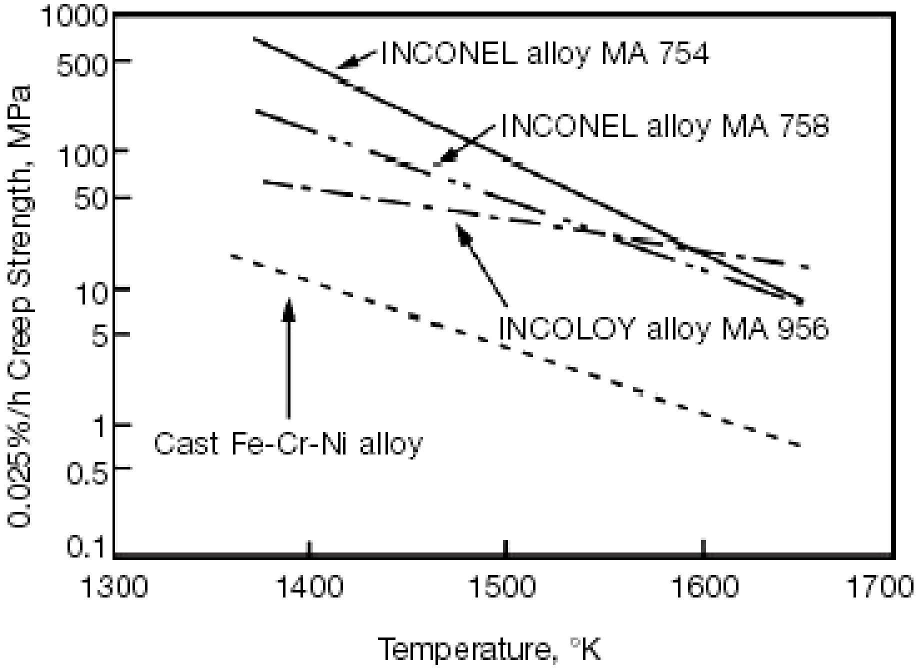

Figure 2.3 Comparison of Creep Strength of MA ODS alloys with cast Fe-Cr-Ni alloy [58].

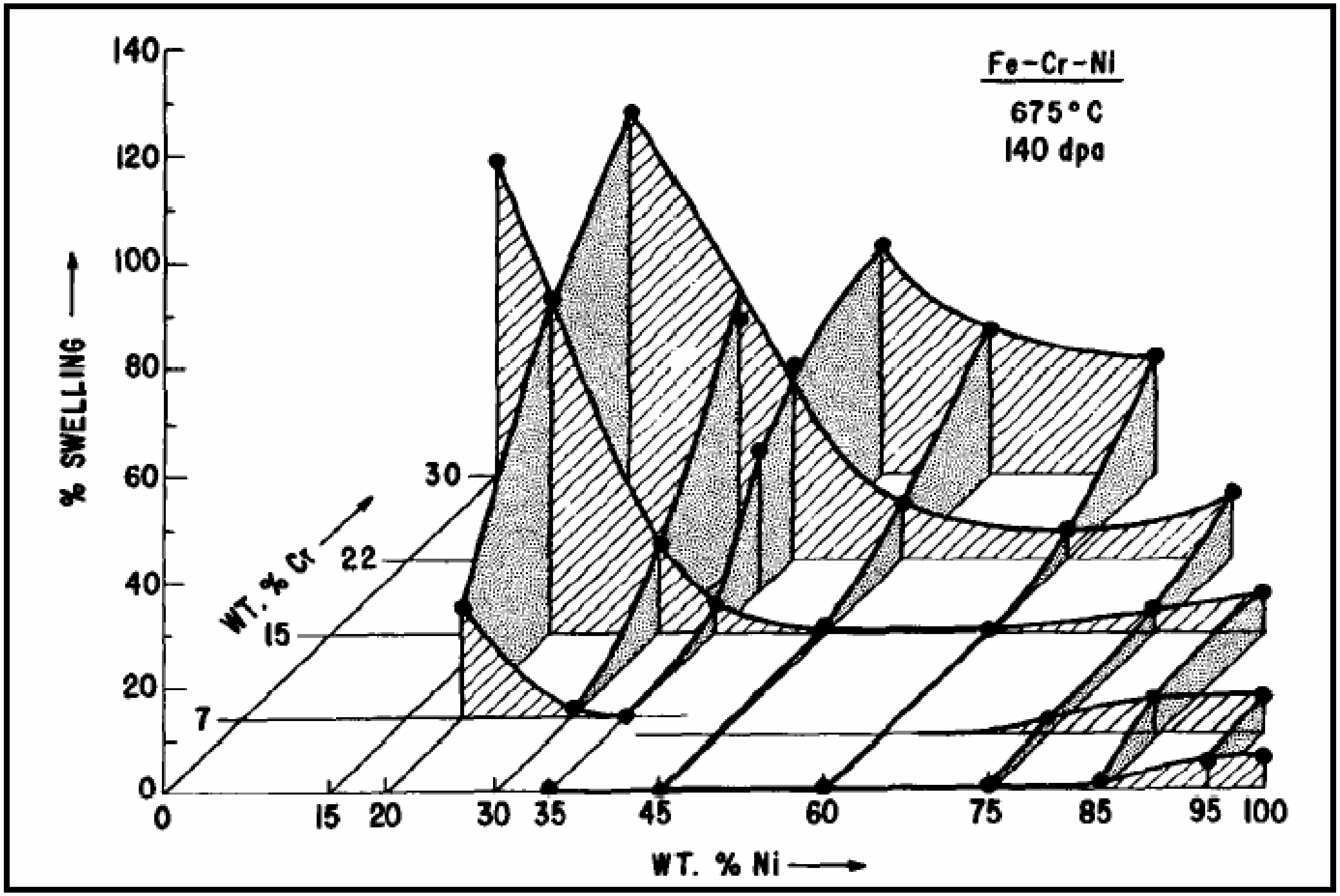

Figure 2.4 Swelling as a function of Cr and Ni content in pure Fe-Ni-Cr alloys bombarded with nickel ions at 675°C and 140 dpa. Figure is from the review by Stiegler and Mansur [61] based on Johnston et al. work [12].

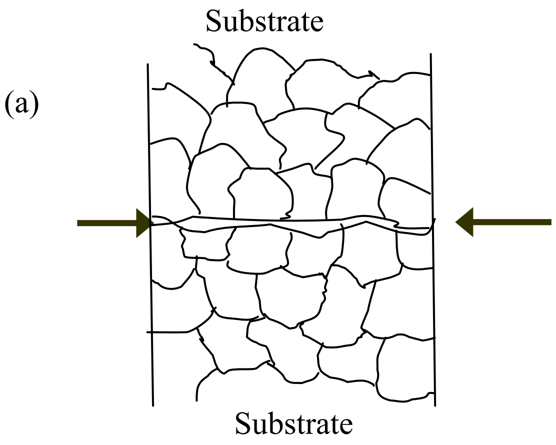

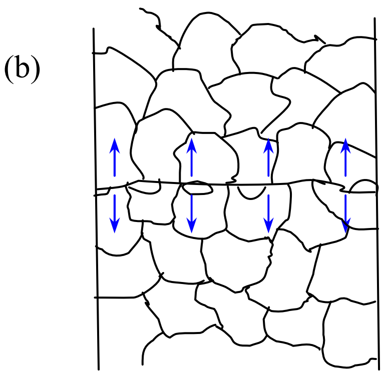

Initial contact area

Stage I - Deformation of asperities leading to larger contact area

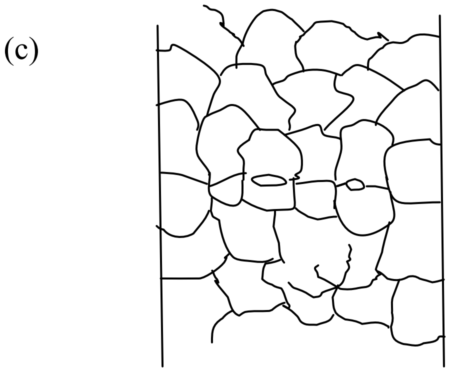

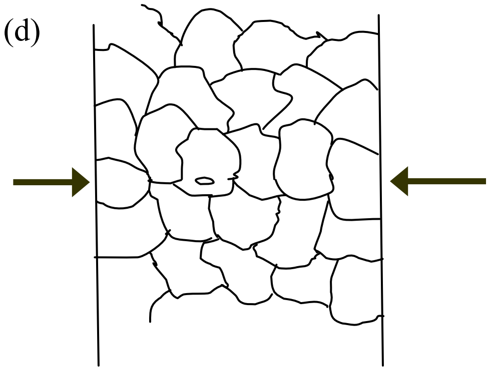

Stage II - Closure of pores and grain boundary migration

Stage III – Elimination of voids by volume diffusion

Figure 2.5 The different stages of diffusion bonding (a) initial contact area, (b) stage I - deformation of asperities leading to larger contact area, (c) stage II - closure of pores and grain boundary migration, and (d) stage III – elimination of voids by volume diffusion [80].

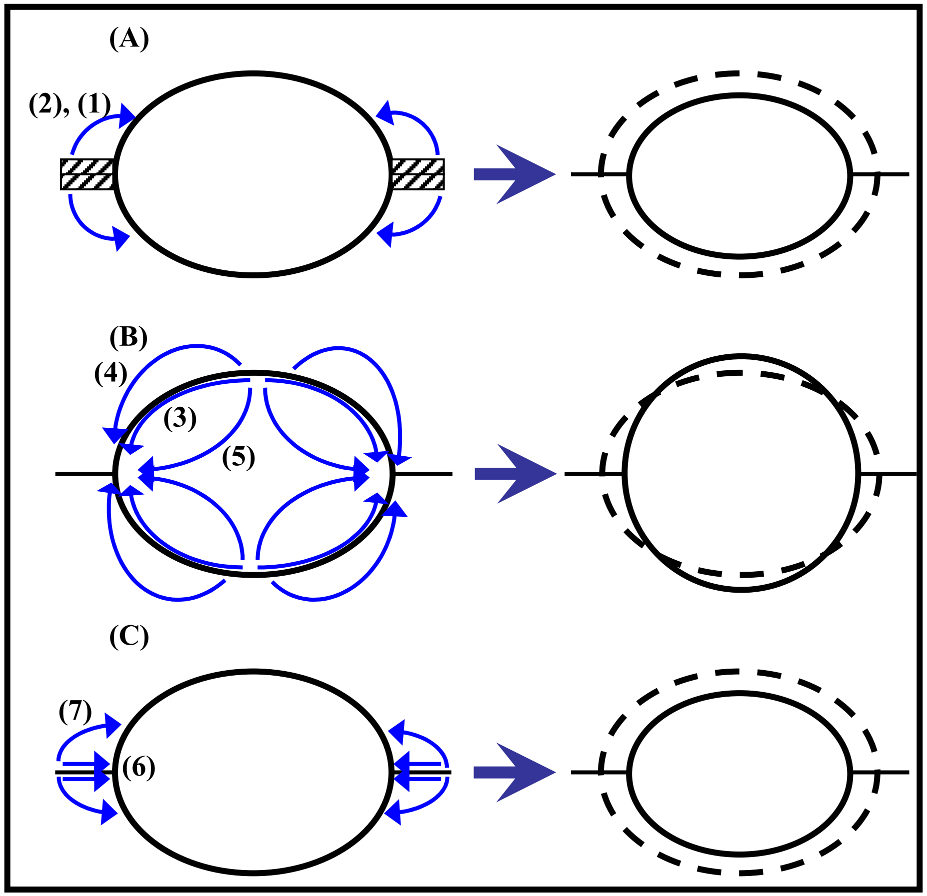

Figure 2.6 Schematic of various mechanisms (1-7) that occur during diffusion bonding (and pressure sintering). Mass transfer happens through (a) bulk deformation mechanisms, (b) surface source mechanisms, and (c) interface source mechanisms [78].

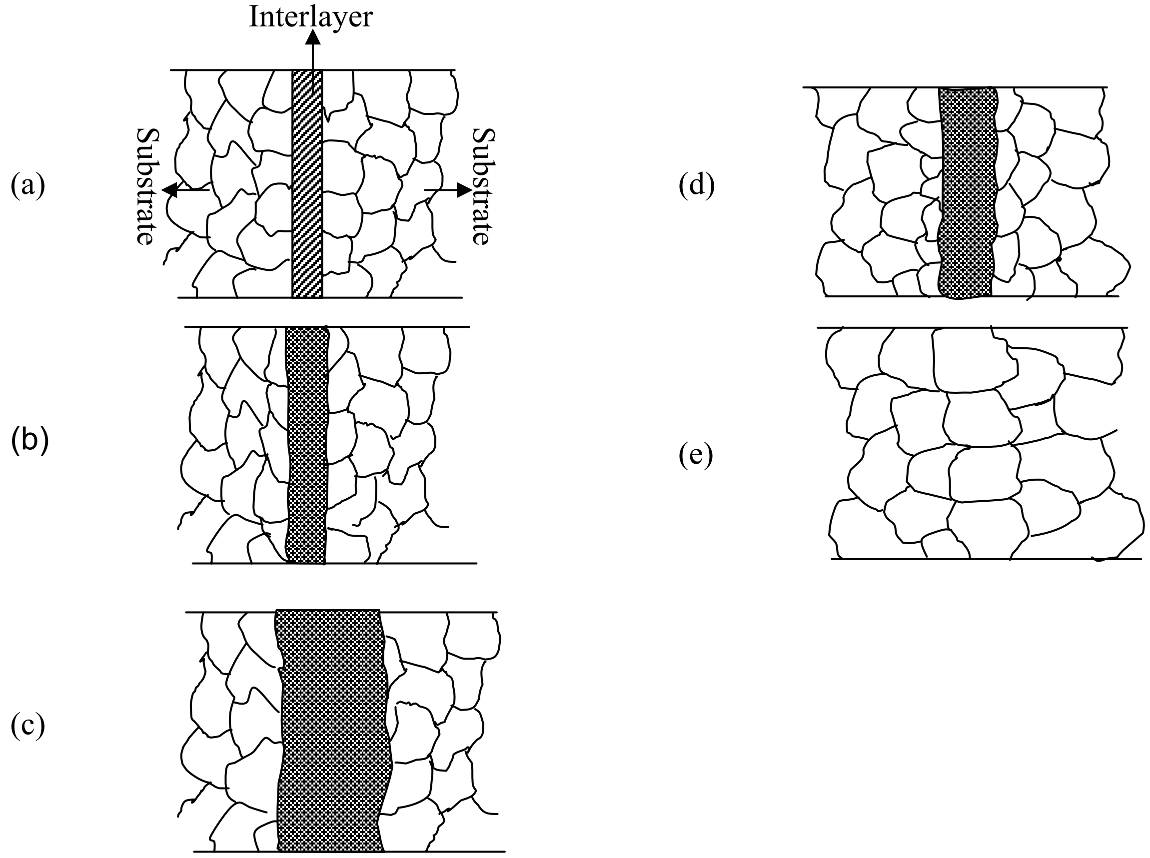

Figure 2.7 (a) Bond setup (b) Melting of interlayer (c) Substrate dissolution (d) Isothermal solidification (e) Homogenization

3. OBJECTIVES OF THE CURRENT RESEARCH

The aim of this project was to develop a successful joining technique to metallurgically bond fuel cans, made of ferritic oxide dispersion strengthened (ODS) alloys, to end caps. The end caps may be made of ferritic ODS alloys or ferritic non-ODS steels. Ferritic ODS alloys were chosen for this research because of their various advantages over austenitic alloys, especially due to their high resistance to void swelling, as mentioned in the literature review. This project aimed to study bonding phenomena associated with ferritic ODS alloys, including the development of the bond microstructure and its relation to the joint properties.

Objectives of the project are:

- Design and implement a bonding process that produces a bond between ferritic ODS alloys with reasonable dispersoid continuity.
- Produce a microstructure with recrystallized grains, similar to that in the base metal, which extends across the bondline.

In the current investigation, joining of two ferritic ODS alloys, MA956 and PM2000, was conducted using two techniques. (1) Transient liquid phase (TLP) bonding was employed due to its potential to join non-weldable alloys with stable oxide layers on the faying surface, and to attain parent metal microstructure; and (2) Solid-state diffusion bonding was also examined as it does not involve melting of the base metal and has the ability to maintain the yttria dispersion and hence, retain the parent metal microstructure.

The following approach was used in this project in order to obtain a successful bonding technique;

(1) Perform bonding with a joint design that minimizes the disturbance to the yttria dispersion.

(2) Use thin film interlayers to reduce the amount of dissolution that occurs during TLP bonding.

(3) Diffusion bonding of recrystallized coarse grain ODS alloys requires high bonding stresses due to the limited plastic flow at low temperatures. The use of fine grain unrecrystallized condition material allowed for higher grain boundary diffusion and led to reduced bonding times and stresses.

(4) The use of fine grain unrecrystallized condition substrates for bonding followed by recrystallization annealing resulted in grain growth across the bondline and in the bulk of the substrates.

The process flow chart for the transient liquid phase bonding and solid-state diffusion bonding involving the investigation of various parameters is given in figure 3.1. The bonds were mechanically tested and compared to the bulk material strength. Fractography was conducted in order to investigate the mechanisms involved in the failure of the bonds.

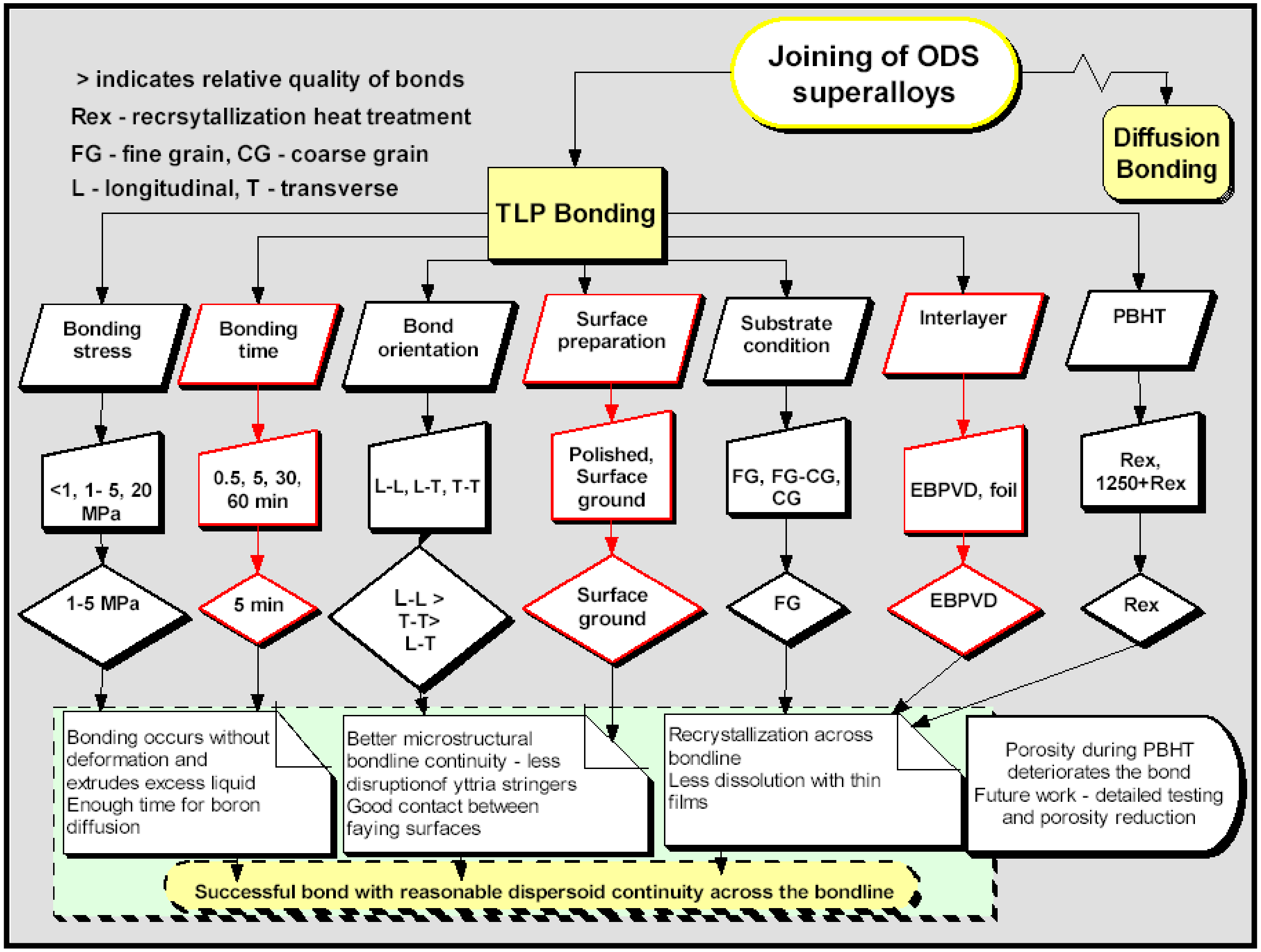

Figure 3.1a Joining Flow Chart – Transient Liquid-Phase Bonding.

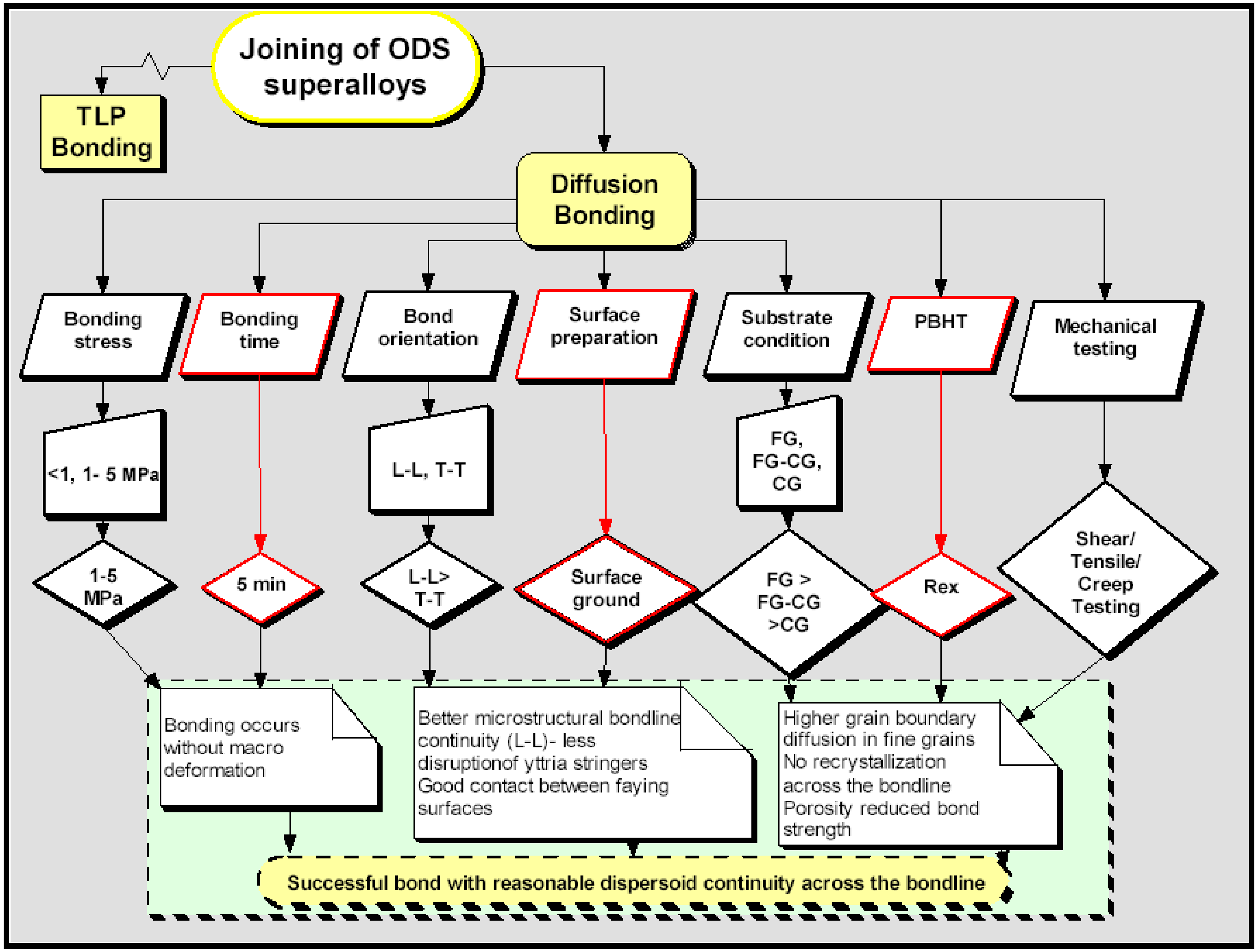

Figure 3.1b Joining Flow Chart – Solid-State Diffusion Bonding.

4. EXPERIMENTAL METHODS

4.1. Preparation of Materials

Substrates: Various ferritic oxide dispersion strengthened materials were supplied by Idaho National Laboratory (INL) (table 4.1). MA956 was received in both the fine grain (unrecrystallized) and the coarse grain (recrystallized) conditions as 11 mm square section billets and 20 mm diameter round bars, respectively. PM2000 used was received in the fine grain (unrecrystallized) condition as 25 mm and 50 mm diameter round bars.

An electric discharge machine (EDM) was used to cut 11 mm x 10 mm x 2 mm thick substrates in the longitudinal and transverse orientations (along and normal to the direction of extrusion, respectively). A schematic of the substrate orientations is shown in figure 4.1. The substrates were then polished using 1200 grit emery paper or surface ground to remove the recast layer formed during EDM cutting. A surface grinder from Gold International Machinery, Inc. was used for surface grinding. These substrates were then cleaned ultrasonically in acetone in order to remove any grease or dirt present on the substrates. These alloys are prone to the formation of a protective oxide layer on the faying surface when exposed to atmosphere. Hence, to avoid such oxide layer formation, the cleaned substrates were stored in acetone.

Interlayers: Electron beam physical vapor deposition (EBPVD) was employed to deposit 250 nm, 500 nm and 1 µm thick boron films to be used as interlayers for TLP Bonding, which react with the faying surfaces of the substrates to form eutectic liquid. Boron film deposition was performed using the CHA-Mark 50 high vacuum deposition system [93], figure 4.2, at the Alabama Microelectronics Science and Technology Center (AMSTC). The deposition parameters are provided in table 4.2. Commercially available 25 µm thick iron-based (Fe-16B-5Si wt %) foil was also used as an interlayer for comparison purposes.

4.2. Joining Procedure

A Gleeble 1500 (figure 4.3), a thermo-mechanical processing system, was employed for bonding trials to allow both rapid heating and the ability to apply pressure. Temperature was monitored using a k-type thermocouple spot-welded to the substrate. A schematic of the bond setup is shown in figure 4.4. POCO carbon blocks were used for effective thermal conduction between the water-cooled copper blocks and the base metal. In general, no additional material is required. However, in the current application carbon forms a eutectic with the iron-based substrates, requiring an additional niobium foil be inserted between the carbon block and the iron-based substrate. Limited joining work was also conducted using a Brew furnace, a radiantly heated (refractory metal heating element) vacuum furnace. In the latter case, only a fixturing load was employed and a relatively low heating rate used (2-4 ºC s^{-1}) for the furnace as compared with the 8-10 ºC s^{-1} used with the Gleeble. Rapid heating rates are necessary in order to prevent excessive boron diffusion during heating to the bonding temperature, which would impede (or possibly even prevent) liquid formation at the bonding temperature. The heating rate used in the Gleeble would be attainable in a commercial induction brazing operation, but is far higher than the heating rates achievable with a commercial vacuum brazing furnace. Furthermore, even the lower 2 ºC s^{-1} heating rate used for furnace brazing in the present project was an order of magnitude higher than the standard furnace brazing practice.

Bonding was conducted at 1250 °C, well above the binary Fe – B eutectic temperature of 1,174 ºC [94] in a vacuum of less than 1 x 10^{-3} Pa. Phase diagrams for the Fe-B and Cr-B systems are shown in figures 4.5 and 4.6, respectively. Different bond orientations, obtained by varying the substrate's alignment, were investigated including longitudinal – longitudinal (L-L), longitudinal – transverse (L-T) and transverse – transverse (T-T), as shown in figure 4.7. The significance of the bond orientation will be discussed in the latter sections. Joining was performed using the base metal in both the unrecrystallized fine grain (FG) and recrystallized coarse grain (CG) conditions. Although, TLP bonding does not require significant bonding stresses (one of the advantages of TLP bonding), the application of compressive stress helps to extrude the excess liquid formed at the bondline, thus reducing the amount of liquid that must be dissolved in to the substrate and reducing the time required for isothermal solidification. Stresses on the order of few MPa fall in the lower limit range of the Gleeble 1500 and it is difficult to obtain a reproducible stress value in this lower range. Hence, a nominal stress range of 1-5 MPa was applied in the current investigation.

Post bond heat treatment (PBHT) was conducted in order to induce recrystallization and for diffusion of boron into the substrates. PBHT was performed in the Brew furnace, in a vacuum of less than 1 x 10^{-3} Pa, at recrystallization temperatures of 1300 °C and 1385 °C for the MA956 and PM2000 materials, respectively. Limited heat treatments below the recrystallization temperature at the bonding temperature were also conducted.

4.3. Metallographic Preparation

Metallographic preparation was conducted using advanced Struers' machines. Samples were cut using Accutom-5 precision cutting machine and were mounted using a Labopress-3 machine. Polishing of the samples was conducted using a TegraSystem autopolisher. The autopolisher consisted of a TegraPol-15 polishing machine with a TegraForce-1 specimen mover and a TegraDoser-5 dosing system. This system can polish up to 3 samples at the same time with excellent control over the surface finish. The polishing settings are shown in table 4.3. The samples were then water cleaned using deionized water and air-dried.

Different etching techniques were initially used for metallographic examination. These were;

(1) A solution of 10 ml hydrochloric acid in 90 ml ethanol/methanol for 1 – 2 minutes

(2) 20% nital for up to 3 minutes at 0.5 A current for electrolytic etching

(3) A solution of 2g copper chloride, 40 ml hydrochloric acid and 40 – 70 ml methanol for 2 - 10 seconds.

The last etchant gave the best results.

4.4. Materials Characterization

The microstructure was evaluated using an Olympus PME 3 optical microscope equipped with digital picture conversion by a using LEICA DC 300 system. A JEOL 840 scanning electron microscope (SEM) operated at 20 kV was used for microstructural characterization for secondary electron imaging at higher magnification. Energy dispersive X-ray spectroscopy (EDS) with back scattering was used for compositional analysis and detection of porosity or secondary phases. Fractography of the tested samples was conducted using the same SEM equipment.

4.5. Mechanical Testing

Room temperature shear testing was conducted using an MTS Q-Test screw-driven system with a 100kN load cell. The shear rig used for testing was based on a design developed by Yan and Wallach [95]. Peak stress values were measured from the maximum load required for fracture over the initial bond area. The grip separation speed was set at 500 μm/min. A schematic of the grips is shown in figure 4.8.

Room temperature tensile testing was conducted on bulk and bonds using Sintech system with a 27 kN load cell. Rectangular tensile samples (figure 4.9 (a)) were prepared using EDM. The cross head speed was set at 250 μm/min.

Creep testing was conducted on bulk PM2000 samples (figure 4.9 (b)) using a Applied Test Systems, Inc. 2410 series lever arm creep testing machines. Testing was done at 1000 °C in air using a 3210 series three zone heating furnace under different loads after a recrystallization heat treatment at 1385 °C for 4 hours.

Table 4.1 Materials

Alloy	As-received condition	Nominal Composition (wt %)						
		Fe	B	Si	Cr	Al	Ti	Y_2O_3
MA956	Fine grain (Unrecrystallized) condition – 11 mm square billets Coarse grain (recrystallized) condition – 20 mm diameter bar	bal	-	-	20	4.5	0.5	0.5
PM2000	Fine grain (unrecrystallized) condition – 25 mm and 50 mm diameter bars	bal	-	-	20	5.5	0.5	0.5
Boron	E-beam physical vapor deposition	-	100	-	-	-	-	-
Fe-B-Si	Foil	bal	16	5				

Table 4.2 Electron Beam Physical Vapor Deposition (EBPVD) Parameters

Element	Emission current	Voltage	Deposition Rate	Power	Thickness
Boron	148 mA	9.58 kV	~ 400 pm / s	2.5 kW	1 μm*

* The thickness used depended on the final thickness of interlayer needed

Table 4.3 Settings for Polishing

Struers Disc	**Lubricant/Suspension**	**Level Pumpspeed (Arbitrary units)**	**Time (seconds)**	**Load (newtons)**	**Disc rpm**
MD Piano	Water	On	60	25	300
MD Largo	DiaPro Allegro/ Largo	4/5	45	25	150
MD Plan	DiaPro Plan	4/5	150	25	150
MD Dac	DiaPro Dac	4/5	150	25	150
MD Mol	DiaPro Mol	6/6	120	25	150
MD Chem	OP-S	5/6	90	25	150

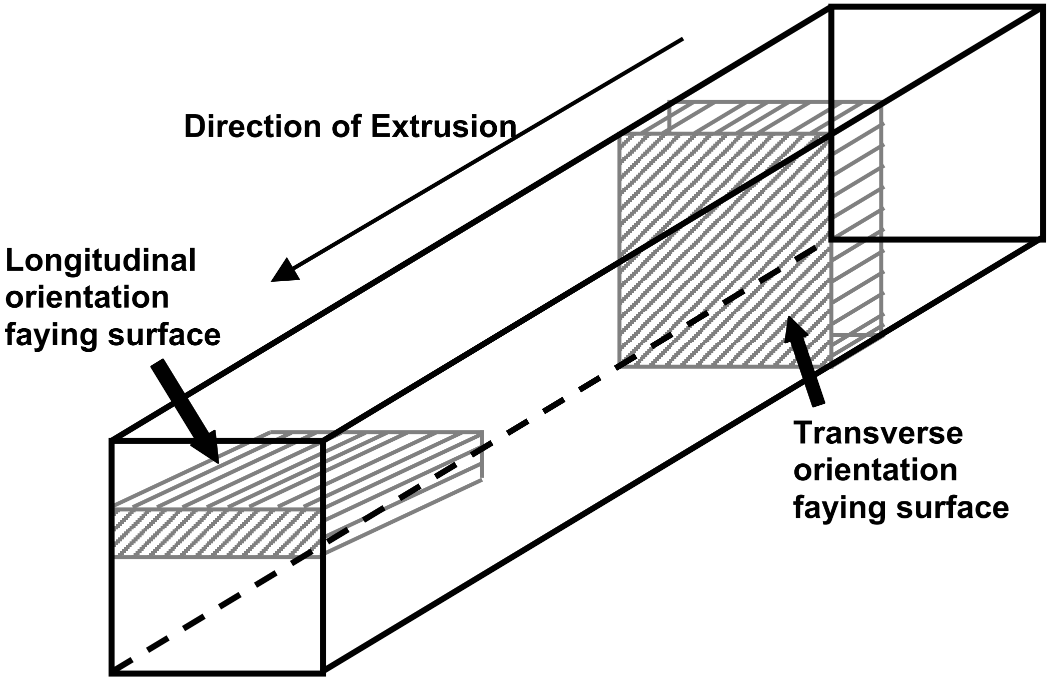

Figure 4.1 Substrates showing transverse and longitudinal orientations.

Figure 4.2 CHA- Mark 50 high vacuum deposition system used for depositing boron thin films [93].

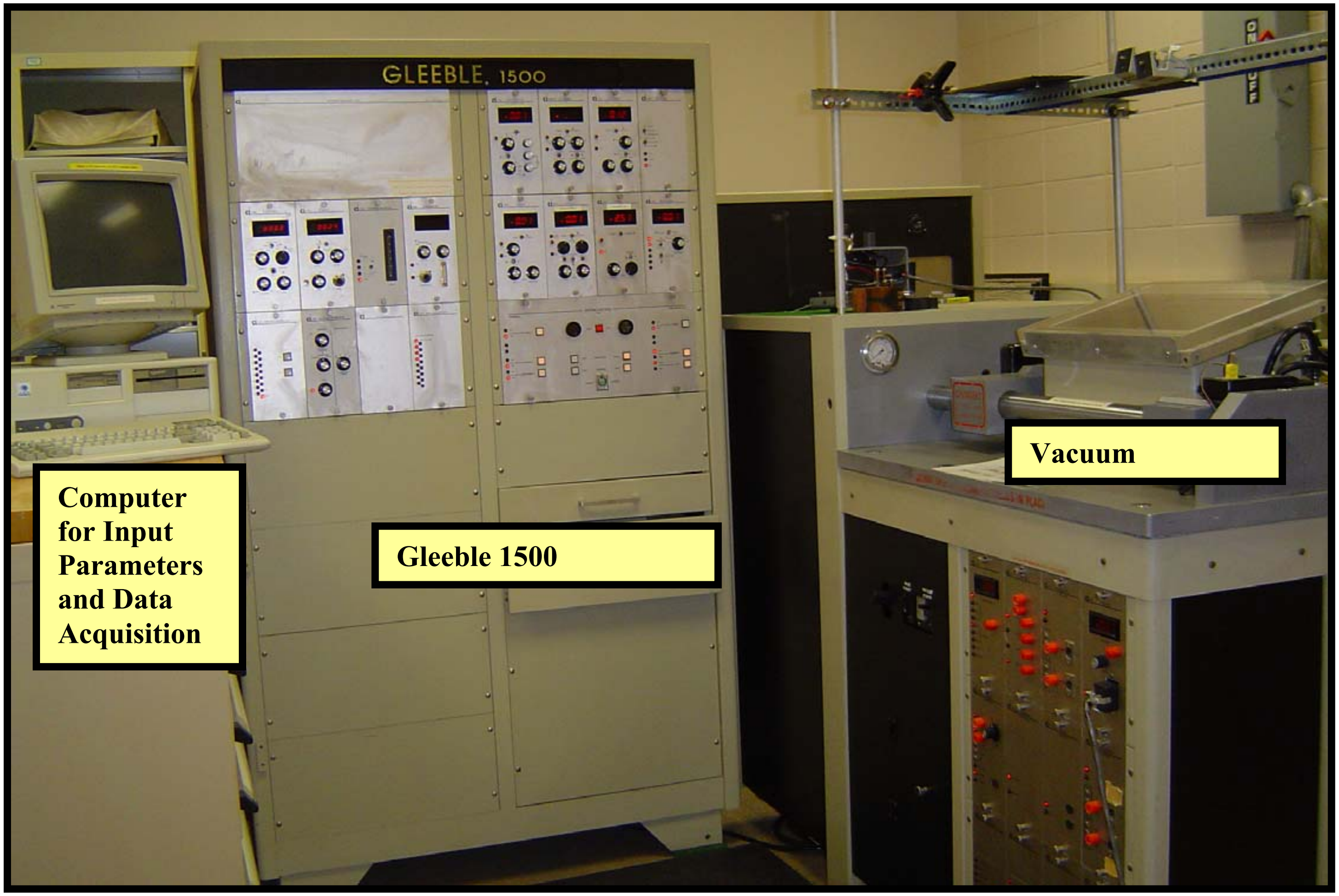

Figure 4.3 Gleeble 1500 thermo-mechanical system used for bonding.

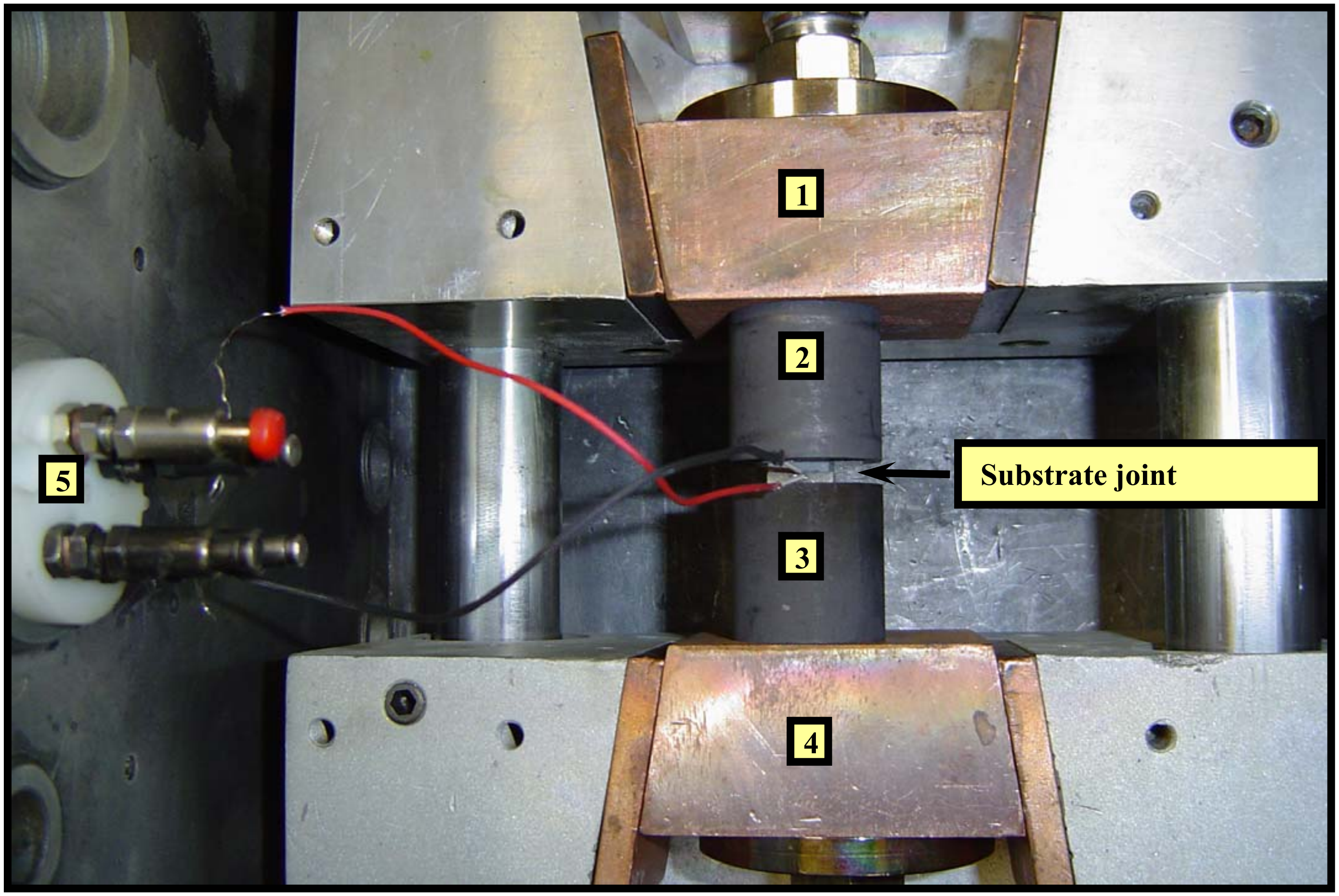

Figure 4.4 Bond set-up 1 and 4 – copper blocks, 2 & 3 POCO carbon blocks and 5 thermocouple connections.

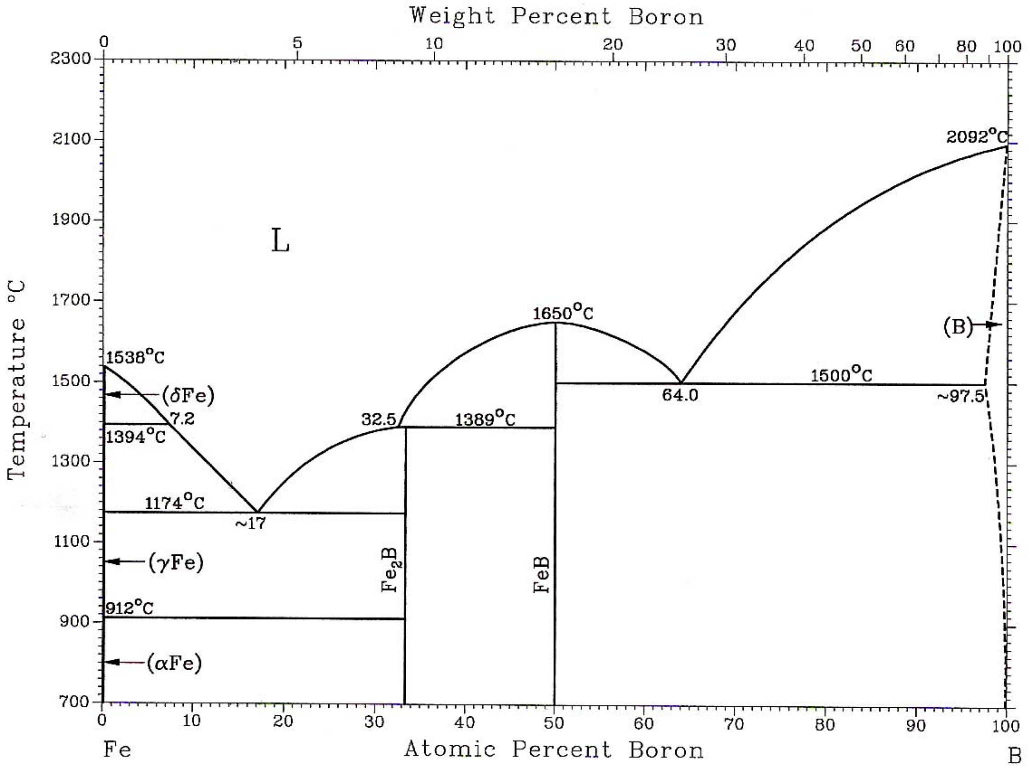

Figure 4.5 Binary phase diagram of the Fe-B system [94].

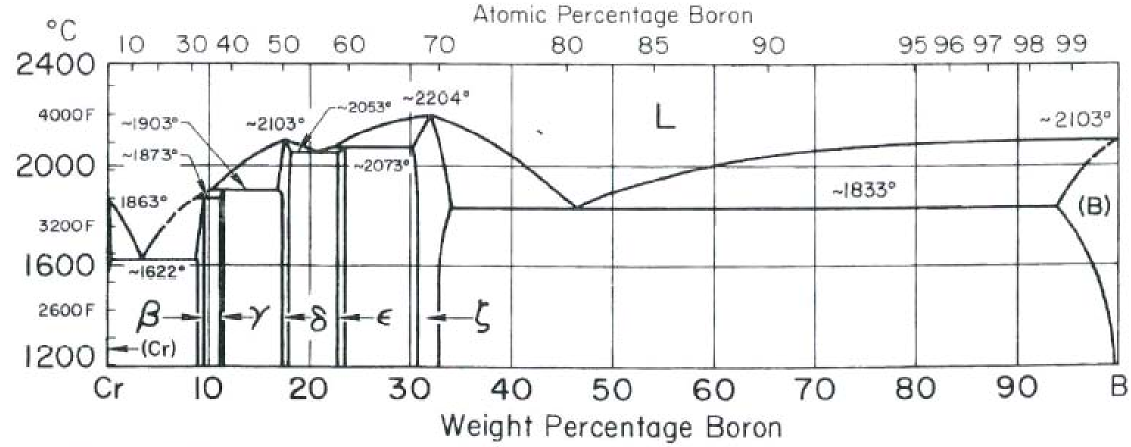

Figure 4.6 Binary phase diagram of the Cr-B system [94].

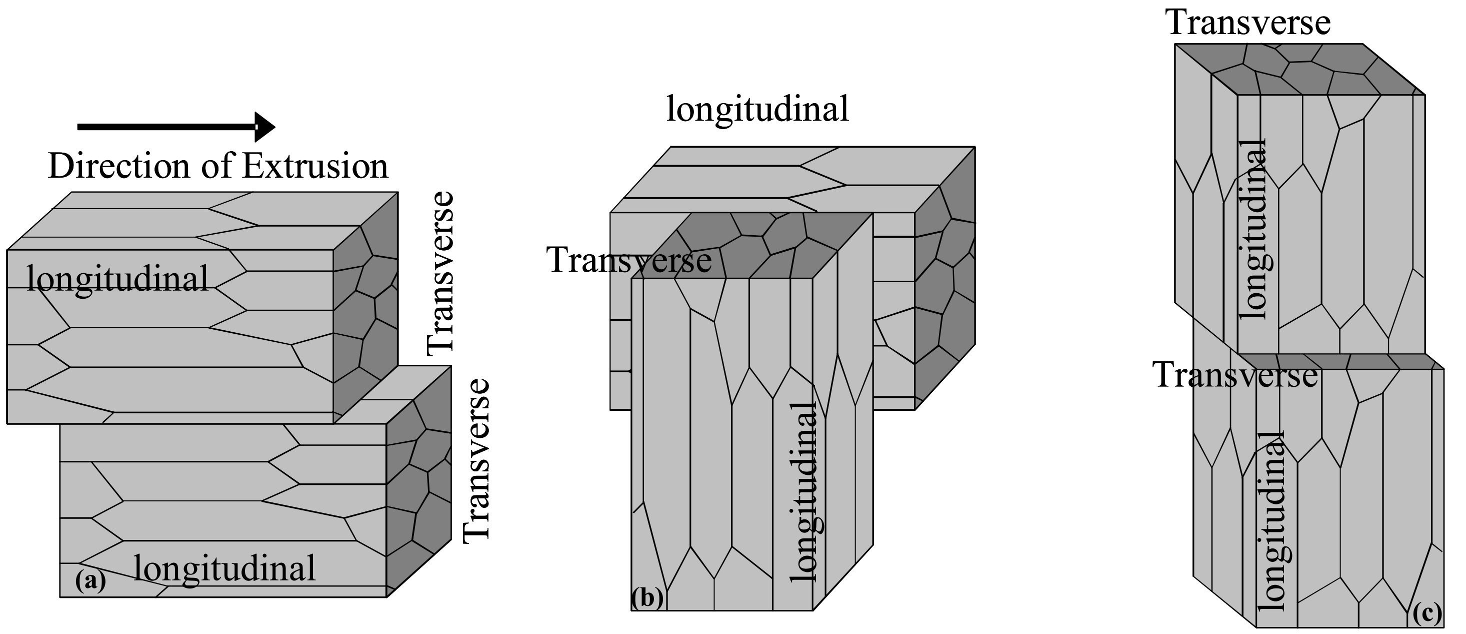

Longitudinal - Longitudinal **Longitudinal - Transverse** **Transverse - Transverse**

Figure 4.7 Substrate orientations with respect to direction of extrusion (a) longitudinal – longitudinal (L-L), (b) longitudinal - transverse (L-T) and (c) transverse – transverse (T-T).

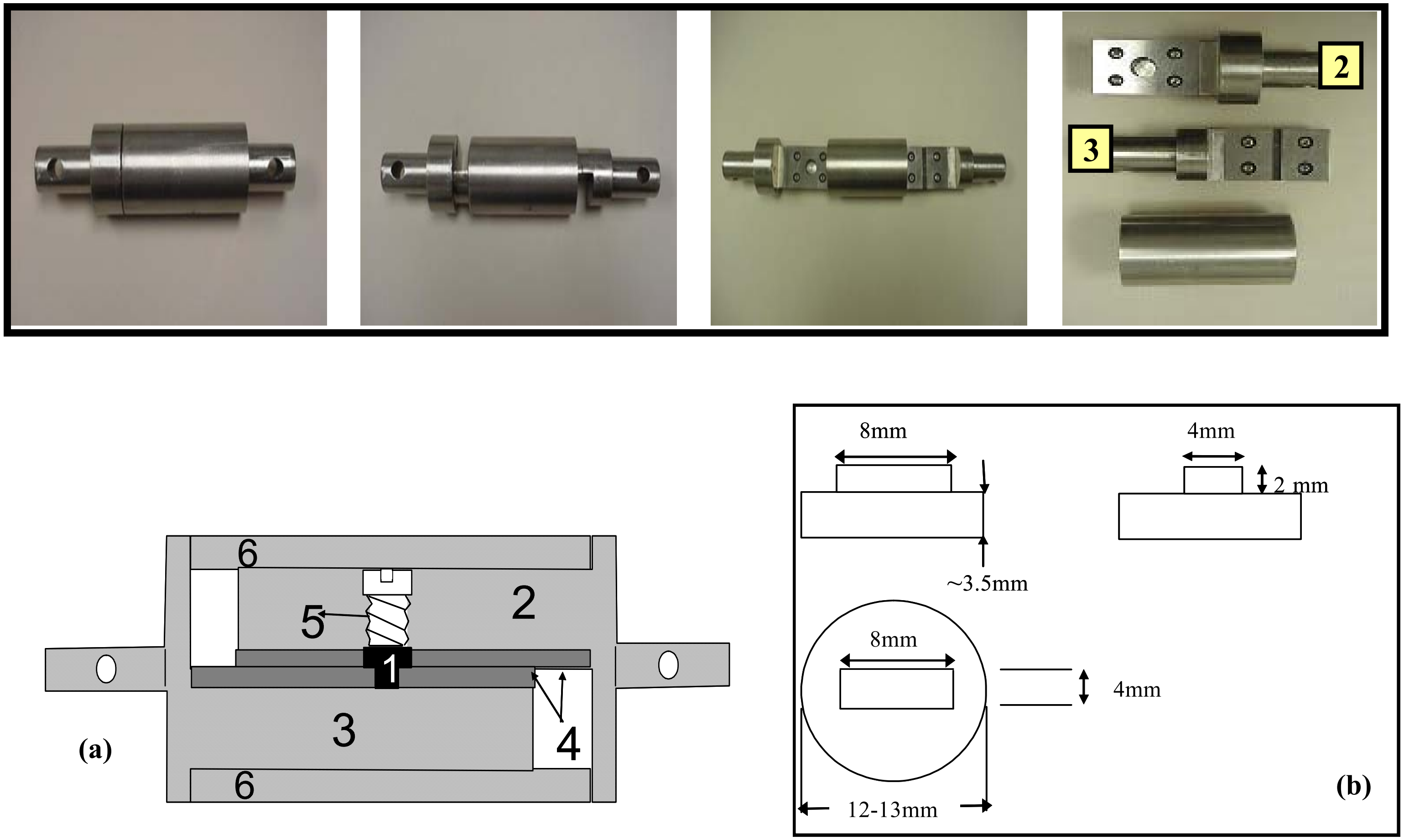

Figure 4.8 Shear testing rig (a) set-up: 1 - Sample, 2 - Large substrate holder (circular grove), 3 - Small substrate holder (rectangular groove), 4 – Tool Steel hardened inserts, 5 – Adjustable screw and 6 – Outer sheath and (b) specimen geometry, based on Yan and Wallach [95].

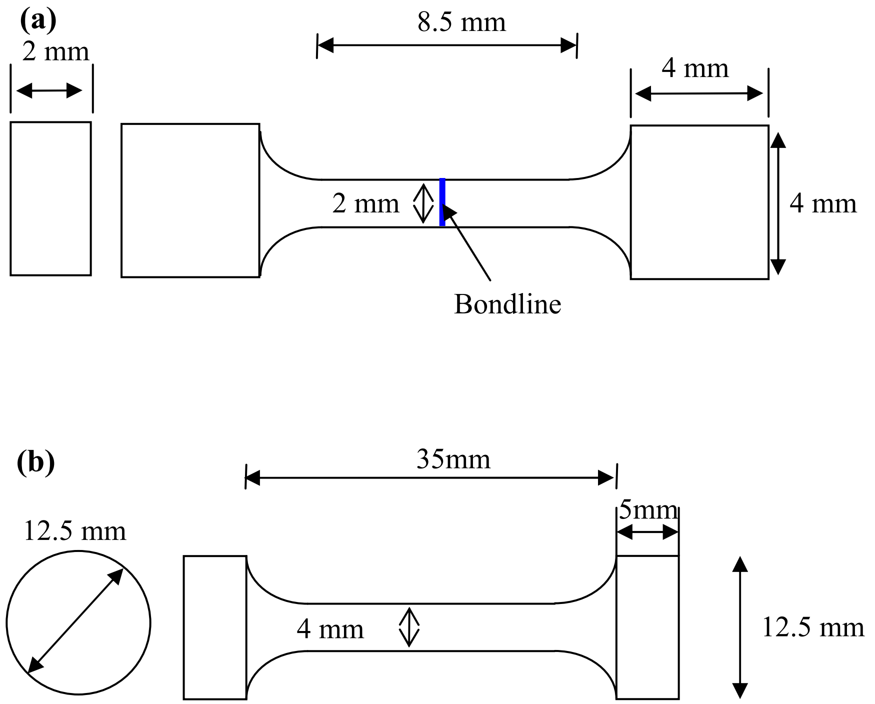

Figure 4.9 Geometry of (a) tensile test specimen and (b) creep test specimen

5. RESULTS AND DISCUSSION

5.1. Parent Metal Microstructure

MA956 was received in both the unrecrystallized and recrystallized conditions, and PM2000 was received in the unrecrystallized condition. ODS alloys, whether in the unrecrystallized or recrystallized condition, possess fine grains in the range of sub μm and coarse columnar grains in the range of millimeters, sometimes extending throughout the length of the sample, respectively [5].

Metallographic analysis was conducted on the as-received materials using the procedure shown in the table 4.3. The as-received fine grain (FG) condition materials possessed a microstructure with a few columnar grains of the order of μm, aligned in the working direction and fine equiaxed grains in the transverse orientation, as shown in figures 5.1-5.4. TEM analysis by Chou [96] and Capdevila et al. [41] of MA956 and PM2000, respectively, revealed subμm grains sizes in the unrecrystallized condition. Fine grains are formed as a result of the very high strains induced during mechanical alloying [5]. The microstructures of the as-received coarse grain (CG) condition samples that had been heat treated for 1 h at 1300 °C show coarse columnar grains of the order of 20 mm aligned in the longitudinal (working) direction, figures 5.5-5.6. The formation of coarse grains in the iron-based ODS alloys is due to primary recrystallization of the fine grains present in the as-consolidated alloy. In the nickel-based ODS alloys, the formation of fine grains occurs as a result of primary recrystallization during mechanical alloying [37]; Coarse grain formation occurs as a result of secondary recrystallization, driven by grain boundary energy, of the primary recrystallized fine grains. The elongated grain structure, as discussed in section 2.2.2.1, is influenced by the oxide particle alignment.

ODS alloys also possess a strong crystallographic orientation [37,42,47,75]. MA956 in the fine grain condition possesses an elongated grain structure with a preferred <110> fiber texture along the working direction [97]. The recrystallization temperature may also be influenced by the grain texture due to the effect on the grain boundary mobility. Favorably aligned grains recrystallize more readily than grains aligned in random orientations with respect to the recrystallization front. Recrystallized ODS alloys possessed either <110> or <111> orientations, or a combination of both. The initial strain induced in the alloy may affect the grain aspect ratio and the formation of preferred texture in the recrystallized ODS alloy.

5.2. Transient Liquid Phase Bonding

It is very important to achieve intimate contact between the faying surfaces of the substrates that are to be joined in order to obtain a sound metallurgical bond. In TLP bonding, the interlayer melts, filling any gaps and thus increasing the contact area across the bond interface.

5.2.1. Bonding Temperature

In the current project, the interlayer material was chosen so that it would form a eutectic with the substrate material. Boron forms a liquid by eutectic reaction with the iron-matrix of the substrate at temperatures above 1174 °C, as shown in figure 4.5 [94]. Bonding should be conducted well above the substrate – B eutectic temperature. Since the necessary phase diagrams were not found in the literature, a temperature of at least 50 ºC above the binary Fe – B eutectic temperature (1174 °C) was used as a reference point for the lower boundary on the bonding temperature, giving a lower limit on the bonding temperature of 1224 ºC. Previous authors [40,69,70,75] have found that bonding should be conducted on fine grain material and followed by recrystallization and hence the upper boundary on the bonding temperature is the recrystallization temperature for the bulk substrate (~ 1300 °C for MA956). Since the latter is not known with certainty and given that batch to batch (and even region to region) variations in properties for ODS alloys are common, the bonding was conducted only at 1250 °C and it was not possible to study a significant range of bonding temperatures.

5.2.2. Bonding Stress

One of the advantages of the TLP bonding technique is that it does not require an applied bonding stress beyond that needed for fixturing [74]. The joint assembly becomes critical with a decrease in the thickness of the interlayer, but better fitting can be obtained by surface finishing with higher tolerance. However, this may prove to be difficult in the case of complex shapes. Applying compressive stresses can improve the fit-up of the joints. The use of compressive stresses extrudes the excess liquid filler volume formed at the bondline, which reduces the amount of liquid filler metal available at the bondline that can be diffused into the substrate and the distance to be diffused by the melting point depressants. Compressive stresses can also improve the flow of the filler metal. Compressive stresses of up to 5 MPa are often used for bonding, and are known to result in a decrease in the porosity and precipitate formation at the bondline [40, 75]. However, compressive stresses of the order of 15 MPa or higher resulted in substrate deformation. In earlier studies by Ekrami et al. [98], a small stress of 100 kPa did not show any significant effect on the bond properties. Hence, in order to extrude the excess liquid formed at the bondline, avoid large scale substrate deformation and improve the joint strength, optimizing the bonding stress is necessary.

In order to obtain an optimum compressive stress at the bonding temperature of 1250 °C, experiments were performed with fine grain material under various compressive stresses: (i) less than 1 MPa, (ii)1-5 MPa and (iii) 20 MPa. Joining conducted with stresses below 1 MPa resulted in no bonding or very weak bonds as 8 out of 10 bonds, failed during handling or machining. In contrast, a high stress of 20 MPa resulted in plastic deformation of the substrates. However, bonding occurred when compressive stresses in the range of 1-5 MPa were used. It should be noted that in order to obtain stresses in the range of 1 – 5 MPa, the required respective load to be applied falls in the lower limits of the Gleeble 1500's loading capability. It was thus difficult to produce a single repeatable load close to this lower limit of the GLEEBLE 1500 and, hence, a bonding stress range of 1 – 5 MPa was used. The applied loads were measured using a compressive load cell.

5.2.3. Bonding Time and Post Bond Recrystallization Treatment

Bonding trials were conducted using MA956 fine grain material with bonding times ranging from 20 to 3600 s at 1250 °C using a 1 μm boron interlayer (figures 5.7 to 5.10). Figure 5.7 shows that there is some second phase precipitation, most likely borides, at the bondline in the 20 s bond. The boride formation at the bondline decreased with an increase in the bonding time up to 1 hour and no large precipitates were observed at the bondline. This may be related to the diffusion of higher amounts of boron away from the bondline, and into the substrate with increasing bonding time. However, some precipitates were still visible in the substrate near the bond region for all the bonding times examined.

Two possible sources of these boride precipitates are the eutectic reaction, which occurs if a sample is cooled prior to completion of isothermal solidification, and solid-state precipitation of borides on cooling, which occurs if the solid-solubility is exceeded. In standard models of the TLP bonding process [83], isothermal solidification occurs under local equilibrium conditions and boride formation at the bonding temperature is not possible. However, Gale and Wallach [99] have previously produced evidence that indicates that borides can form at the bonding-temperature under non-equilibrium conditions. In general, the morphology of the eutectic is sufficiently distinctive to allow this to be distinguished from other boride-containing microstructural features. However, with very thin interlayers, a lamellar eutectic is not always formed on cooling a sample that has almost, but not entirely, isothermally solidified and so it can be difficult to distinguish the different sources of borides.

After 5 minutes at 1250 ºC, no lamellar eutectic was apparent, although some precipitates with high chromium concentration were observed. Boron cannot be detected by the EDS system employed in this study, but chromium is a relatively strong boride former and chromium borides are stable at the recrystallization temperatures used here, so these precipitates are more likely to be chromium borides.

Secondary precipitates near the bond region were also observed by Khan [75]. Laser microprobe mass spectrometry (LAMMS) analysis of these precipitates showed peaks for iron, chromium and boron. It was reported that these borides of iron and chromium were of the form $(Fe,Cr)_2B$. In the present study, chromium borides are stable at temperatures higher than for iron borides. Khan observed that most of the precipitates were removed after a heat treatment at 1200 °C for 2 hours, but some fine stable particles richer in chromium than iron were present, indicating that the remaining particles were chromium borides. In other experiments conducted by Wei [77], who diffusion brazed MA956 using a 1-2 μm thick Fe-13B-5Si wt% sputter coating as an interlayer, precipitation of secondary phases at the bondline occurred. However, the electron diffraction patterns for these particles could not be indexed to $(Fe,Cr)_2B$, Cr_2Si, Fe_2Si or Fe_3Si phases which suggests that these precipitates might be metastable phases of B and Si. Markham [40] found high amounts (up to 95%) of chromium in the precipitates that formed during brazing of a nickel-based ODS alloy, MA754, using BNi1a filler metal. Electron diffraction images of these particles showed a Cr_2B structure and suggested that these borides might have formed from solid solution during cooling to room temperature.

Other possible sources of bond-line particles are yttria dispersoids and the substrate matrix's own oxide (the latter both from the faying surface and formed in the bulk during processing of the ODS alloy [48]). These will be carried into the bond-line by dissolution of the substrates and will tend to agglomerate as a result of convection in the liquid, leading to clumps of yttria and/or other oxides. In addition, uncontrolled recrystallization at the bond-line can produce new fine grains with a morphology similar to that of a precipitate.

Separating out the different precipitates or precipitate-like features was challenging due to the limited spatial resolution of the SEM-based EDS available for the study. Particles for which chromium or titanium, but no oxygen, were detected were assumed to be borides, and regions:

- with no detectable compositional difference with the bulk were assumed to be new substrate grains;
- that were rich in yttrium were assumed to contain agglomerated yttria;
- that were rich in aluminum were assumed to be substrate oxides, since aluminum is not a boride former; and
- that were rich in both oxygen and chromium/titanium may have contained either oxides or a mixture of borides and oxides, since chromium and titanium are both oxide and boride formers.

On this basis, all of these phases were present at the bond-line in the as-bonded condition. The oxides remained stable for all conditions examined, as would be expected. New fine grains coarsened during PBHT. Individual alloy borides were not encountered after PBHT, but some may have been present clumped with oxides. The most marked distinction between "good" and "bad" bonds was the extent of uncontrolled fine grain formation at the bond-line, which occurred either during bonding and/or PBHT.

The melting of the interlayer and dissolution of the substrate occur very rapidly [83, 84, 85, 90]. Once the local equilibrium between the liquid and the substrate is reached, diffusion of boron into the substrate occurs. This results in a lowering of the local boron content and, hence, raising the local melting temperature. Solidification of the liquid commences and the liquid zone shrinks at the bonding temperature leading to isothermal solidification of the joint. Isothermal solidification requires less time than homogenization of the bond as the process occurs in the liquid phase. The time required for isothermal solidification was calculated based on Tuah-poku et al.'s work [83], as tabulated in table 5.1.

$$W = W_0 . [1 + \{(C^B - C^{L\alpha})/ C^{L\alpha}\} . (\rho^B/ \rho^S)] \qquad \text{Equation 5-1}$$

$$t = (\pi W_0{}^2/16 D_s{}^\alpha). (C^B/C^{\alpha L}) \qquad \text{Equation 5-2}$$

where W is the maximum width of the liquid interlayer, W_0 is the initial interlayer liquid thickness, C^B is the melting point depressant (boron) concentration in the interlayer (100% in this case), $C^{\alpha L}$ is the solidus composition (≈ 0.2 wt% [100]), $C^{L\alpha}$ is the liquidus composition (≈ 3.1 wt% [94]), D_s^α is the diffusion coefficient of solute (boron) in the substrate ($1.5 \times 10^{-7} \exp(-88/RT)\ m^2s^{-1}$, R – kJ K^{-1} mol^{-1} [101]), and ρ^S and ρ^B are the densities of the substrate (8.0×10^6 kg m^{-3}) and boron interlayer (2.47×10^6 kg m^{-3}), respectively.

The time calculated for isothermal solidification using a 1 μm thick boron interlayer is approximately 340 s at 1250 °C. However, the use of compressive stresses extrudes the excess liquid formed at the bondline, thus reducing the amount of liquid that must be diffused into the substrate. In addition, liquid penetration at the grain boundaries in a fine grain material increases the solid-liquid interfacial area and further reduces the time required for isothermal solidification [102]. Hence, it is possible for isothermal solidification to occur in less than 340 s. This agrees with the bond microstructures observed earlier. The formation of borides at the bondline in the 20 s at 1250 °C bond may be due to allowing insufficient time for diffusion of boron into the substrate or for isothermal solidification of the joint. Hence, such borides were not observed in the bonds with longer bonding times (≥ 5 min at 1250 °C) as here there was sufficient time for completion of isothermal solidification. The decrease in the amount of boron available at the bondline due to the applied pressure and diffusion of boron into the substrate also reduced the likelihood of precipitation of secondary phases i.e., borides.

5.2.4. Recrystallization in the Bulk ODS Alloy

In mechanically alloyed ODS alloys, recrystallization occurs at very high homologous temperatures, of the order of 0.9 of the absolute melting temperatures, resulting in coarse columnar grains along the direction of extrusion [37]. Longitudinal and transverse cross sections of as-received MA956 and PM2000 in the fine grain condition are shown in figures 5.1 - 5.4. In general, heat treatments at 1300 °C and 1385 °C for 1 h are sufficient to induce recrystallization in MA956 [103] and PM2000 [32], respectively. However, a delay in recrystallization was observed in the as-received fine grain condition MA956 material as shown in figures 5.11 and 5.12, where grains extended only up to a few hundred μm in the working direction and up to 40-60 μm in the transverse orientation. In contrast, grains in the recrystallized as-received coarse grain MA956 extended throughout the length of the specimen (up to 20 mm) along the working direction and up to a few hundred μm in the transverse orientation, as shown in figures 5.5 and 5.6. A similar coarse microstructure was not obtained even after extended recrystallization heat treatment of initially fine grain MA956 of up to 8 h at 1300 °C, as shown in the bonds, figures 5.7 - 5.10. Heat treated unbonded bulk material exhibited larger grains than those in the bonded bulk material. It should be noted that some variation in the recrystallization behavior within the bulk material was also observed.

Dislocations are developed and stored as a result of plastic deformation of the material during hot or cold working [104]. Some dynamic recrystallization may occur in conventional alloys. In ODS alloys, a fine grain structure is retained up to the order of 0.9 of the absolute melting temperature. These dislocations do not occur in thermodynamic equilibrium. These dislocation arrangements are mechanically stable in the deformed sample. With the provision of sufficient thermal energy the dislocations destabilize, leading to recovery of the material as a result of annihilation or rearrangement of the dislocations. Along with recovery, recrystallization of the material occurs, which proceeds by generation and movement of grain boundaries. These recovery and recrystallization processes result in a decrease in the stored strain energy. Fine grains undergo grain growth in order to reduce the total grain boundary energy and this occurs either by shrinking some grains while others grow, or by growth of a few grains at the expense of non-growing grains. In mechanical alloying [5, 25, 26, 27], the alloying powders undergo strains of the order of 9, resulting in the formation of very fine grains with large amounts of stored energy. These powders are compacted and heat treated to achieve the final microstructure. Nucleation is initiated by the bowing of a grain boundary [105]. Bhadeshia [37] suggested that when the grains are very small, the grain boundary junctions themselves act as pinning agents for the grain boundary bulging, thus retarding the nucleation, see figure 5.16. In such cases, a higher activation energy is required for nucleation to occur. It has been observed that the recrystallization temperature of MA ODS alloys varies with the heating rate, preannealing process and mechanical deformation induced in the sample [106, 107] and recrystallization may be delayed by using a higher heating rate. Increase in deformation reduced the temperature at which recrystallization occurs and non-uniform cold deformation resulted in an increase of recrystallization nuclei, leading to the formation of small equiaxed grains [108, 109]. Therefore, any variation in the mechanical alloying process and the applied heat treatments is likely to have an effect on the final microstructure of the ODS alloys.

Unfortunately, due to unknown thermomechanical history of the current batch of alloys it was difficult to correlate their microstructure with their mechanical alloying process conditions. The difference in the recrystallization behavior of the ODS alloys may thus be attributable to their prior thermo-mechanical treatment.

In other studies, significant variation in the response to recrystallization was observed in two virtually identical batches of MA754 [40], although the as-joined microstructures were similar. The variation in the recrystallization behavior was attributed to a difference in the concentration of stringers, which retard the grain growth, in the two batches.

5.2.5. Bond Orientation

In general, with equiaxed materials which possess isotropic properties, the orientation of the work pieces (substrates) to be joined might not be significant [98, 110]. Mechanically alloyed oxide dispersion strengthened alloys, such as MA956 and PM2000 have a preferred grain orientation. In the past, joining of iron-based and nickel-based ODS alloys has been conducted using various techniques [16 - 18, 40, 43, 67, 69 - 71, 75, 98, 110, 111], although, the influence of the orientation of the substrate faying surface on the joint development was not investigated. Hence, in this project, bonds with different orientations with respect to the working direction were studied, namely transverse to transverse (T-T), longitudinal to transverse (L-T), and longitudinal to longitudinal (L-L) orientations, as schematically shown in figure 4.7. Figure 4.1 shows the substrate preparation.

Joining the substrates with faying surfaces in the L-L orientation, see figures 5.10 and 5.13, resulted in a relatively indistinct bond line as compared to the T-T and L-T orientations, shown in figures 5.14 and 5.8, respectively. Secondary recrystallization occurred at the bondline to a varying extent for the different bond orientations. The thickness of the region with unwanted fine grain formation in the T-T bonds varied from 10 to 40 μm. In MA957, a ferritic ODS alloy, bonds prepared using a 25 μm iron-based foil [75] in the T-T orientation resulted in the formation of a 'step-like' grain structure which extended up to 2 mm. Such step-like recrystallization was not observed in MA956 and PM2000 bonds, although, a planar grain boundary was observed at the bondline which was attributed to the presence of aluminum and the higher concentration of chromium in these latter alloys. Second phase particles (rich in boron) precipitated at the bondline. The absence of boron induced recrystallization in the bonds was attributed to the combined effect of the formation of borides at the bondline and the presence of an oxide layer on the faying surface, which suffered erosion due to melt-back and thus restricted the diffusion of boron into the substrates. However, other bond orientations were not investigated.

In the longitudinal- transverse (L-T) orientation, fine equiaxed grains were formed at the interface in the longitudinal substrate of the L-T bond, which occurred occasionally up to 100 μm away from the bond (see figure 5.8). In the transverse substrate, it was difficult to distinguish the fine grains that might have formed as a result of boron induced recrystallization from other recrystallized grains due to their similar grain sizes. In MA754, a nickel-based ODS alloy, bonds [40] were prepared with two bond orientations;

(a) the elongated grains of the substrate aligned perpendicular to the bondline (transverse-transverse orientation) and (b) one of the substrates aligned perpendicular to the elongated grain structure (longitudinal-transverse orientation). A thick region of recrystallized grains was observed in both these conditions. In the L-T orientation bond, the recrystallized grains in the substrate were more equiaxed than in the T-T orientation bond and fine equiaxed grain formation occurred in the substrate, with the elongated grains aligned parallel to the working direction, similar to the results observed in the current study. Markham attributed the formation of fine equiaxed grains in the longitudinal substrate as resulting from two competing forces acting normal to each other: (a) the inherent nature of the alloy tending to produce elongated grains in the working direction, and (b) the formation of recrystallized grains in the substrate due to the diffusion of boron from the bondline into the substrate.

The L-L joints investigated in the current study showed minimal disruption, figure 5.10, at the bondline as compared to the T-T and L-T bond orientations. The thickness of the secondary recrystallization varied from minimal (zero) up to 20 μm, figure 5.13. EDS analysis across the bondline in the L-L orientation showed uniform composition, figure 5.15. Although the amount of liquid formed was several times larger than the as-deposited interlayer thickness, the use of compressive stresses extruded the excess liquid formed at the bondline and reduced the amount of boron that remained to diffuse into the substrates. Further, the use of compressive stresses reduced porosity at the bondline [40, 75].

The coarse columnar grain structure in the ferritic ODS alloys occurs as a result of the nano size yttria particles [41, 42], aligned in the extrusion direction, that retard the grain growth in the transverse direction. These dispersoids increase the activation energy required for grain boundary migration to take place [112]. Any disturbance to the yttria alignment can result in the formation of fine equiaxed grains. The number of yttria stringers cut by the bond line, which is governed by the substrate orientation, is higher when the faying surface is machined in the transverse orientation as compared with the longitudinal orientation. During transient liquid phase bonding, the faying surface of the substrates reacts with the interlayer forming liquid and further dissolution then occurs. Hence, some uncontrolled recrystallization in the substrates can be expected.

Kokawa et al. [102] observed that the grain boundaries act as preferential diffusion paths for melting point depressants and increase the solid-liquid interfacial area. Hence, grain boundaries contribute to increasing the rate of diffusion of the liquid and, therefore, reducing the total time required for isothermal solidification. Deviations from a planar solid-liquid interface to a saw-tooth like structure have been observed due to dominated wetting at grain boundaries. Grain boundary misorientation has also been used as a measure to investigate liquid penetration. High misorientation grain boundaries possess a large grain boundary energy and more liquid penetration was observed at these grain boundaries than at small angle grain boundaries. MA956 possesses an elongated grain structure with preferred <110> fiber texture along the working direction in the fine grain condition [97]. The faying surface of a substrate may be treated as a long grain boundary. The substrates when prepared in the L-L orientation, i.e., with the elongated grains arranged parallel to the faying surface, have fewer grain boundary junctions on the faying surface than when prepared in the T-T and L-T orientations. The extent of the liquid penetration at the grain boundaries, which might cause the solid-liquid interface to deviate from a planar to saw-tooth like structure, may be relatively lower in the L-L orientation than in the T-T and L-T orientations and, hence, resulting in smaller thickness of the disruption of the parent metal microstructure.

5.2.6. Substrate Condition

Earlier researchers [40, 75, 98] have observed that bonding in the fine grain condition, followed by recrystallization, resulted in grain growth across the bondline. The influence of the grain condition on bond development was, therefore, investigated by joining MA956 using both fine grain (FG, unrecrystallized) and coarse grain (CG, recrystallized) conditions. The bond types included FG-FG, FG-CG and CG-CG conditions in the L-L bond orientation. As observed earlier, figures 5.10 and 5.13, a minimal (zero) thickness of the secondary recrystallization (no secondary recrystallized grains) was obtained in the FG-FG bonds. In the FG-CG bonds, however, the thickness of the layer of fine grains formed at the bondline was larger in the FG substrate (from 20 up to 40 μm) as compared with the CG substrate (10 μm), figure 5.17. Secondary recrystallized grains were observed even after the post bond recrystallization heat treatment, figure 5.18. A planar interface at the bondline was observed in the CG-CG bonds and no grain growth across the bondline took place, figure 5.19. A smaller thickness of the secondary recrystallization area, 10 – 15 μm, was observed in the CG-CG bonds than in the FG-CG bonds.

The influence of grain boundaries on the TLP bonding phenomena was earlier reviewed by Zhou et al. [85]. Grain boundaries are known to alter the kinetics of the process, and Zhou et al. listed several factors that influence the TLP bonding process kinetics:

a) Enhanced diffusion due to grain boundaries: A higher rate of solute transfer occurs at the grain boundaries than in the bulk at temperatures below 0.5 – 0.75 T_m, where T_m is the absolute melting temperature. At these temperatures grain boundary diffusion coefficient (D_{gb}) may be 10^5 times or higher than lattice diffusion coefficient (D_l). At temperatures higher than 0.75 T_m, D_{gb}/D_l is of the order of 10^3 or less.
b) Solid/liquid interface curvature: An increase in the solid/liquid interfacial curvature increases interfacial diffusion.
c) Solid/Liquid interfacial area: Greater diffusion of the solute into the substrate occurs as a result of the formation of a larger liquid/solid interfacial area at the grain boundaries.
d) Grain boundary migration: This increases the solid/liquid interfacial area and, hence, increases the diffusion of the solute.
e) Grain boundary segregation: Grain boundaries act as getters of solute atoms, leading to solute segregation at the grain boundaries.

The ratio of grain boundary diffusion coefficient to lattice diffusion and apparent diffusivity was calculated as follows.

$D_l = D_{0\,l} \exp(-Q_l/RT)$ Equation (5-3)

$D_{gb} = D_{0\,gb} \exp(-Q_{gb}/RT)$ Equation (5-4)

$D_{app} = D_l + (\delta/l)\, D_{gb}$ Equation (5-5)

Where, D_l and D_{gb} are the diffusion coefficients, $D_{0\,l}$ (2×10^{-4} m^{2}s^{-1}) and $D_{0\,gb}$ (1.1×10^{-2} m^{2}s^{-1}) are the diffusion constants, Q_l (251 kJ mol^{-1}) and Q_{gb} (174 kJ mol^{-1}) are the activation energies of lattice and grain boundary, respectively, R is the universal gas constant (8.314 J mol^{-1}K^{-1}), T is absolute temperature, D_{app} is apparent diffusivity, δ is grain boundary region effective thickness and l is the average grain size. The respective values in the parenthesis are for ferritic iron [78].

The calculated value of D_{gb}/D_l at the bonding temperature is approximately 2.41×10^4. Unlike conventional alloys, MA ODS alloys do not undergo grain growth and retain their fine grain size at temperature up to 0.9 times their absolute melting temperature (T_m) [37]. Hence, although the bonding temperature, 1250 °C, in the current investigation is greater than 0.75 T_m, the grain boundary diffusivity can be significant. Considering the values for fine grain size and coarse grain size PM2000 of 1 μm [41] and 10 mm, respectively, and assuming a value of δ = 5 nm, the grain boundary diffusion contribution to the apparent diffusivity is much higher than two orders of magnitude.

The grain boundary influence on the solute diffusion increases with decrease in the grain size. The amount of solute diffused into a polycrystalline substrate increased from around 1.25 times to 3 times compared to that in a single crystal substrate as the grain size decreased from 40 μm to 5 μm [85].

Ekrami and co-workers [98, 110] observed grain growth across the bondline in bonds made using MA758, a nickel-base MA ODS alloy, after recrystallization heat treatment. However, the joint grain size at the bondline when joining in the fine grain (grain size less than 2 μm) condition was larger than those when joining in the coarse grain condition. Ekrami attributed this to the large amounts of stored energy present in the fine grain material compared to the coarse grain material. This stored energy might have promoted grain growth at the bond line during recrystallization in the FG-FG bonds. Pénisson and Vystavel [113] used a 3 μm thick polycrystalline nickel coating as a filler metal to join polycrystalline molybdenum to bicrystal molybdenum. After heat treating this sandwich structure, the authors observed an 8 μm thick Mo-Ni intermetallic phase adjacent to the bicrystal and a 50 μm thick recrystallized zone in the polycrystalline molybdenum. A higher concentration of nickel was observed in the recrystallized zone as compared with the non-transformed polycrystalline substrate. Wetting was observed at the bicrystal grain boundary only when the $\gamma_{GB} > 2\,\gamma_{SL}$ condition was satisfied, where γ_{GB} and γ_{SL} are the grain boundary and solid-liquid interface energies, respectively. A high grain boundary energy promotes the wetting phenomenon. In the present investigation, the unrecrystallized FG substrate was polycrystalline and the faying surface of the recrystallized CG substrate, although polycrystalline, may be treated as a single or a bicrystal interface because recrystallized MA956 possesses coarse columnar grains in the longitudinal direction. As boron cannot be detected using EDS, it can be inferred from Pénisson and Vystavel's work that the secondary recrystallized zone at the joint interface of the FG-CG joint is likely due to the diffusion of boron into the substrate. The larger thickness of fine grains in the fine grain substrate can be related to: (i) a greater amount of base metal dissolution in the fine grain substrate due to higher grain boundary liquid penetration, and (ii) the larger amounts of stored energy present in the unrecrystallized fine grain MA ODS alloys, as compared with the recrystallized coarse grain substrate. A significant amount of interlayer liquid penetration into the base metal at the grain boundaries has been observed in fine grain nickel joints compared to joining coarse grain nickel [102]. The equiaxed grains observed at the bondline in the FG substrate were larger than those observed in the coarse grain substrate. Some variation in the thickness of the secondary recrystallization region can be observed along the length of the MA956 bonds, figure 5.17. The variation in the recrystallized grain sizes and their thicknesses might be attributable to inhomogeneities in the parent metal. Markham [40] observed uneven recrystallization at the ODS braze interface, although he did not observe any significant variation in the LAMMS analysis of the interlayer coatings. He suggested that the differences in the recrystallization behavior at the joints must be due to variations in either the stored energy or the grain size of the parent metal. This thickness of the recrystallized zone, 10 – 15 μm (figure 5.19), in the CG-CG bonds, corresponds approximately to a substrate dissolution thickness of around 12 μm. The smaller recrystallized zone thickness might be attributed to a decrease in the interlayer liquid penetration into the base metal due to the presence of few (or no) grain boundaries at the bondline.

On the basis of the above discussion, the large solid/liquid interfacial area provided by the grain boundaries in the fine grain condition material encourages faster diffusion of boron into the substrate and leads to rapid isothermal solidification. The amount of boron available at the bondline might be sufficiently low that boron induced secondary recrystallization does not occur, unlike in the bonds prepared using coarse grain substrates. The coarse grain substrates in MA956, due to their elongated grains, that are aligned parallel to the faying surface in the L-L bond orientation act as single crystal material in which the solute transfer occurs, mainly, by volume diffusion. It is known that volume diffusion is slower than grain boundary diffusion except at high T/T_m, where T_m is absolute melting temperature [85, 102]. Hence, the diffusion of boron into the coarse grain substrate is slow as compared to that in the fine grain substrate. This results in the availability of large amounts of boron at the bondline in the coarse grain bonds, which may be enough to cause secondary recrystallization. It has been observed in the past [40, 75], that boron induced recrystallization occurs at the bondline when an “appreciable amount” of boron (a melting point depressant) is available. As the boron interlayer reacts with the substrate to form a eutectic liquid some uncontrolled recrystallization in the substrates can be expected.

The above results suggest that TLP bonding of unrecrystallized fine grain material to itself (FG-FG) can result in better bonds than bond involving recrystallized material (FG-CG or CG-CG), as has been observed previously by Khan [75].

5.2.7. Interlayer Composition and Thickness

The extent of secondary recrystallized grains and boride formation at the bondline in MA956 bonds decreased as the thickness of the boron interlayer decreased. The formation of secondary recrystallized fine grains and borides at the bondline was reduced for a 500 nm boron interlayer, figure 5.20, due to the decrease in the dissolution of the substrate and the amount of interlayer liquid formed, when compared to the bonds obtained for a 1 μm interlayer. The thickness of the liquid formed for each thickness is given in table 5.1. A limited comparison was made with a conventional 25 μm Fe–16B-5Si wt% foil interlayer. Bonding was conducted at 1190 °C, above the melting point of the foil (i.e., the Fe-B eutectic point [94]). A well wetted bond was observed when iron-based foil was used and this bond contained surprisingly few borides after cooling to room temperature. However, the bondline remained distinct and recrystallized grain growth across the bondline did not occur, figure 5.21. Excessive dissolution of the substrates and formation of borides has been observed with the use of a foil interlayer by other researchers [40, 75]. Bonding with such foil interlayers produced a thick layer (up to 2 mm) of uncontrolled recrystallization. Thus, satisfactory bonds were not achieved with the foil interlayer, unlike those observed with the thin (≤ 1 μm) EBPVD boron interlayers which produced microstructural continuity of the substrate grains across the bond-line after PBHT.

5.2.8. TLP Bonding of PM2000

Microstructure:

Bonding was conducted at 1250 °C using 250 nm and 1 μm thick boron interlayers in the L-L orientation. The bonds were heat treated at a recrystallization temperature of 1385 °C for up to 2 hours to induce grain growth in the bulk and across the bondline. The use of a 250 nm thick interlayer resulted in grain growth across the bondline and no boron-induced secondary recrystallization at the bondline was observed, figure 5.22. Recrystallization in the bulk also took place, leading to coarse grains of the order of mm. However, the use of 1 μm thick interlayers resulted in a zone of recrystallized grains at the bondline, which extended from 100 to around 200 μm, figure 5.23. The secondary recrystallization observed in the 1 μm bonds may be explained in terms of the amount of boron available at the bondline. Markham [40] observed that recrystallization occurs only when a boron rapid diffusion of an "appreciable amount" of boron takes place, although the exact quantity of boron required to induce secondary recrystallization was not specified. In the current study, it proved difficult to calculate the amount of boron available at the bondline due to:

a) the application of compressive stresses, which extruded the excess amounts of liquid formed at the bondline.

b) significant variations in the base metal grain size and composition from batch to batch and region to region within the same batch, which arose due to differences in the prior thermomechanical processing of the alloy during production. The details of the processing were not available, due to proprietary commercial considerations.

A large amount of porosity was also observed in post bond recrystallization heat treated PM2000 bonds, both in the bulk and in the bond region, as shown in figures 5.23 and 5.24. A detailed study of the as-received PM2000 material was conducted and can be found in the appendix. The study shows that the porosity is an inherent defect of the material and is not due to the TLP bonding process. Significant compositional variations in the received PM2000 material, as compared to the nominal PM2000, were observed. In earlier studies [32, 33, 35], some porosity was observed, which was attributed to the release of the trapped gases, typically hydrogen or argon, used in the powder processing. Chen and Jones [32] used a dual-stage heat treatment in an attempt to decrease the porosity created in the material. The heat treatment did result in a decrease in the porosity, but, failed to eliminate it completely.

Bonding conducted in the T-T orientation also showed results similar to those for the L-L orientation bonds. Bonding occurred using fine grain material, figure 5.25. However, after post bond recrystallization heat treatment, although recrystallization occurred in the substrate, pore formation also occurred, figure 5.26. Porosity developed at the bondline and created gaps between the two substrates. Earlier studies [32, 33], have shown that the grain boundaries act as preferred paths for the release of entrapped gases. The bond interface might also act as a favorable site for gas release leading to pore formation at the bondline. It has been reported that the formation of pores at the bondline decreases the contact area between the two substrates and thus a deterioration in the bond [75].

5.3. Solid-State Diffusion Bonding

5.3.1. MA956

5.3.1.1.Effect of substrate condition

Bonding was conducted using MA956, both in the fine grain (grain size < 1 μm) and coarse grain (grain size of the order of mm) conditions. Bonds were achieved when joining a MA956 substrate in the fine grain condition to a similar material, Fig. 5.27(a), in the L-L bond orientation under unusually low stresses, 1 – 5 MPa at 1250 °C for bonding times up to only 6-8 minutes, followed by the above mentioned PBHT to induce recrystallization across the bondline. Some grain growth across the bond-line was achieved in the fine grain condition to fine grain condition bonds, Fig. 5.27(b). However, occasional voids were observed at the bond-line. Bonding also occurred when joining a fine grain condition substrate to a coarse grain condition substrate, in the L-L orientation, Fig. 5.28. Here, the joint shows no unbonded regions, but when joining two coarse grain condition MA956 substrates, bonds with large unbonded regions were observed, figure 5.29.

Acceptable bonds with no large unbonded regions were obtained only when a fine grain condition material was involved. A submicron grain size can lead to a higher grain boundary diffusion and, hence, result in a significant increase in the bonding rate [78, 114, 115]. During diffusion bonding, the grain boundaries intersect with the voids in the bond. In a polycrystalline material, it is more likely that the void will come in contact with more than one grain boundary. These grain boundaries act as preferred paths through which the atoms diffuse to the voids resulting in void closure. Hill and Wallach [78] considered the surface to be elliptical in cross-section, but Orhan et al. [115] suggested that the surfaces need not be straight sided or elliptical and considered the case where the surface took the shape of a sine wave. In both studies, a significant increase in the grain boundary diffusion was observed when the grain size was less than 10 μm. MA956 in the fine grain condition has a grain size less than 1 μm [96]. Hence, grain boundary diffusion may have contributed significantly when fine grain MA956 was used for the bonds. Unrecrystallized ODS alloys possess large amounts of stored energy [37], which might also have contributed to the bonding of MA956 when joining unrecrystallized material to itself or unrecrystallized material to recrystallized material, but not when joining recrystallized material to itself. Similar results were obtained in bonding experiments, when fine grain material was involved (fine grain - fine grain or fine grain - coarse grain bonds), using MA6000 [69], a Ni-base ODS alloy, and MA956 (in transverse orientation of the faying surfaces) [70]. In the former, joining of coarse grain MA6000 resulted in poor quality bonds. Bucklow [70] used bonding stresses of up to 200 to 300 MPa to bond MA956 fine grain to coarse grain condition material. A 20 μm thick layer of random fine grains at the surface of the fine grain material at the joint interface with no epitaxial growth across the bondline was observed. The formation of fine grains at the bondline was attributed to the mechanical damage induced in the material during specimen preparation. However, the use of electropolishing techniques to prepare the bonding surfaces improved the bondline microstructure and some epitaxial growth was observed. Bucklow [70] also reported some unwanted fine grains in the core of the coarse grain material and similar defects were observed in the current study, figure 5.30. These defects probably arose due to either powder lumps of alloying material spalling from the balls in the mill, thus varying the local composition and grain size, or improper heat treatment [31]. Zhang et al. [71] observed a 5-8 μm tooth-like structure at the joint interface of the recrystallized coarse grain MA956 bonds for stresses higher than 40 MPa. The use of higher stresses, up to 72 MPa, was not successful in removing voids at the bondline. A transverse boundary remained at the bondline, which was reported to be due to the presence of an oxide layer on the faying surfaces prior to bonding. Bonding at low stresses was not successful. MA956 bonds made using 16 MPa had 2 μm thick voids, resulting in poor mechanical properties. The current results agree with the literature. Recrystallized coarse grain MA956 possesses very high creep strength and, hence, requires high stresses and temperatures for bonding to occur, whereas in the present work unrecrystallized fine grain material was bonded using 1-5 MPa compressive stresses. The differences in these bonding phenomena might be attributed to significant contributions from grain boundary diffusion and volume diffusion in the fine grain condition material as compared to the contribution from volume diffusion alone when using a coarse grain condition material [75, 78].

5.3.2. PM2000

Yttria stringers are aligned in the direction of extrusion, resulting in elongated grains [37, 50]. The number of yttria stringers cut by the bondline is governed by the orientation of the substrate. To study the effect of substrate orientation on bond microstructural development, diffusion bonding of PM2000 was performed in the fine grain condition both in the transverse to transverse (T-T) orientation and longitudinal to longitudinal (L-L) orientation. Bonding occurred in both these orientations, at low pressures 1 - 5 MPa, and for bonding times of up to 6-8 minutes, figures 5.31 and 5.32. However, only occasional unbonded regions were observed at the bond interface in the transverse orientation.

Due to the post bond heat treatment at 1385 °C for 2 hours, recrystallization occurred in the substrate leading to coarse columnar grains, although grain growth across the bondline was not observed, see figure 5.33. Significant variations in the response to heat treatment within the same batch were observed in PM2000. A common major defect in the MA ODS alloys is porosity and a large amount of porosity was observed in the bonds after recrystallization heat treatment, figure 5.34, unlike the bond shown in figure 5.33 which was made from material from the same batch. Variations in porosity in the unbonded material, subjected to a similar thermal cycle, were also observed. Details are reported in the appendix.

Regions of secondary recrystallized fine grains that extended up to 10 -12 µm were observed at the bondline in some bonds, figure 5.35. These might be due to the strains induced into the faying surface during surface preparation (surface grinding) [70]. Substrate preparation techniques, such as electropolishing, that are used to produce smooth surface finishes, and post bond moving zone recrystallization heat treatments might lead to the minimization of unbonded regions and also to obtain recrystallization across the bondline [70]. However, these were not investigated in the present work.

The current diffusion bonding technique using fine grain material under unusually low bonding stresses resulted in the successful formation of metallurgical bonds. However, the release of the shielding gas, used in the milling, during PBHT resulted in pore formation in the bonds which can seriously degrade the bond strength. A detailed survey was conducted on the PM2000 as received material, which revealed significant variations in both the composition and porosity along the length of the bar. More details are provided in the appendix.

5.3.3. Room Temperature Mechanical Testing

5.3.3.1.Shear Testing

To evaluate the mechanical properties of the bonds, room temperature shear tests were performed. Tests were conducted on PM2000 diffusion bonds, fabricated using unrecrystallized fine grain substrates bonded to material in a similar condition followed by recrystallization heat treatment, in both transverse and longitudinal orientations. For comparison, shear tests were also conducted on bulk material in both the as-received unrecrystallized fine grain condition and after recrystallization heat treatment. The peak shear stress values of the tests in the transverse and longitudinal orientations are shown in figure 5.36. The peak shear stress of the recrystallized bulk material was lower than the as-received unrecrystallized bulk material, which is as expected due to a larger grain size and hence, a decrease in the grain boundary strengthening in the recrystallized material. Some variation in the peak shear stress with orientation of the substrate was also observed. The transverse orientation showed higher peak shear stress as compared to the longitudinal orientation in the bulk material and the bonds. However, the variation in the bond strength with orientation was not large as compared with the bulk strength. In PBHT bonds, microstructural continuity was not observed unlike in the bulk material. Hence, significant variation in the PBHT bonds with orientation was not observed. Average peak shear strengths of the PBHT bonds in the T-T and L-L orientations were of the order of 70% and 80% of that of the bulk recrystallized material, respectively. Fractography was conducted using the JEOL-840 SEM. Fracture surfaces of the bonds and the bulk exhibited planar shear and secondary cracking, figures 5.37 and 5.38. In general, bonds which failed at the bondline showed planar shear, figure 5.38 (a-b), and those which failed in the bulk showed mixed planar shear and secondary cracking, figure 5.38 (c-d). The former failed at a lower peak stress (71% of the peak shear stress of recrystallized bulk PM2000) as compared to the latter (78% of the peak shear stress of recrystallized bulk PM2000).

5.3.3.2.Tensile Testing

Room temperature tensile testing was conducted on diffusion bonds prepared using fine grain PM2000 in the L-L orientation. For comparison, tests were also done on samples of the bulk material. The bonds were tested both in the as-bonded condition and after PBHT for two different times: (a) 5 s and (b) 300 s at the bonding temperature (1250 °C). In the unrecrystallized (fine grain) condition, the 5 s bond, 300 s bond and bulk material showed average strengths of 800 MPa, 833 MPa and 1GPa, respectively, see figure 5.39. In the unrecrystallized condition, a maximum bond strength of about 83% compared to that of the bulk material were obtained in the 300 s bond. In the recrystallized (coarse grain) condition, the 5 s bond, 300 s bond and bulk material showed average strength of 577 MPa, 499 MPa and 522 MPa, respectively. In the recrystallized condition, a maximum bond strength of about 110% compared to that of the bulk material was obtained in the 5 s bond. An increase in the tensile stress of the as-bonded samples was also observed with increasing bonding time. The strength of the as-bonded samples increased from 800 MPa to 833 MPa as the bonding time increased from 5 s to 300 s at 1250 °C, which may be related to the increasing bond area with increase in the bonding time. However, a decrease in the bond strength was observed in the recrystallized condition, from 577 MPa to 499 MPa, as the bonding time increased from 5 s to 300 s at 1250 °C. This decrease in the bond strength may be due to the variation in the porosity developed during the PBHT in the bonds. Some variation in the material's response to heat treatment has already been noted earlier in this study, section 5. The unrecrystallized bonds showed a flat fracture surface, and failure occurred at the bondline. PBHT samples showed some elongation and failed near the bond region at a lower stress than as-bonded samples, showing a 45 °C inclination to the gage length. This might be due to the deformation of the large recrystallized grains near the bondline. The fracture surfaces revealed a large number of voids under light microscopy, mainly due to the porosity developed in the material during PBHT. The increase in grain size also resulted in a decrease in the peak stress.

5.3.3.3. Creep Testing

Initial creep rupture tests were conducted on PM 2000 bulk material after a recrystallization heat treatment of 4 h at 1,385 ºC. The data obtained is summarized in table 5.2. An example of a crept specimen is shown in figure 5.40. The voids (pores) observed in the sample can be a combination of the typical stress rupture void formation and pores formed in the bulk material during heat treatment.

Table 5.1 Total liquid width and time required for isothermal solidification of the joint for different interlayer thicknesses.

Interlayer (boron) thickness (W_0)	Total liquid width after interlayer melts (C^E = 3.8 wt %)	Total liquid width at liquid – solid equilibrium ($C^{L\alpha}$ = 3.1 wt %)	Time for isothermal solidification
2 µm	19.2 µm	23.2 µm	1360 seconds
1 µm	9.6 µm	11.6 µm	340 seconds
500 nm	4.8 µm	5.8 µm	85 seconds
250 nm	2.4 µm	2.9 µm	21 seconds

Table 5.2 Results obtained to date for creep rupture testing of bulk PM 2000, after heat treating 4h, 1385 ºC

Thermal Exposure Prior to Creep Testing		**Creep Rupture Life**		
Temp. (ºC)	**Time (h)**	**Temp. (ºC)**	**Stress (MPa)**	**Life (h)**
1,385	4	1,000	13	> 185
			50	> 500
			85	~ 0

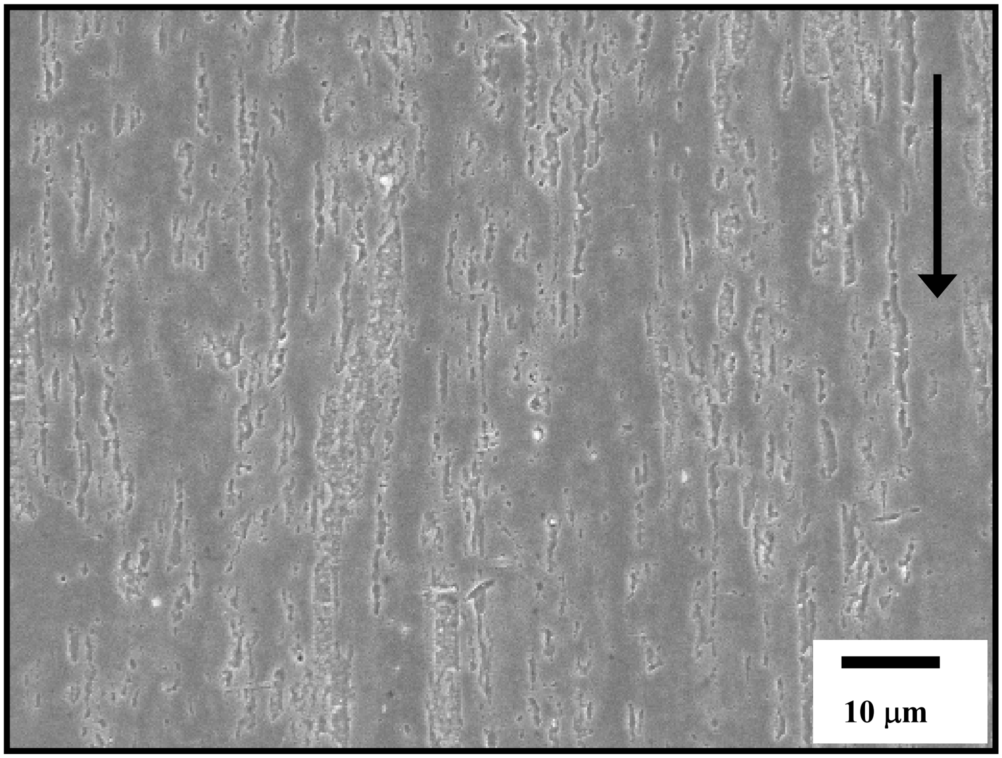

Figure 5.1 MA956 Fine grain material in the as-received condition (longitudinal orientation). The black arrow shows the working direction.

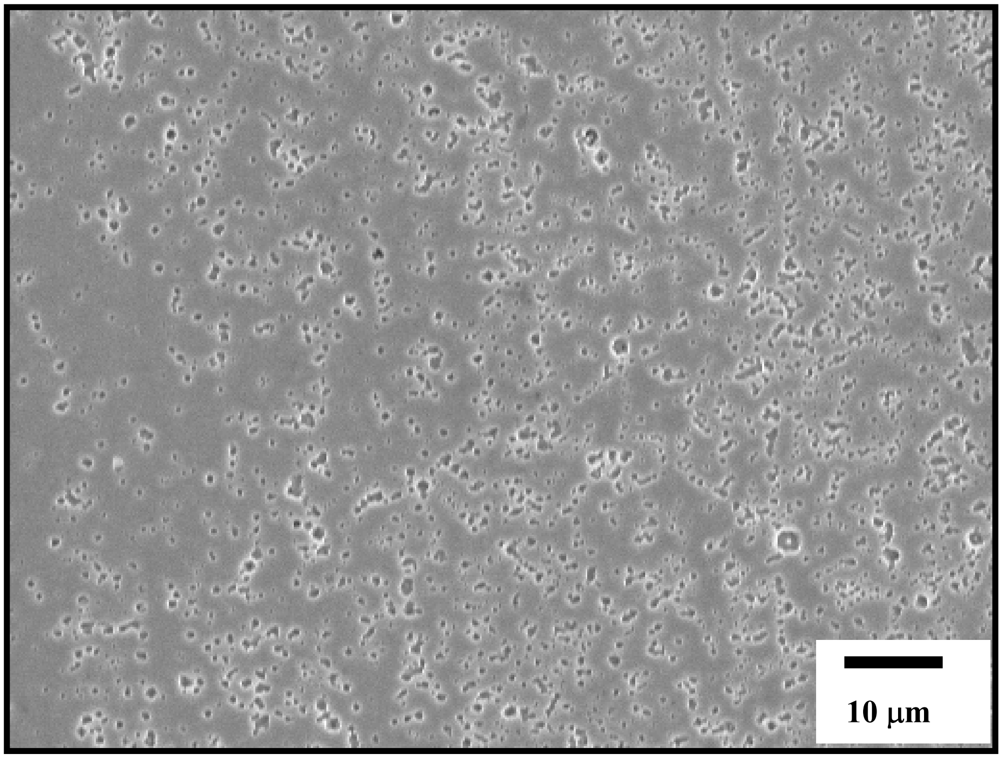

Figure 5.2 MA956 Fine grain material in the as-received condition (transverse orientation).

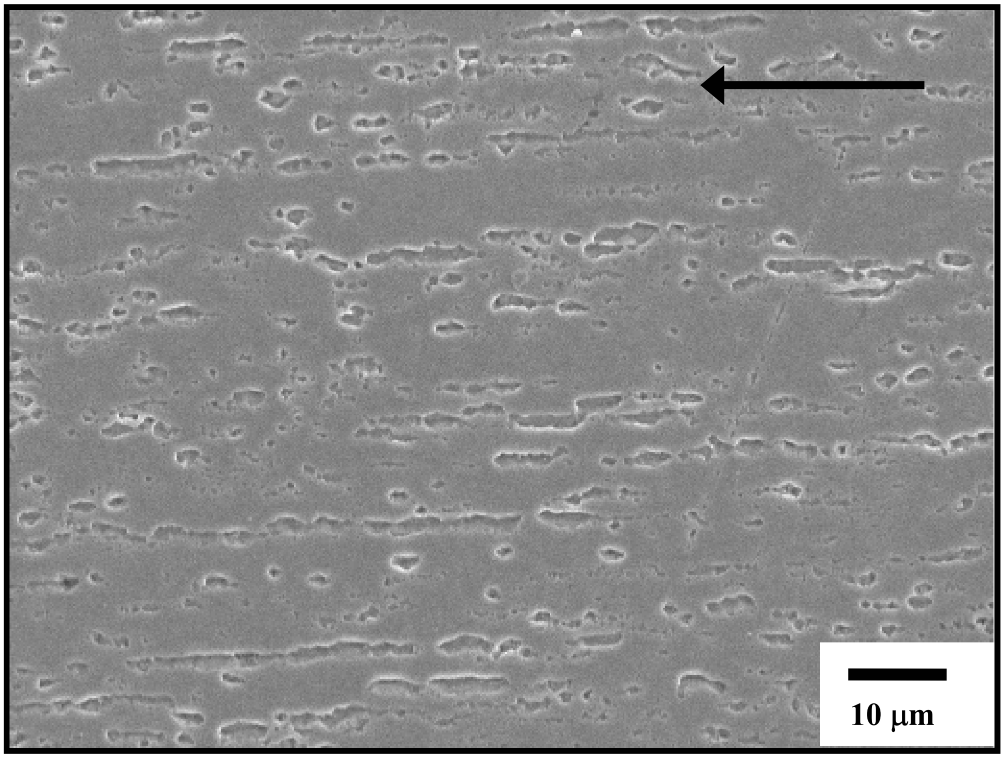

Figure 5.3 PM2000 Fine grain material in the as-received condition (longitudinal orientation). The black arrow shows the working direction.

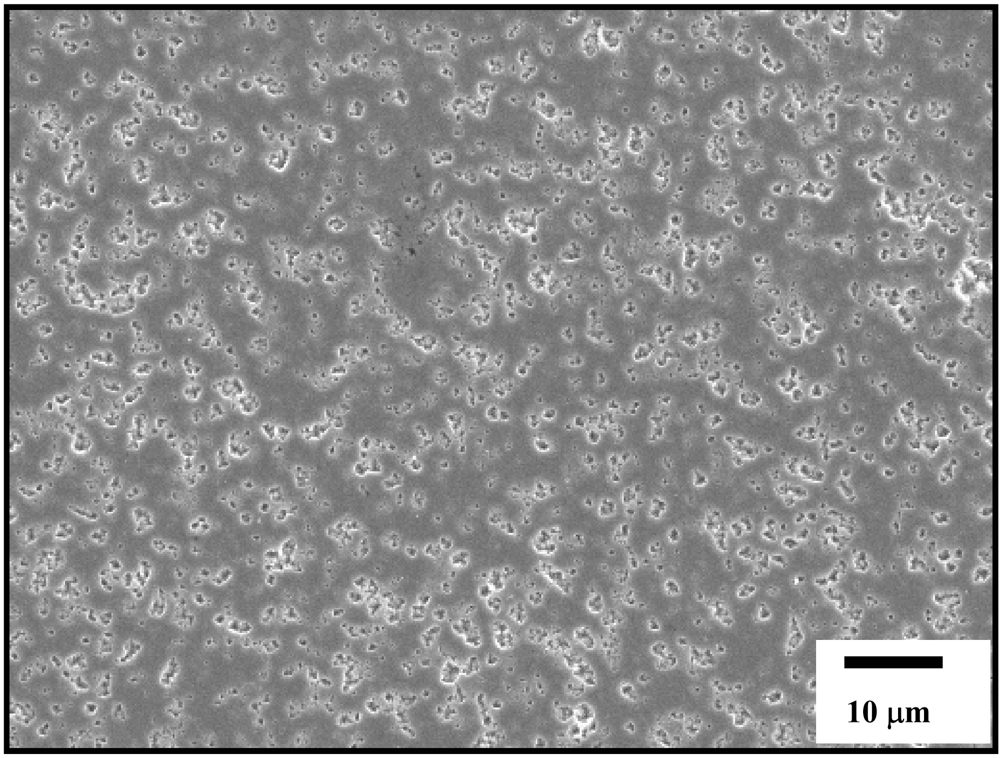

Figure 5.4 PM2000 Fine grain material in the as-received condition (transverse orientation).

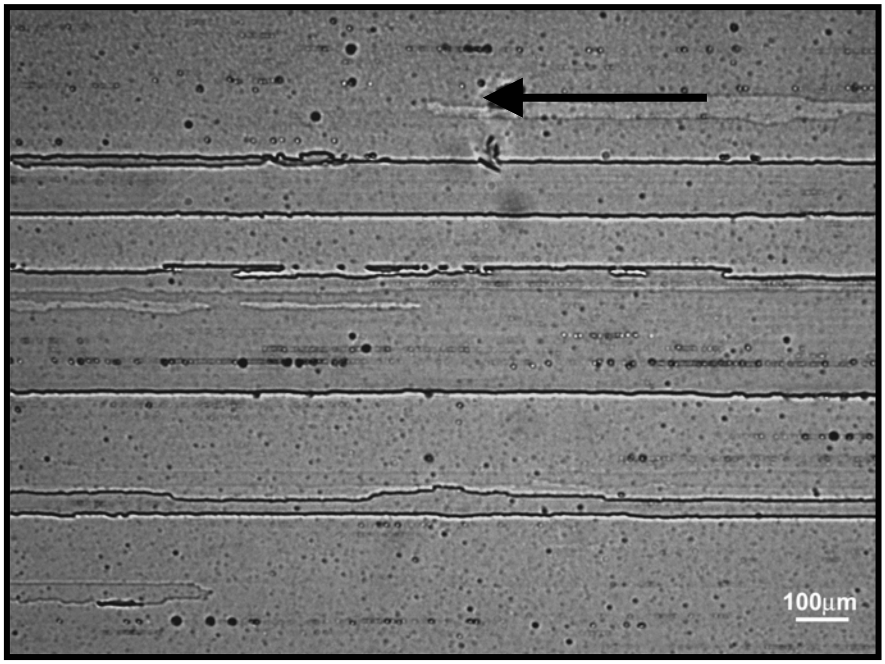

Figure 5.5 MA956 As-received coarse grain material heat treated for 1 h, 1300 °C (longitudinal orientation). The black arrow shows the working direction.

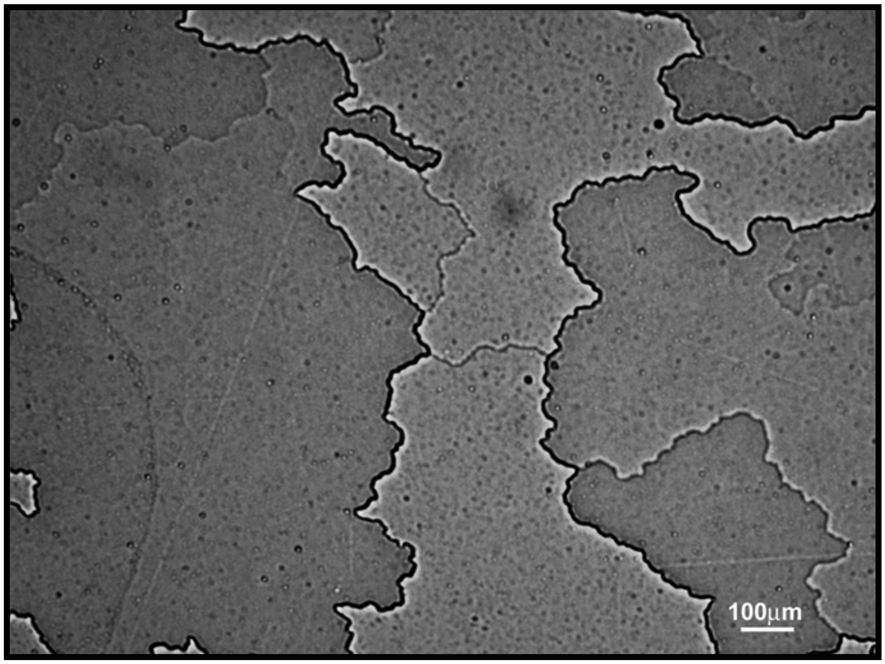

Figure 5.6 MA956 as-received coarse grain material heat treated for 1 h, 1300 °C (transverse orientation).

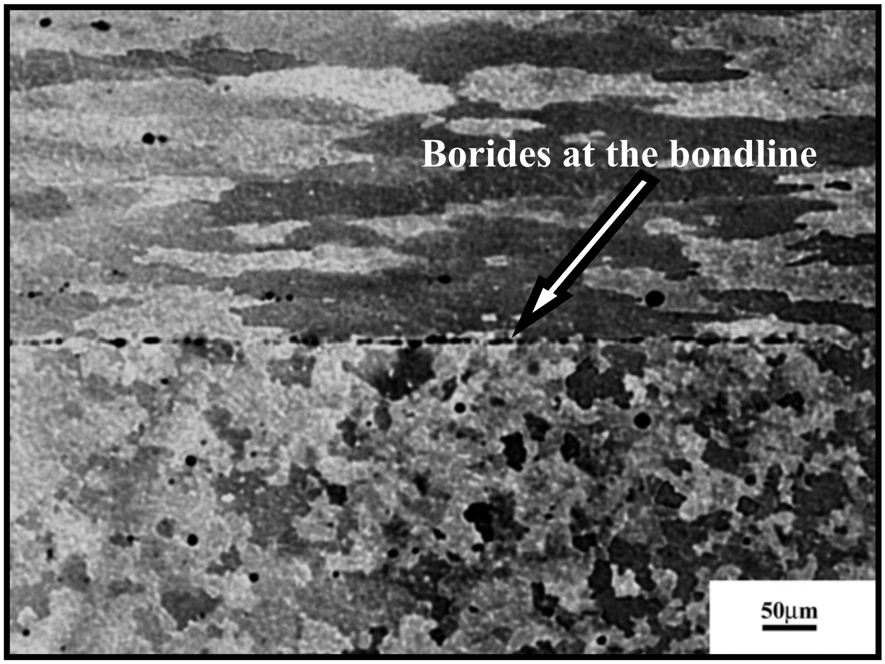

Figure 5.7 MA956 fine grain material, Longitudinal – Transverse orientation bond, 20 s, 1250 °C + PBHT 8 h, 1300 °C, showing the presence of borides at the bondline.

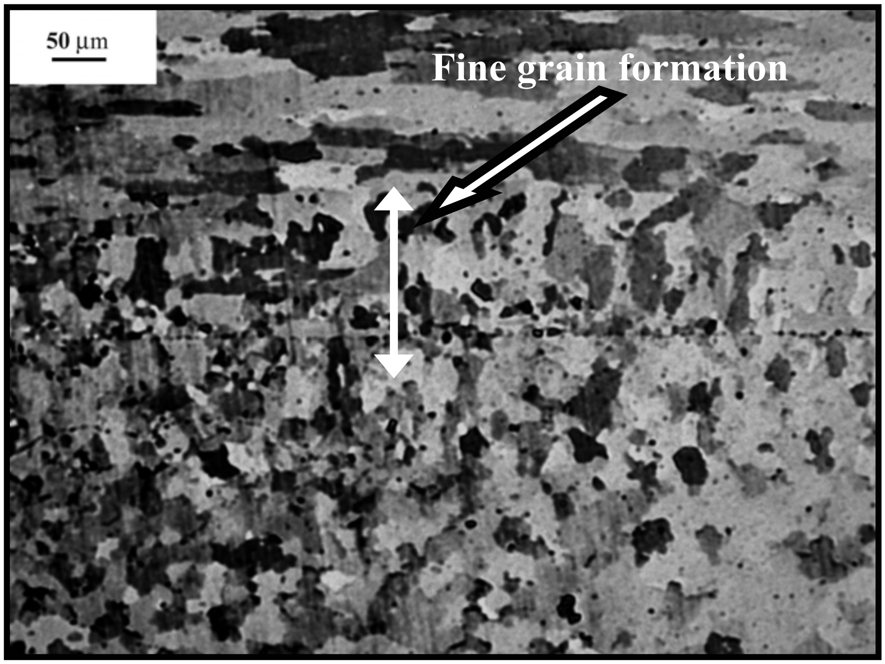

Figure 5.8 MA956 fine grain material, Longitudinal – Transverse orientation bond, 5 min, 1250 °C + PBHT 8 h, 1300 °C, showing the presence of recrystallized grains at the bondline.

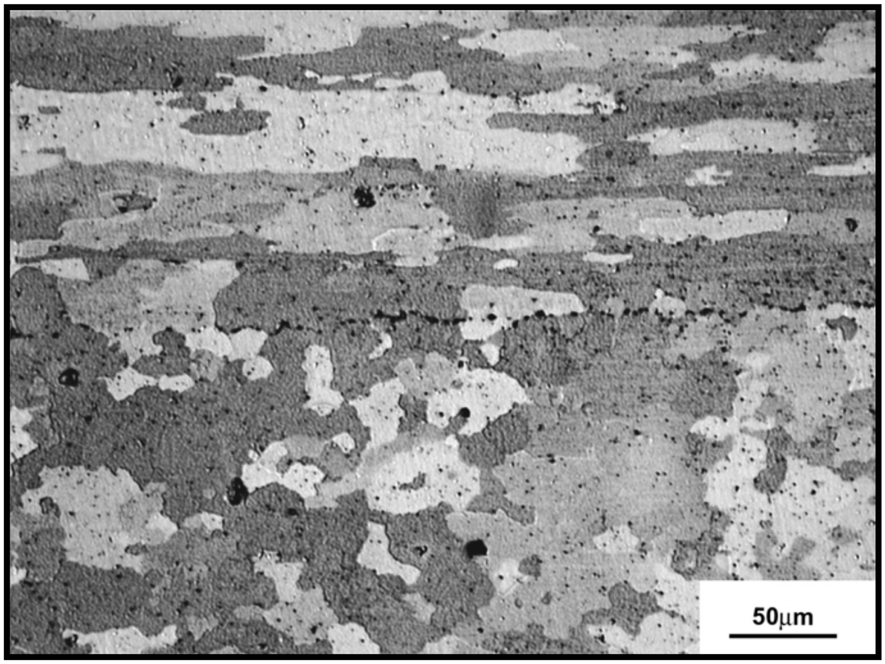

Figure 5.9 MA956 fine grain material, Longitudinal – Transverse orientation bond, 30 min, 1250 °C + PBHT 8 h, 1300 °C.

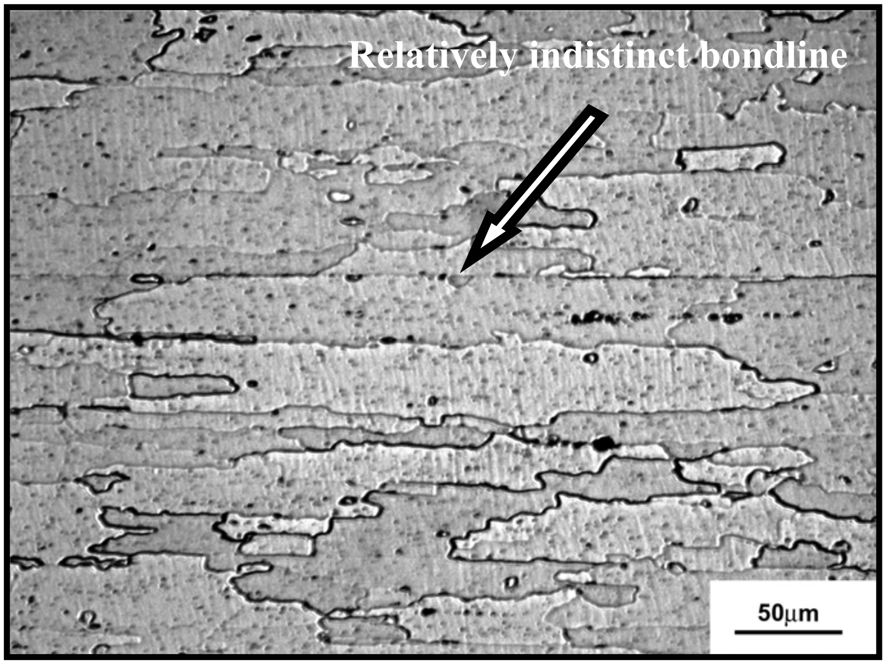

Figure 5.10 MA956 fine grain material, Longitudinal – Longitudinal orientation bond, 1 h, 1250 °C + PBHT 8 h, 1300 °C, showing relatively indistinct bondline.

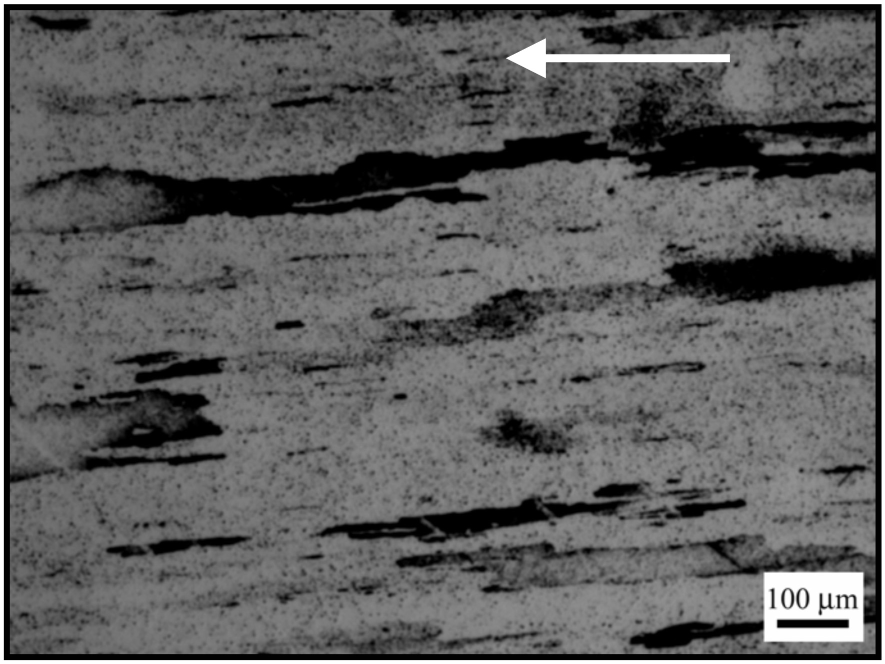

Figure 5.11 MA956 after recrystallization of initially as-received fine grain material 1 h, 1300 °C (longitudinal orientation). The arrow shows the working direction.

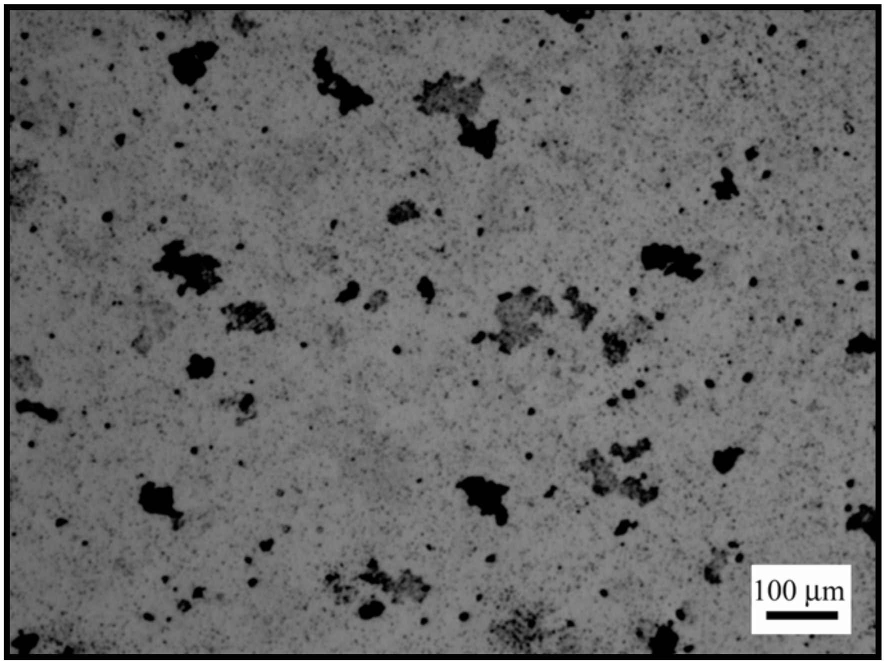

Figure 5.12 MA956 after recrystallization of initially as-received fine grain material 1 h, 1300 °C (transverse orientation).

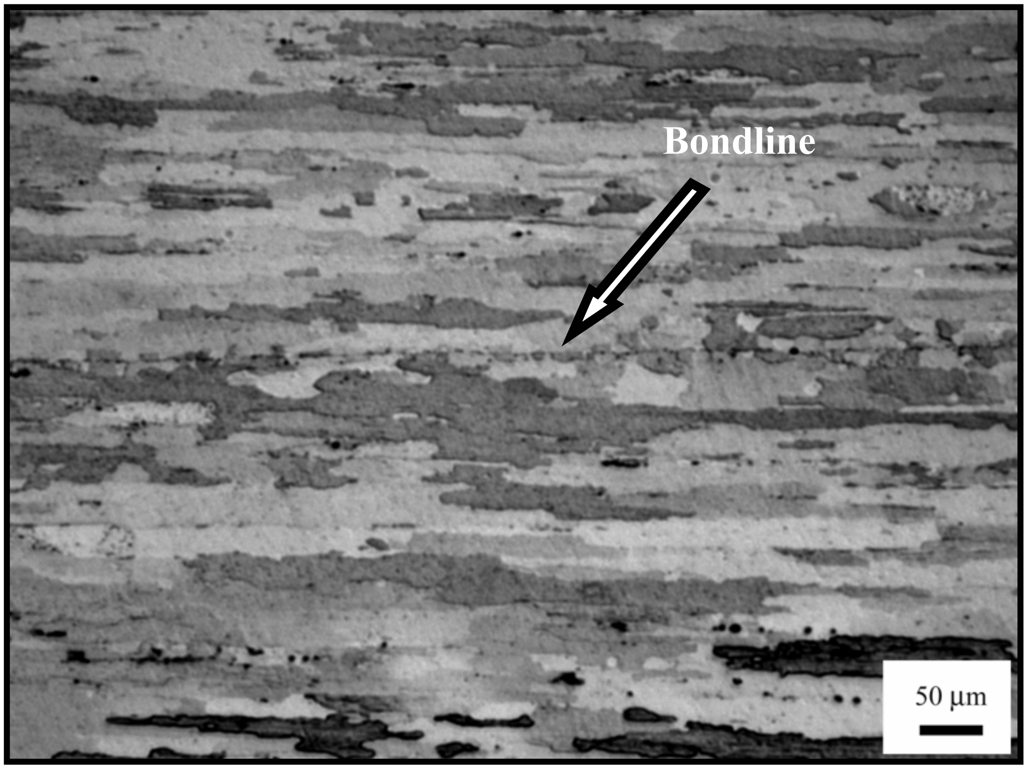

Figure 5.13 MA956 fine grain bonds 1 µm boron interlayer longitudinal – longitudinal 120 s, 1250 °C + PBHT 1 h, 1300 °C .

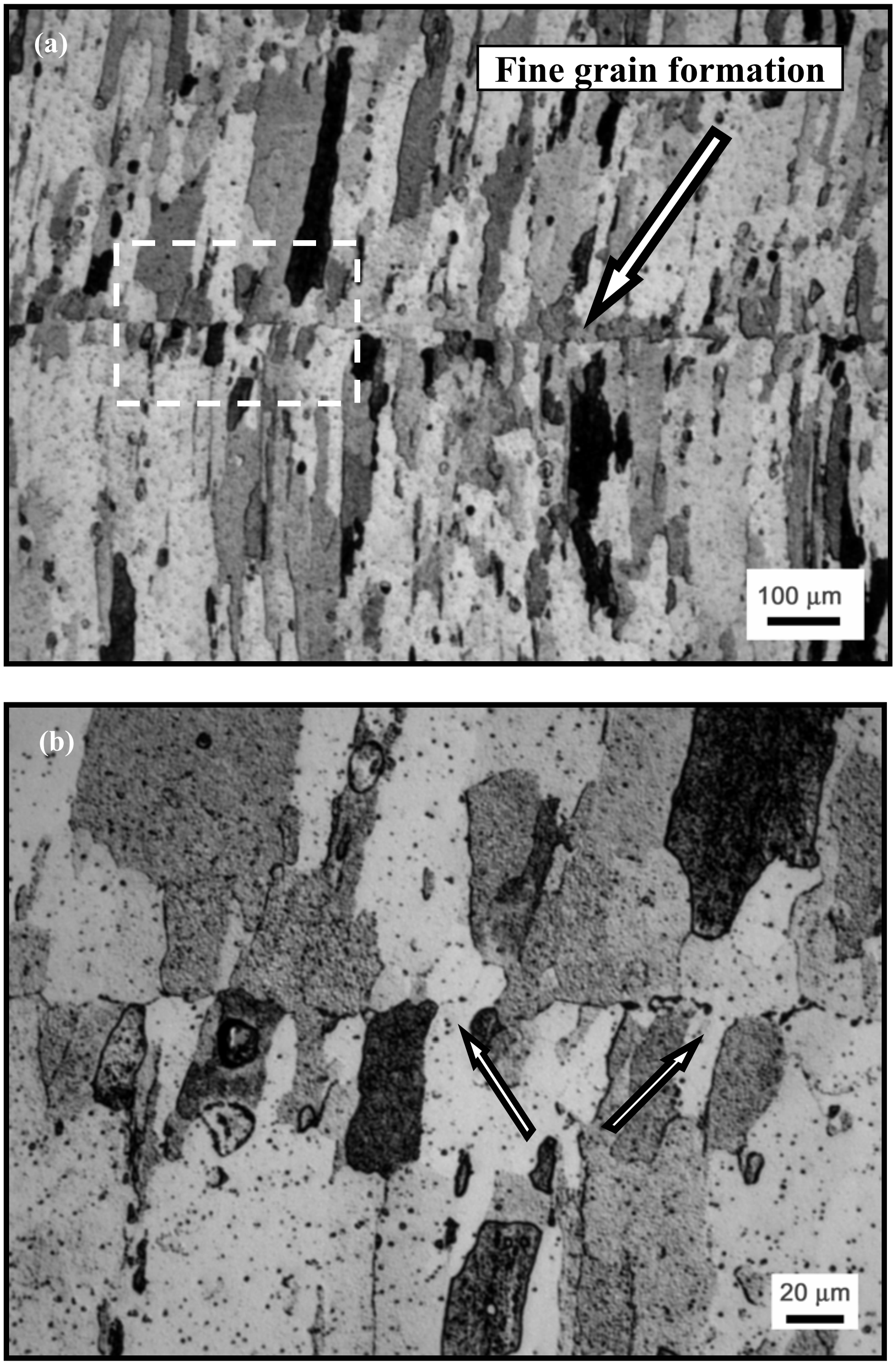

Figure 5.14 MA956 fine grain bonds 1 µm boron interlayer transverse –transverse, (a) 343 s + PBHT 1 h, 1300 °C and (b) Inset in (a) showing recrystallized grains at the bondline. Some grains (indicated by arrows) also extend through the bondline.

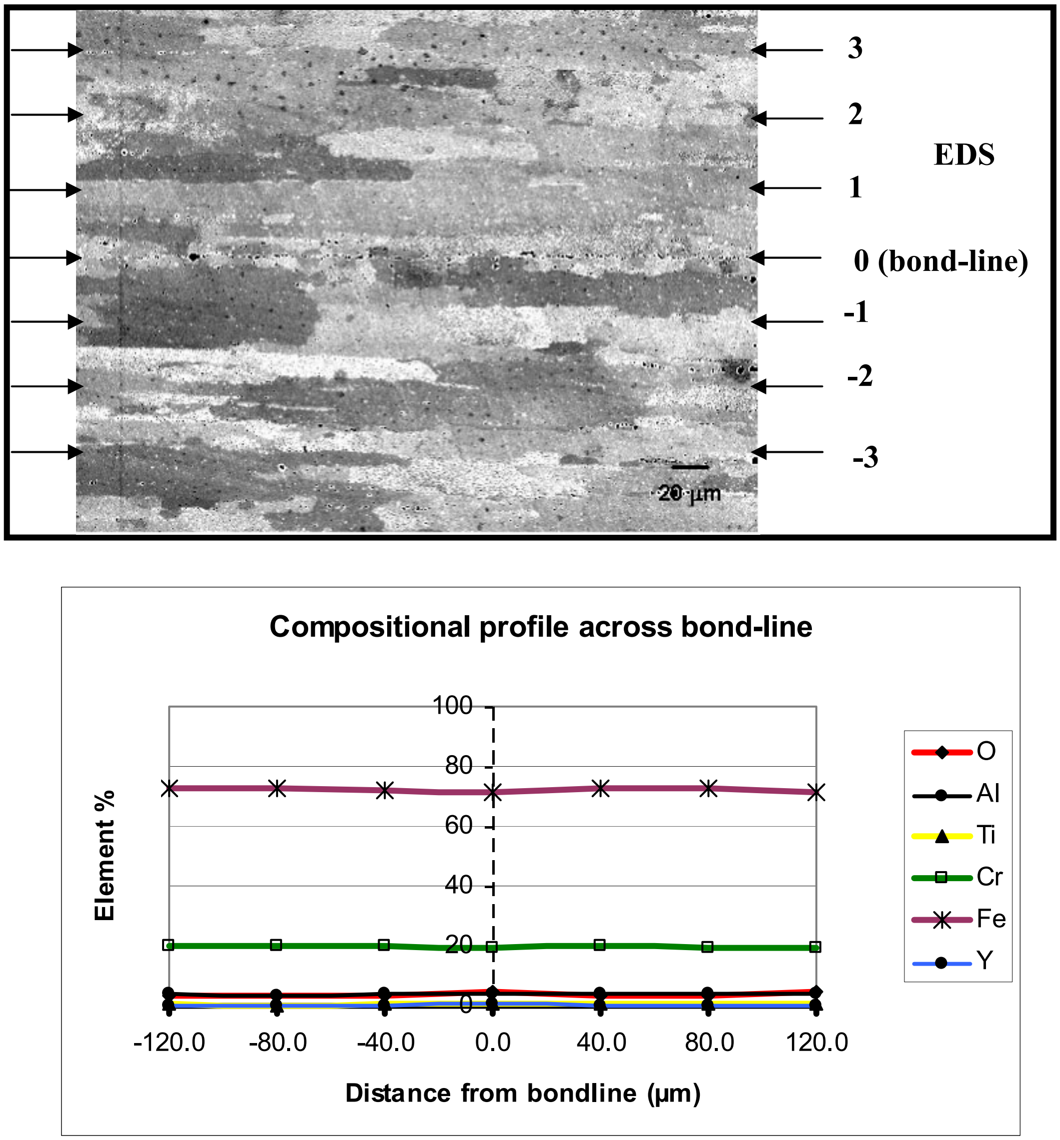

Figure 5.15 Compositional profiles showing uniform distribution of the alloying elements across the bondline of the bond shown in figure 5.13.

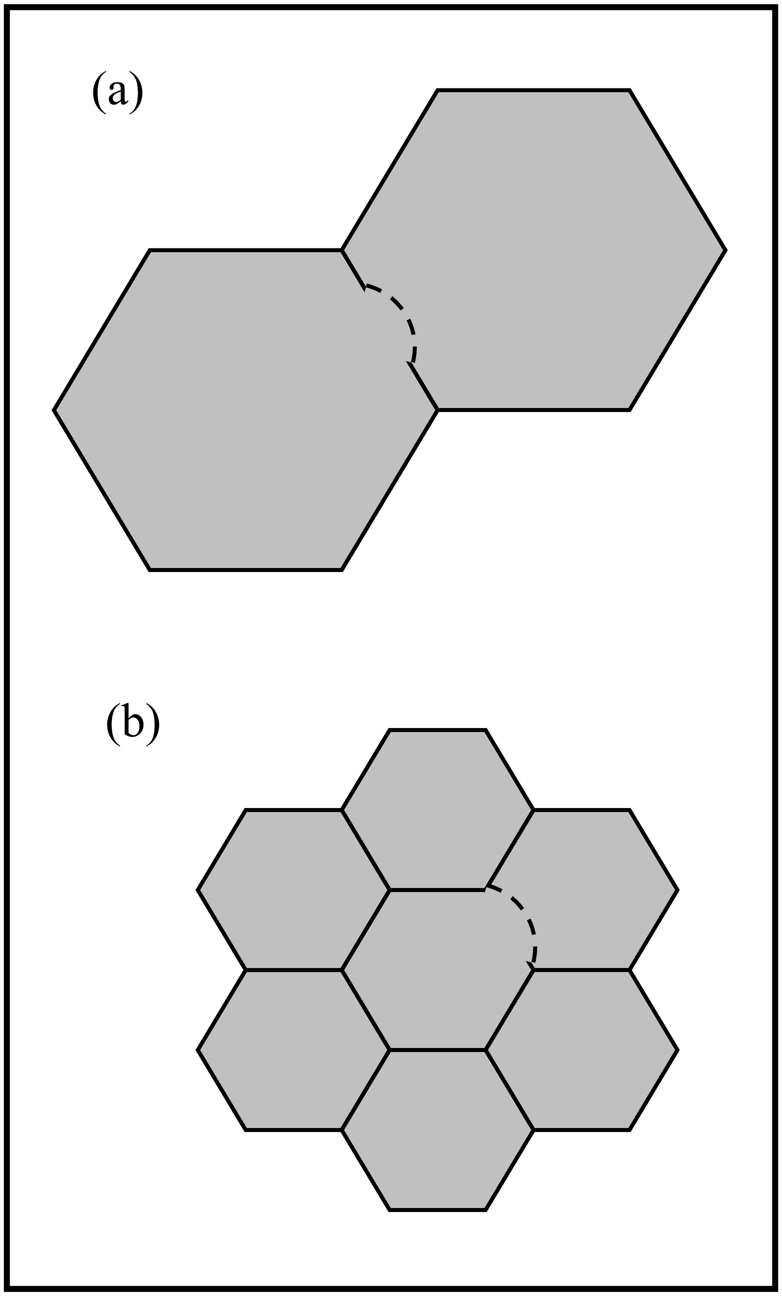

Figure 5.16 Effect of the grain size on recrystallization. (a) Large grains (widely spaced grain boundaries) undergo bulging in the grain boundary. (b) In fine grains, the grain boundary junctions act as pinning agents, delaying nucleation in recrystallization based on Bhadeshia [37].

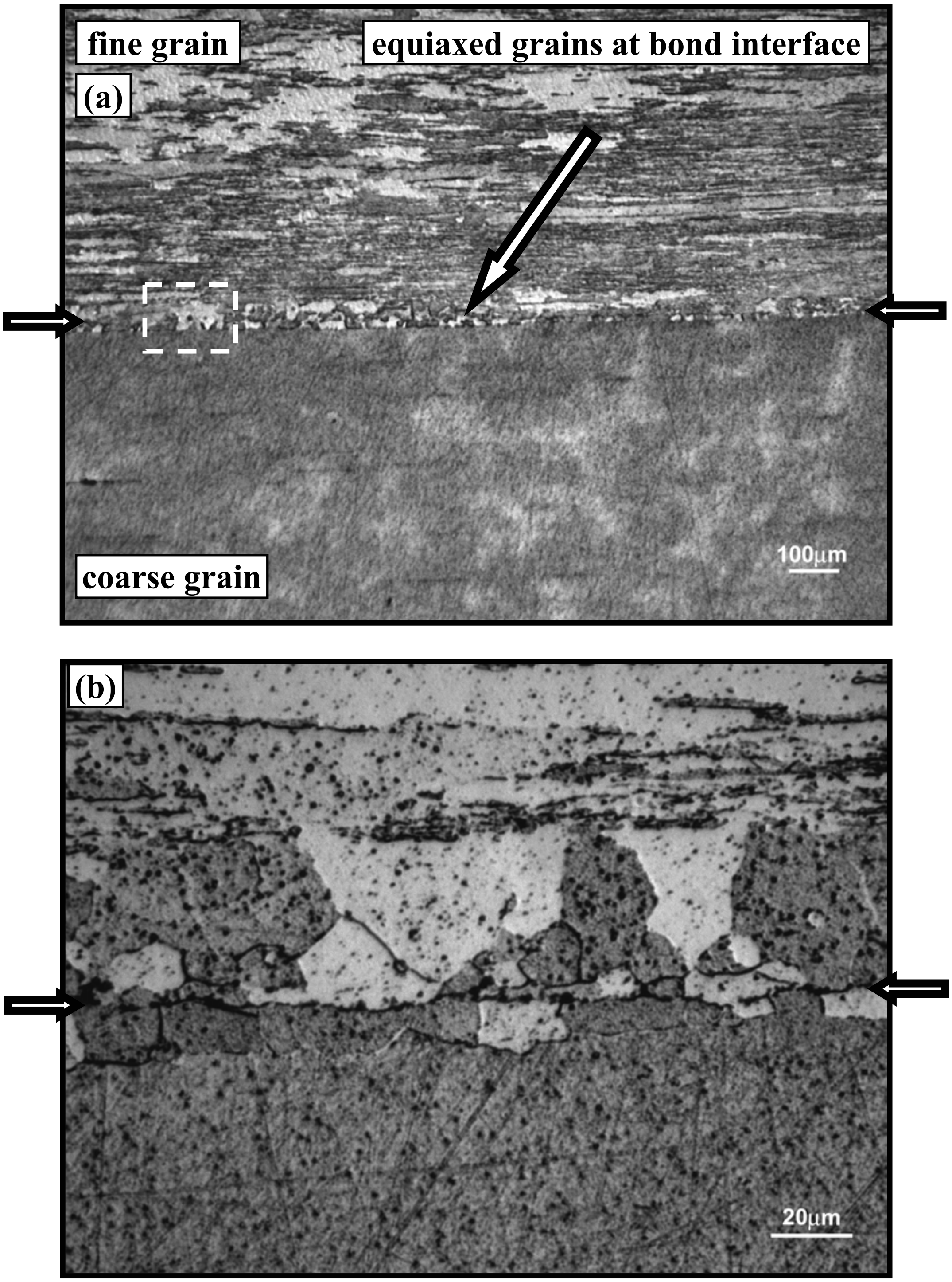

Figure 5.17 (a) MA956 fine grain to coarse grain condition (FG-CG) bond in L-L bond orientation 99 s, 1250 °C, as-bonded. (b) same view at higher magnification. Arrows show the bondline.

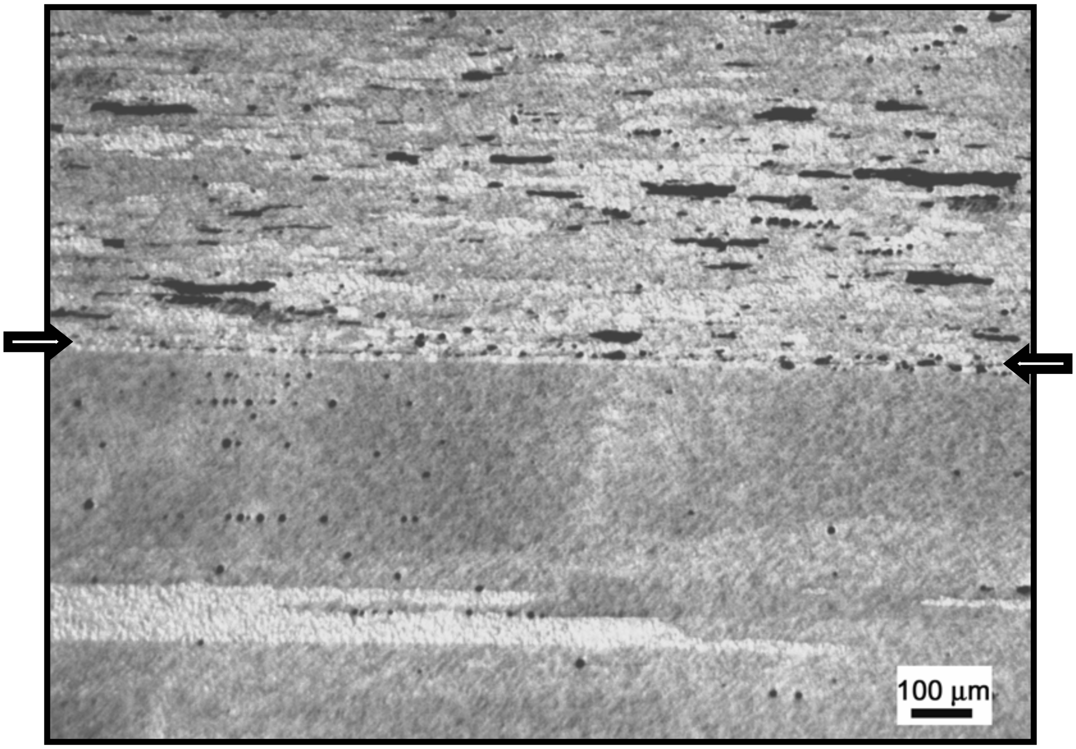

Figure 5.18 MA956 fine grain to coarse grain condition (FG-CG) bond in L-L bond orientation same bond as in figure 5.17 after recrystallization heat treatment (1 h, 1300 °C). Arrows show the bondline.

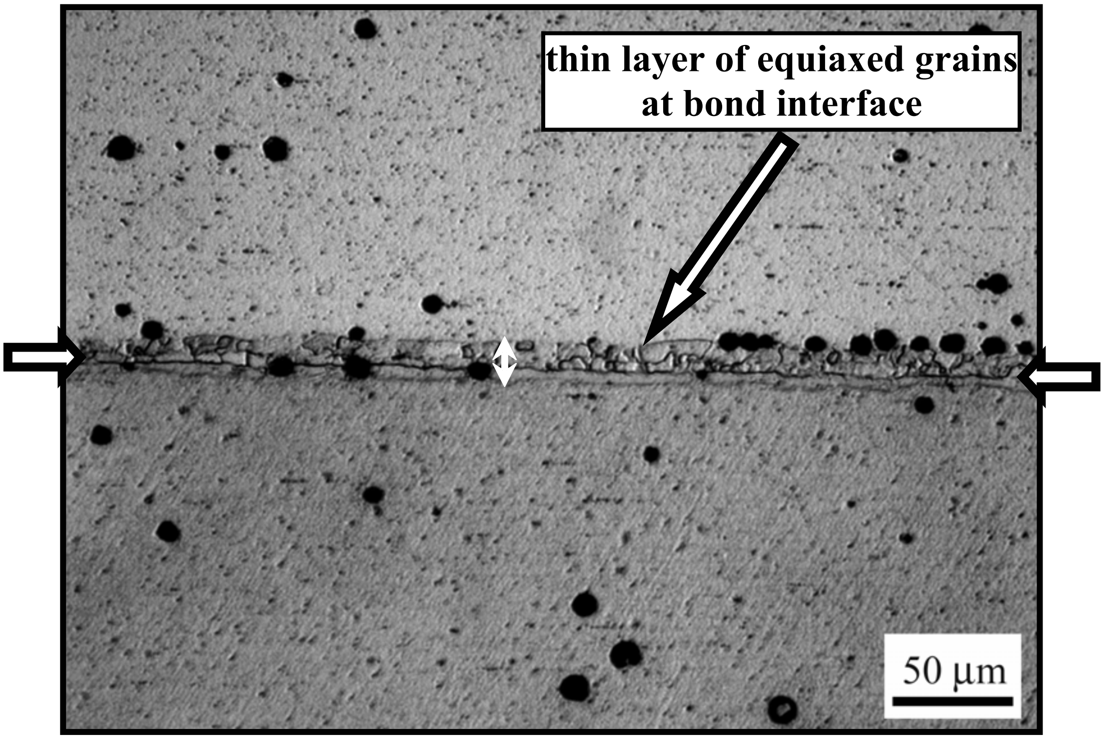

Figure 5.19 MA956 coarse grain – coarse grain (CG-CG) bond in the L-L orientation 1 µm boron interlayer, 240 s, 1250 °C + PBHT 1 h, 1300 °C, white double-head arrow shows the thickness of the recrystallized zone.

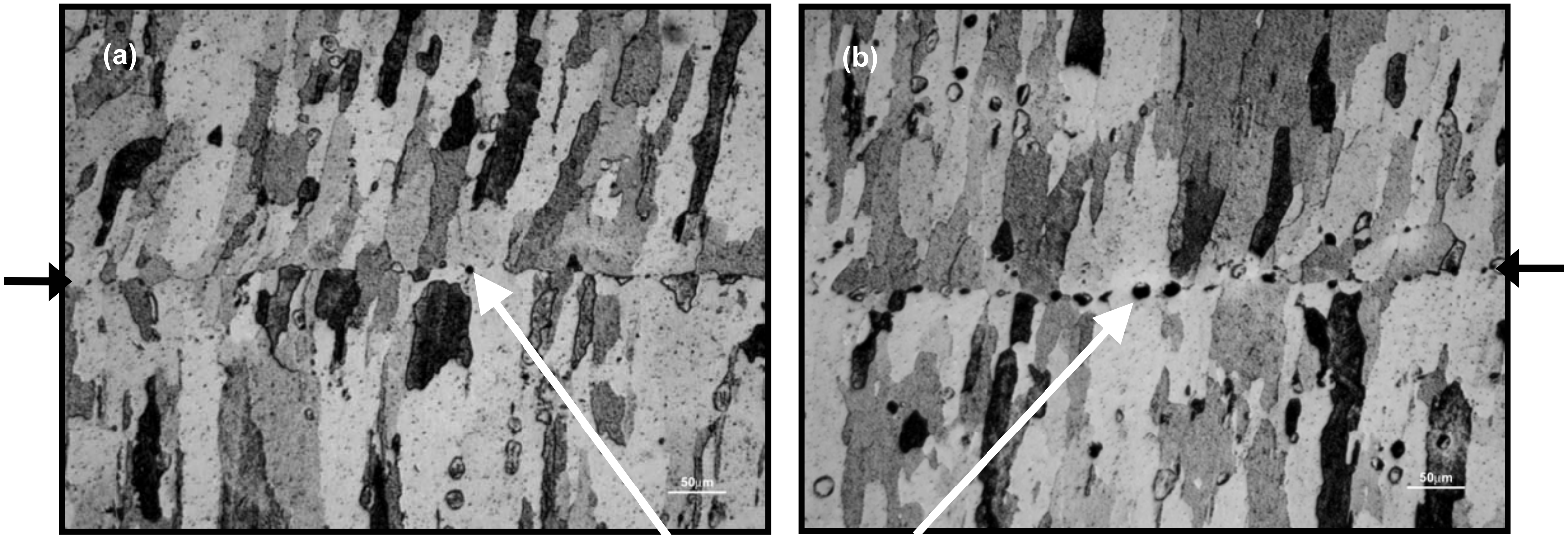

Borides and fine grains at bondline

Figure 5.20 Effect of interlayer thickness: MA956 fine grain T-T orientation bond with (a) 500 nm (b) 1 µm boron interlayer PBHT (1 h, 1250 °C + 1 h, 1300 °C)

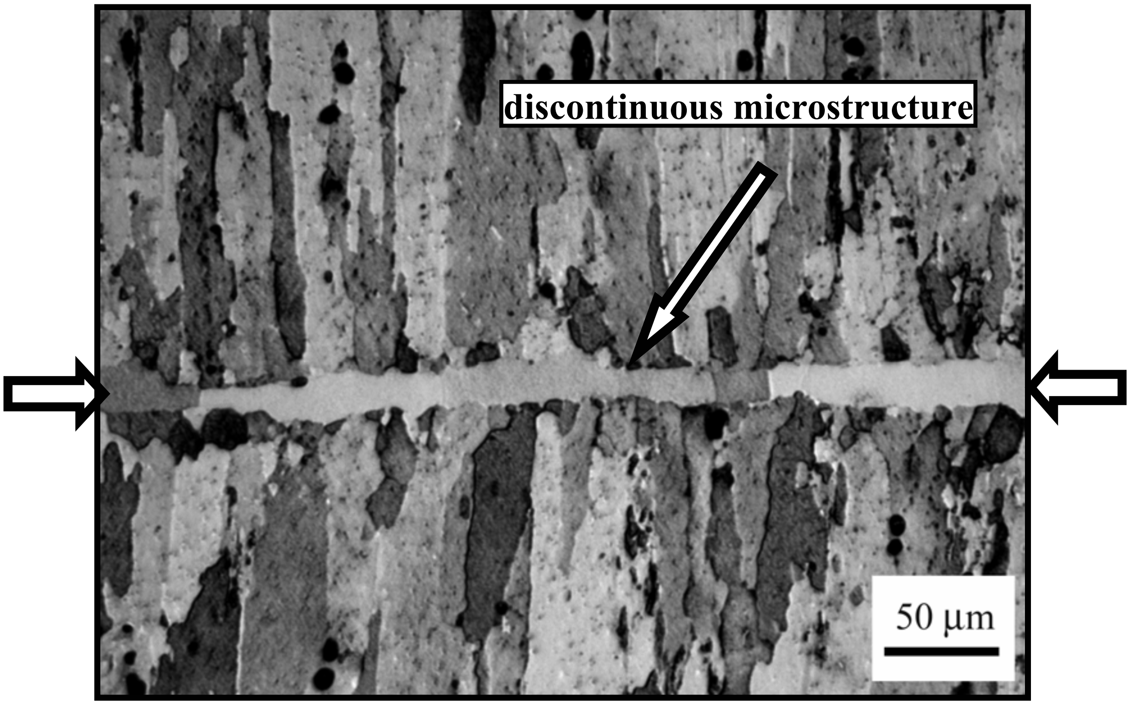

Figure 5.21 MA956 fine grain bonds T-T orientation 25 µm Fe-16Si-5B foil 150 s, 1190 °C + PBHT 1h, 1300 °C

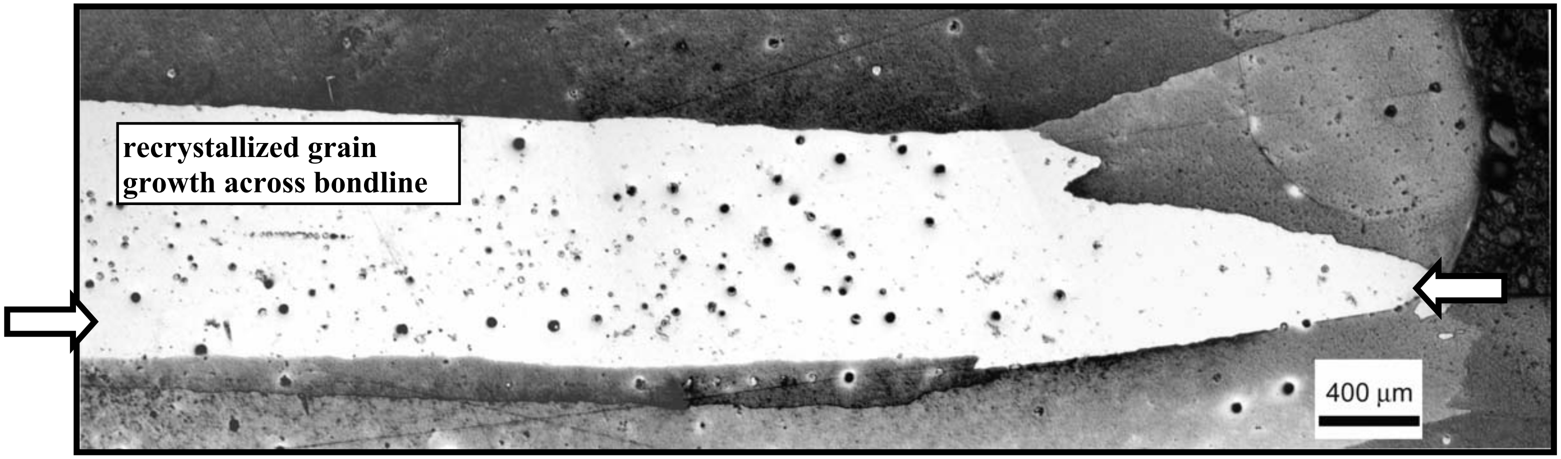

Figure 5.22 PM2000 fine grain bond L-L orientation 250 nm boron interlayer, 30 s, 1250 °C + PBHT 2 h, 1385 °C

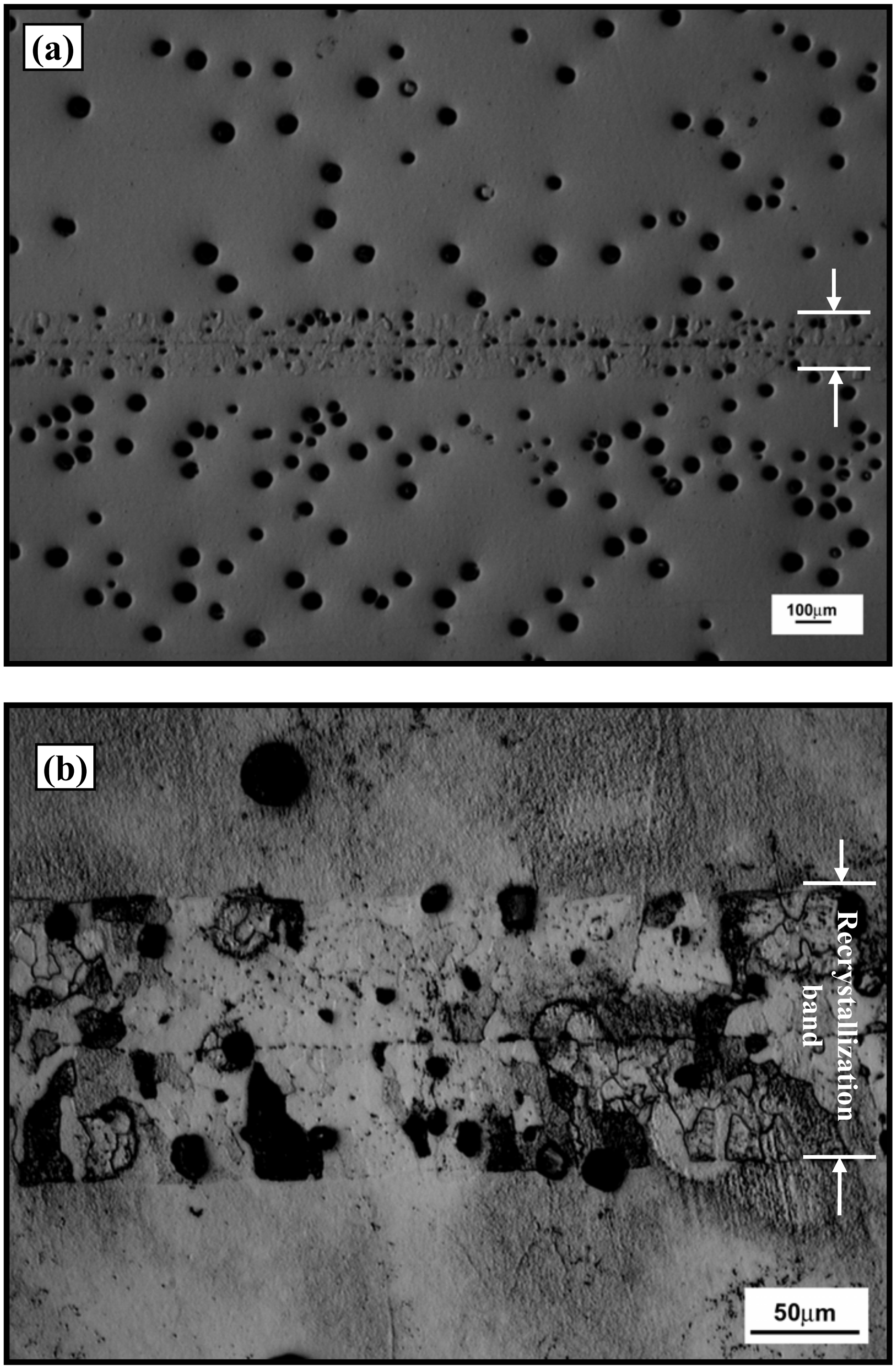

Figure 5.23 PM2000 fine grain –fine grain L-L bond orientation, 1 µm B interlayer 310 s, 1250 °C + PBHT 2h, 1385 °C (a) unetched (b) same bond etched and at higher magnification. Figure shows secondary grains and pores formed during PBHT.

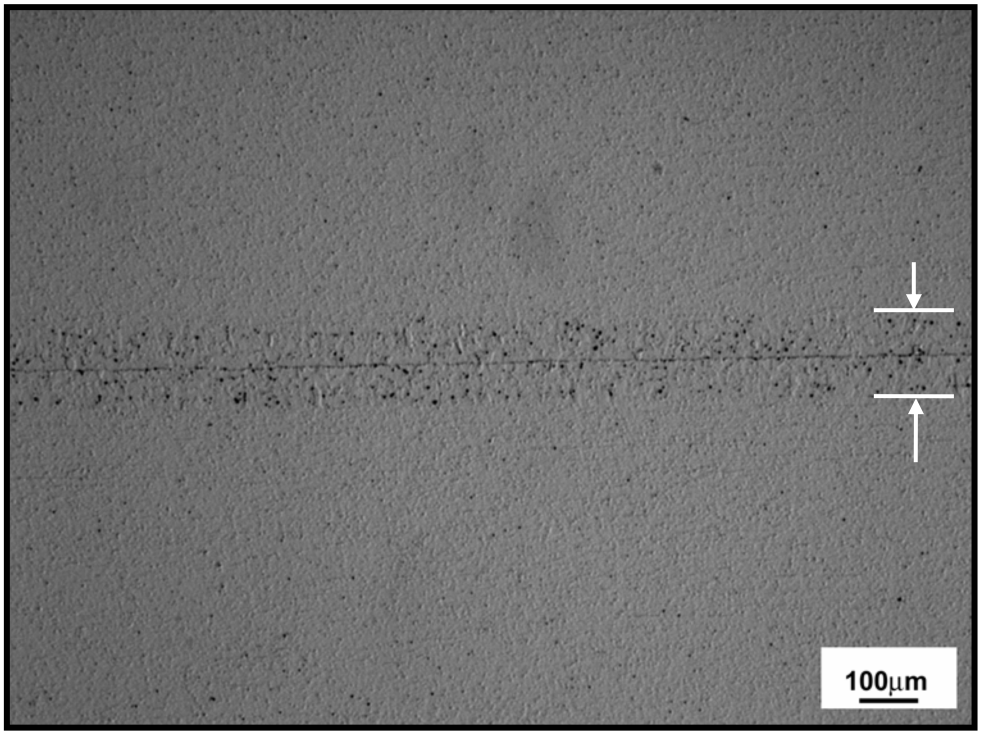

Figure 5.24 PM2000 fine grain –fine grain L-L bond orientation 1 μm B interlayer 310 s, 1250 °C in the as-bonded condition.

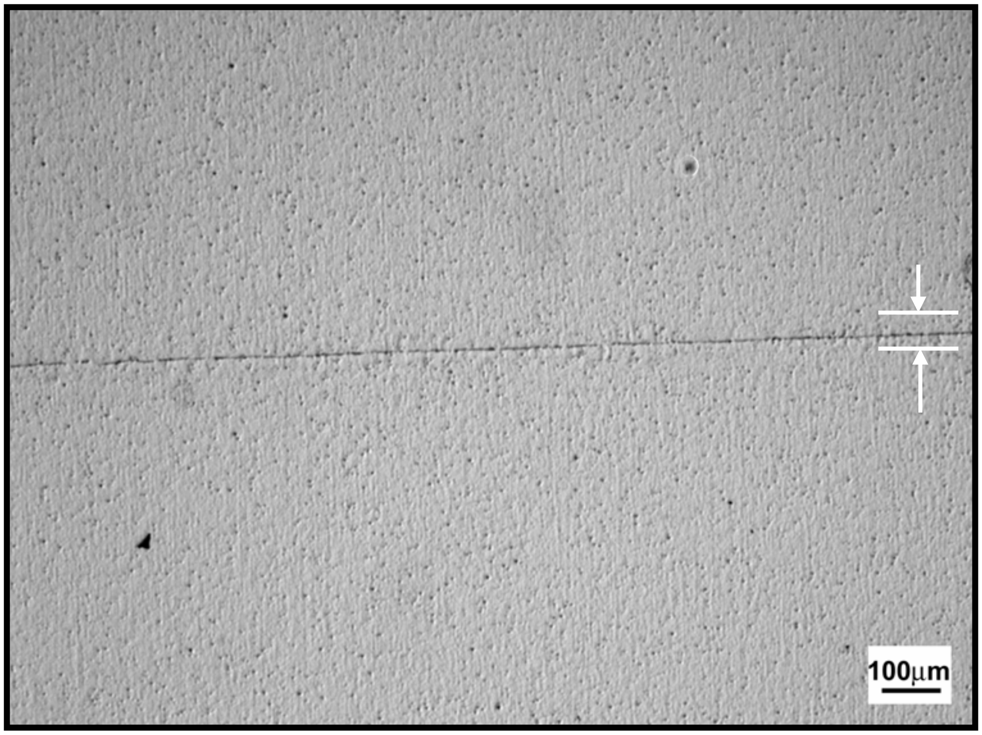

Figure 5.25 PM2000 fine grain –fine grain T-T bond orientation 1 µm B interlayer 300 s, 1250 °C in the as-bonded condition.

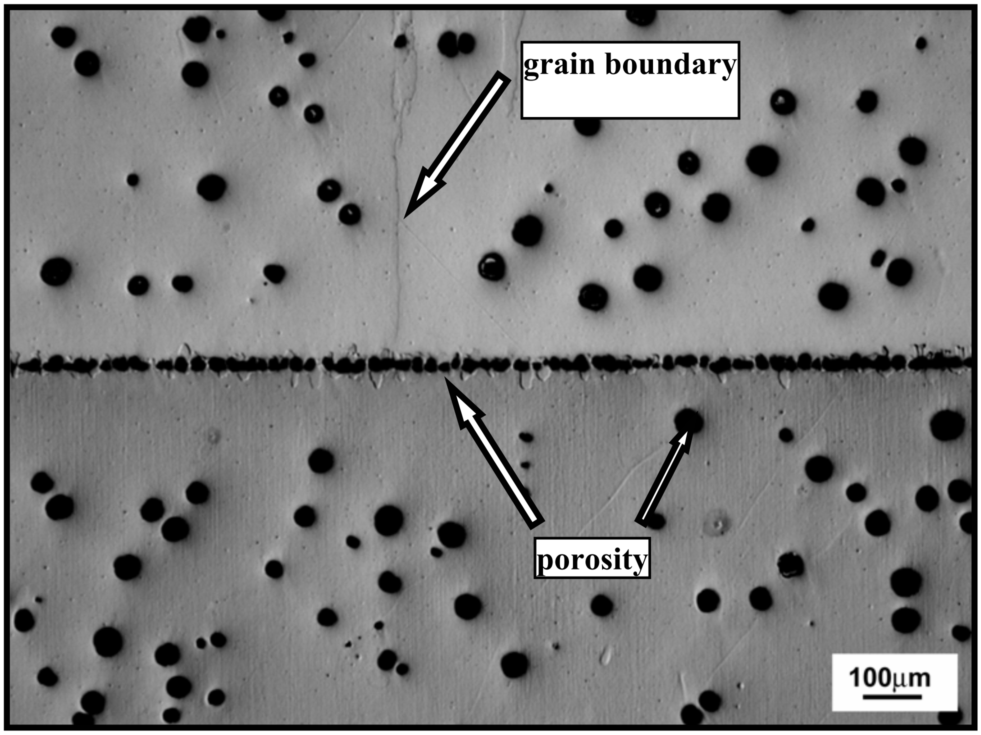

Figure 5.26 After recrystallization PBHT 2 h, 1385 °C of the same bond in figure 5.25. Notice the formation of porosity during PBHT both at the bondline and in the substrate.

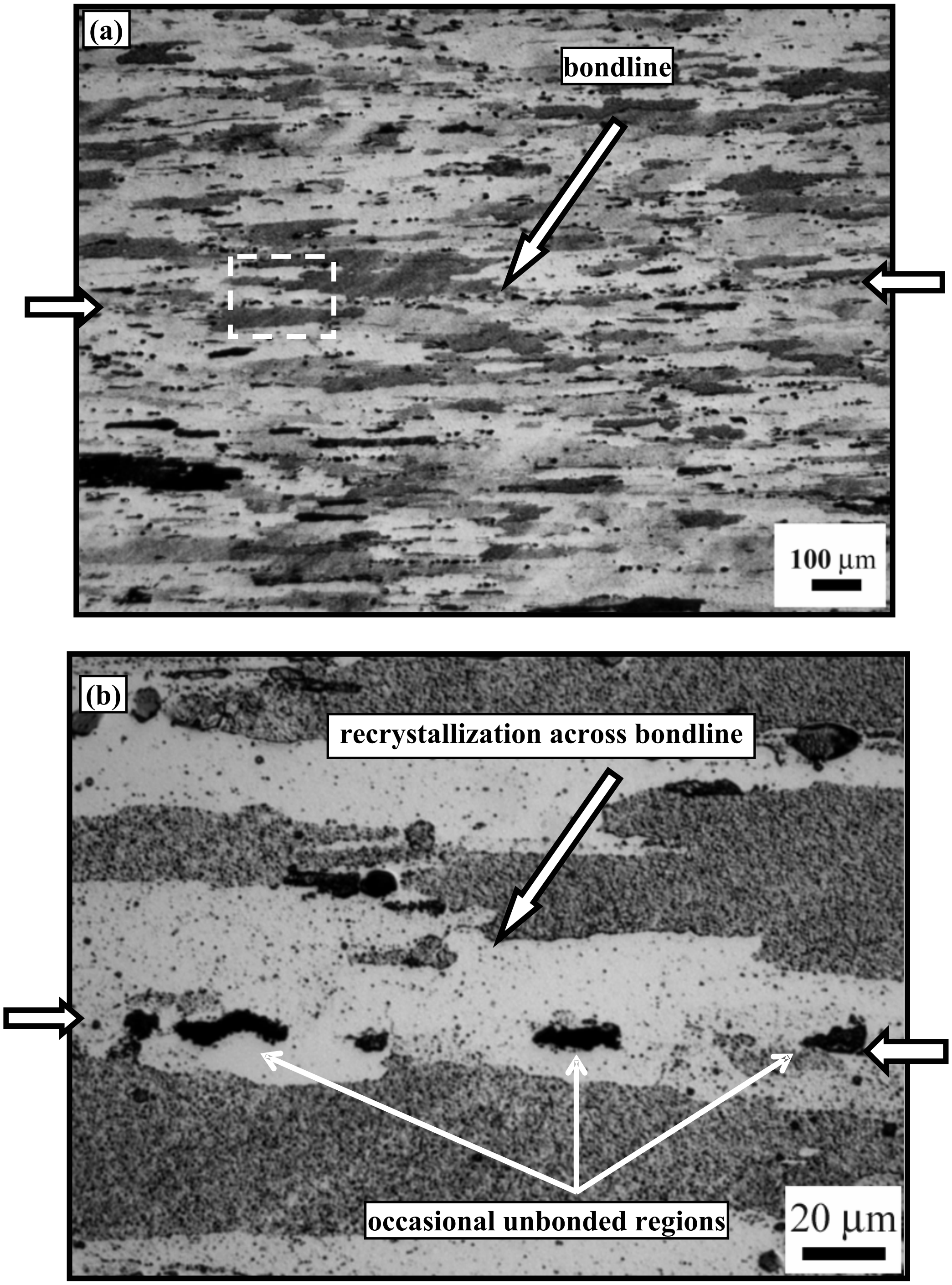

Figure 5.27 MA956 L-L orientation fine grain - fine grain bond 121 s, 1250 °C (PBHT 1 hr, 1300 °C) (a) bondline barely visible (b) recrystallized grain growth across the bondline in the inset region in (a).

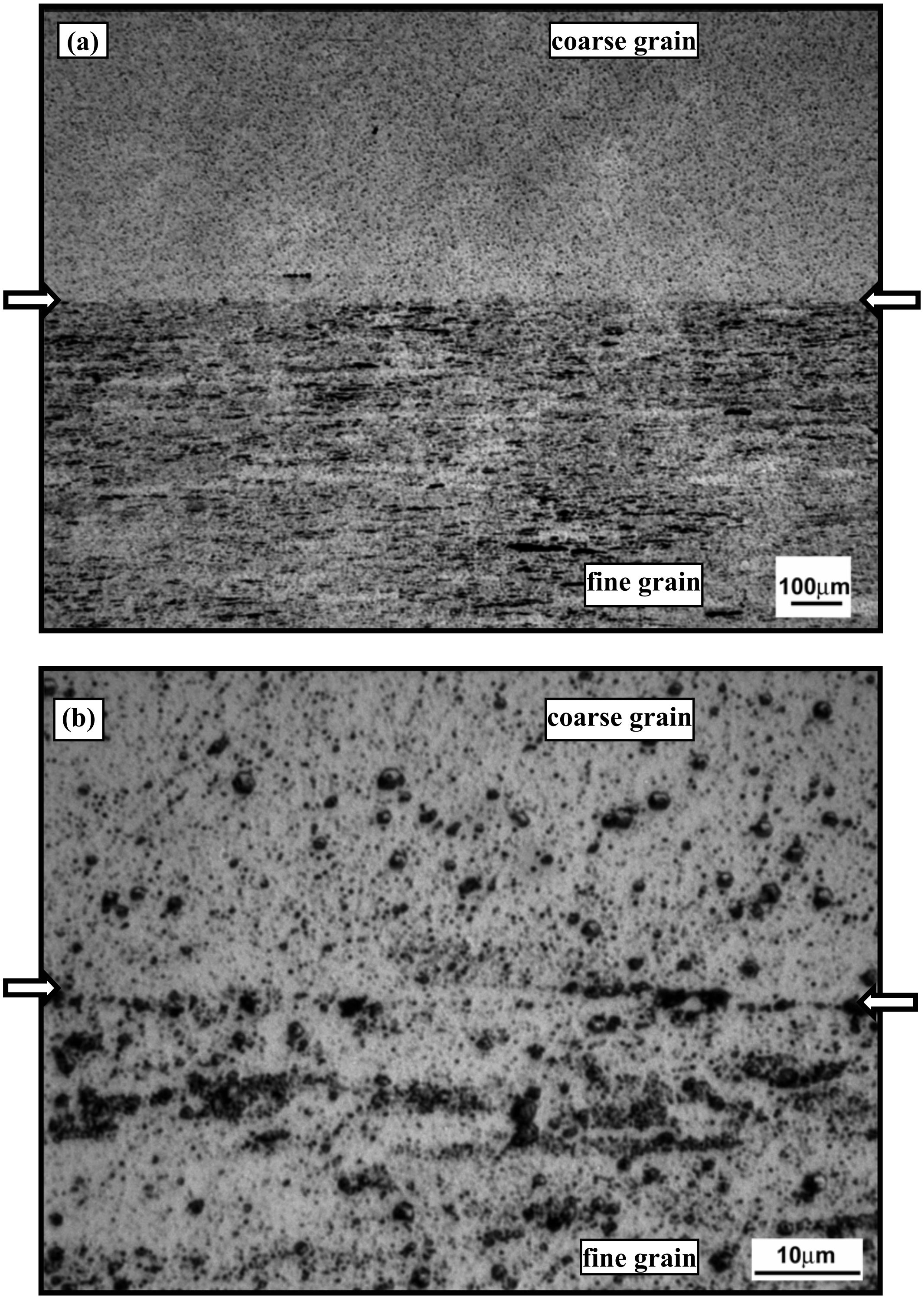

Figure 5.28 (a) MA956 L-L orientation bond coarse grain – fine grain bond 170 s, 1250 °C (as-bonded). (b) same bond as in (a) at a higher magnification.

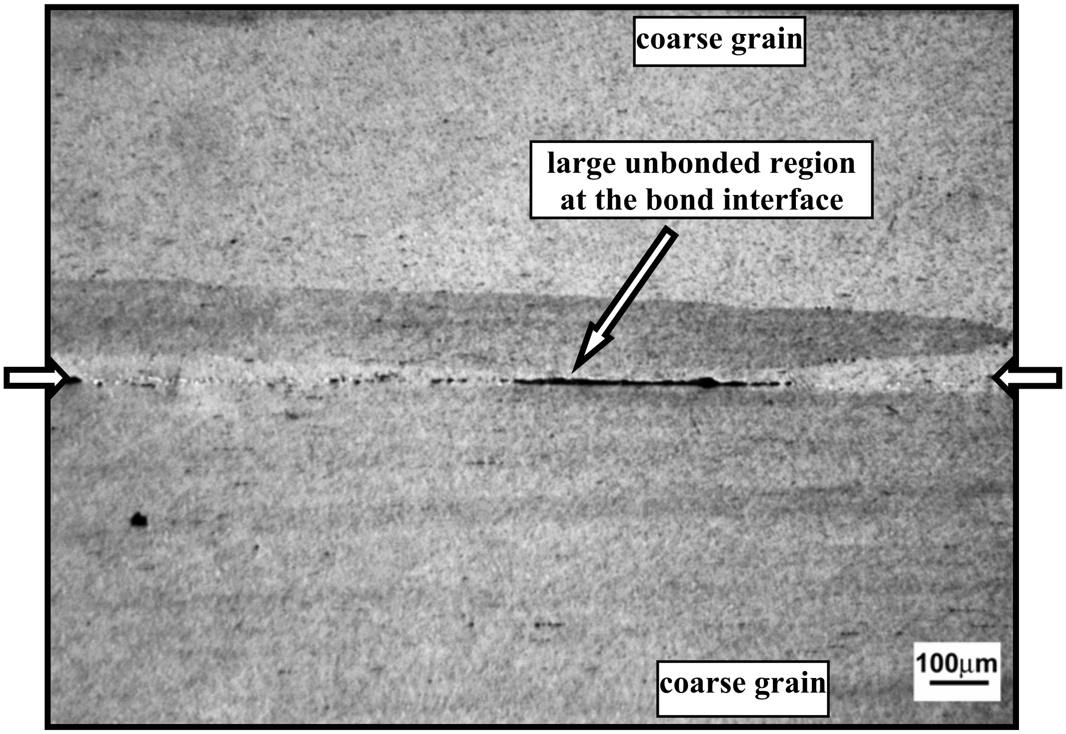

Figure 5.29 MA956 L-L orientation coarse grain (CG-CG) bond 174 s, 1250 °C bond in the as-bonded condition.

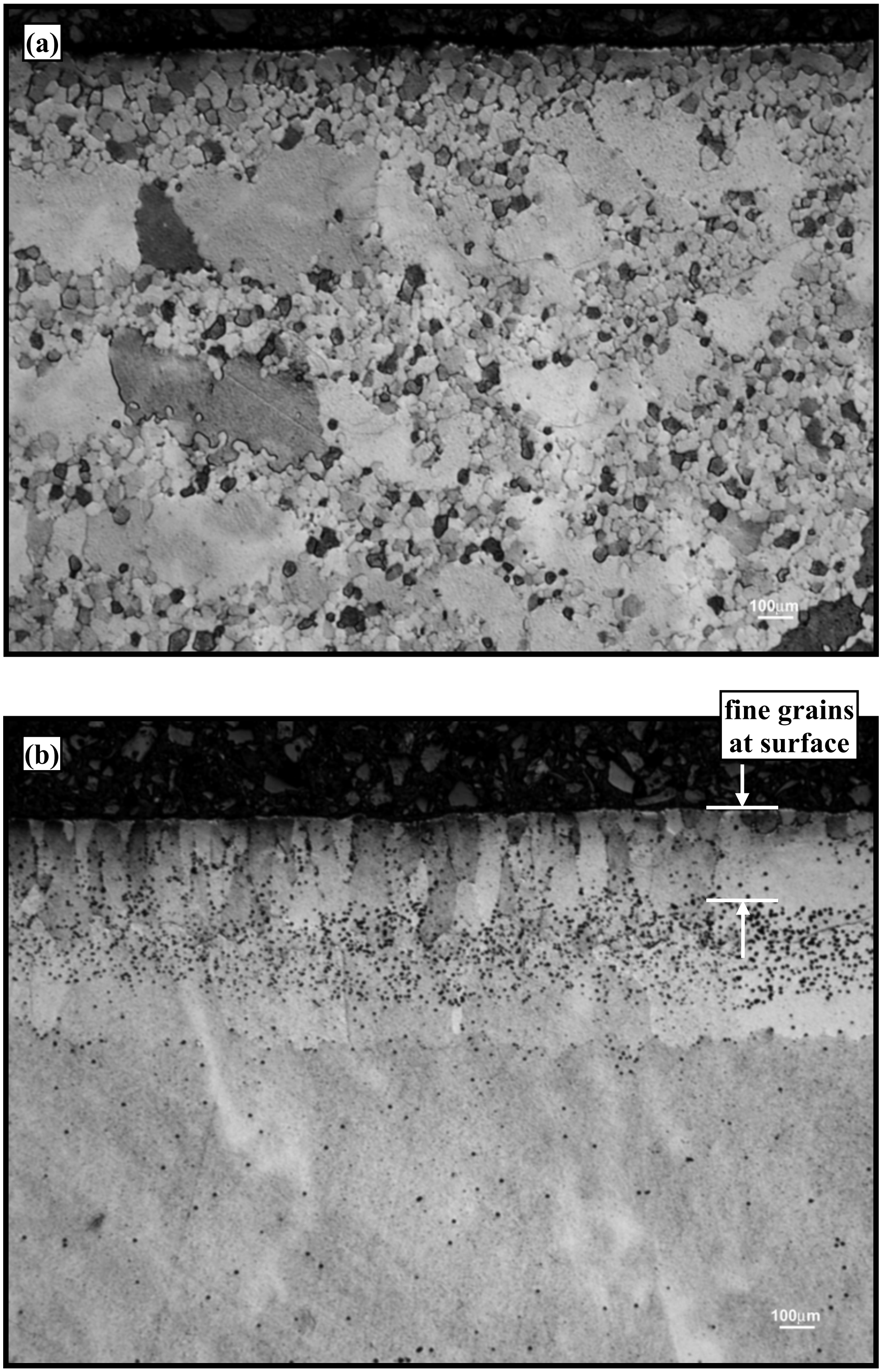

Figure 5.30 Defects in PM2000 material: (a) unwanted fine grains in the recrystallized material 1 h, 1385 °C, (b) fine grains at the surface

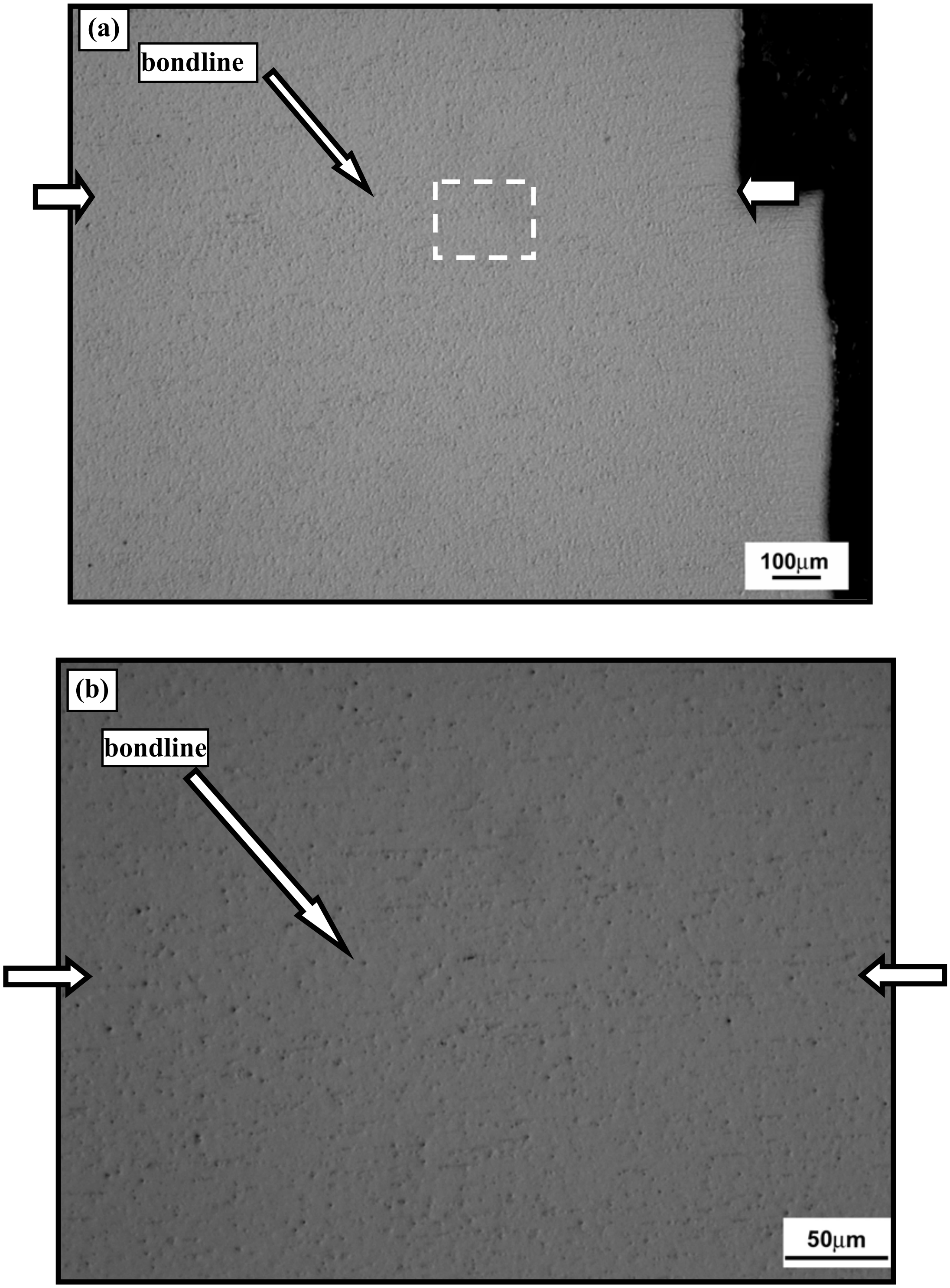

Figure 5.31 (a) PM2000 L-L orientation fine grain bond 310 s, 1250 °C (a) as-bonded (unetched) condition and (b) inset shown in (a) at higher magnification.

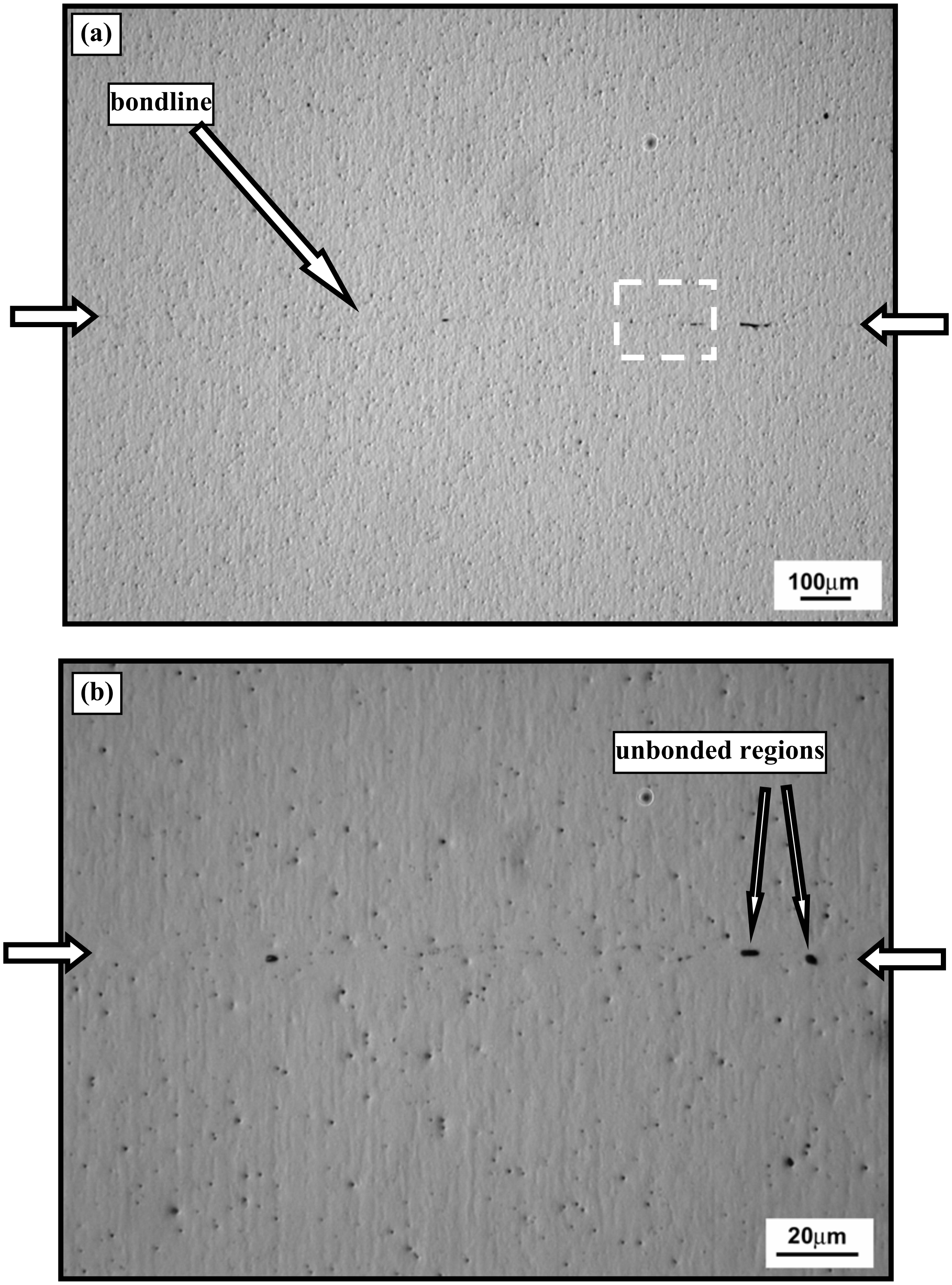

Figure 5.32 PM2000 T-T orientation fine grain bond 300 s, 1250 °C (a) as-bonded (unetched) condition and (b) inset shown in (a) at higher magnification.

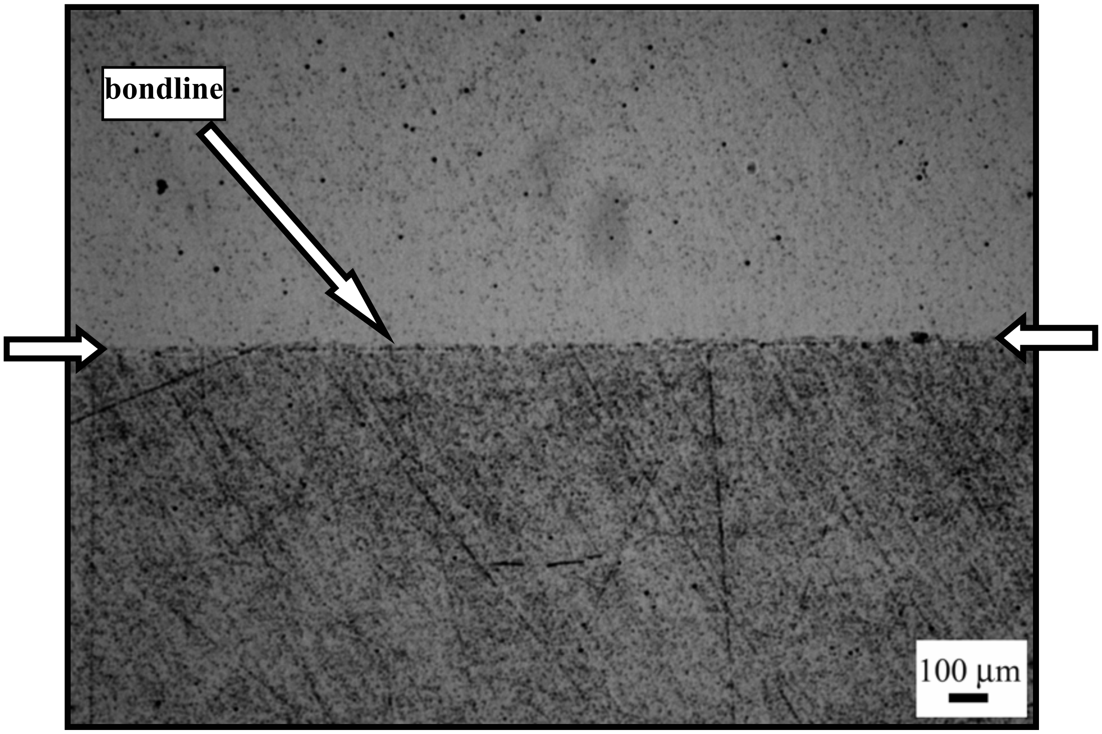

Figure 5.33 PM2000 L-L orientation fine grain bond 380 s, 1250 °C + PBHT 2 h, 1385 °C. Note: Top and bottom surfaces are two separate large substrate grains. Recrystallization occurred in the substrates but no grain growth across the bondline was observed.

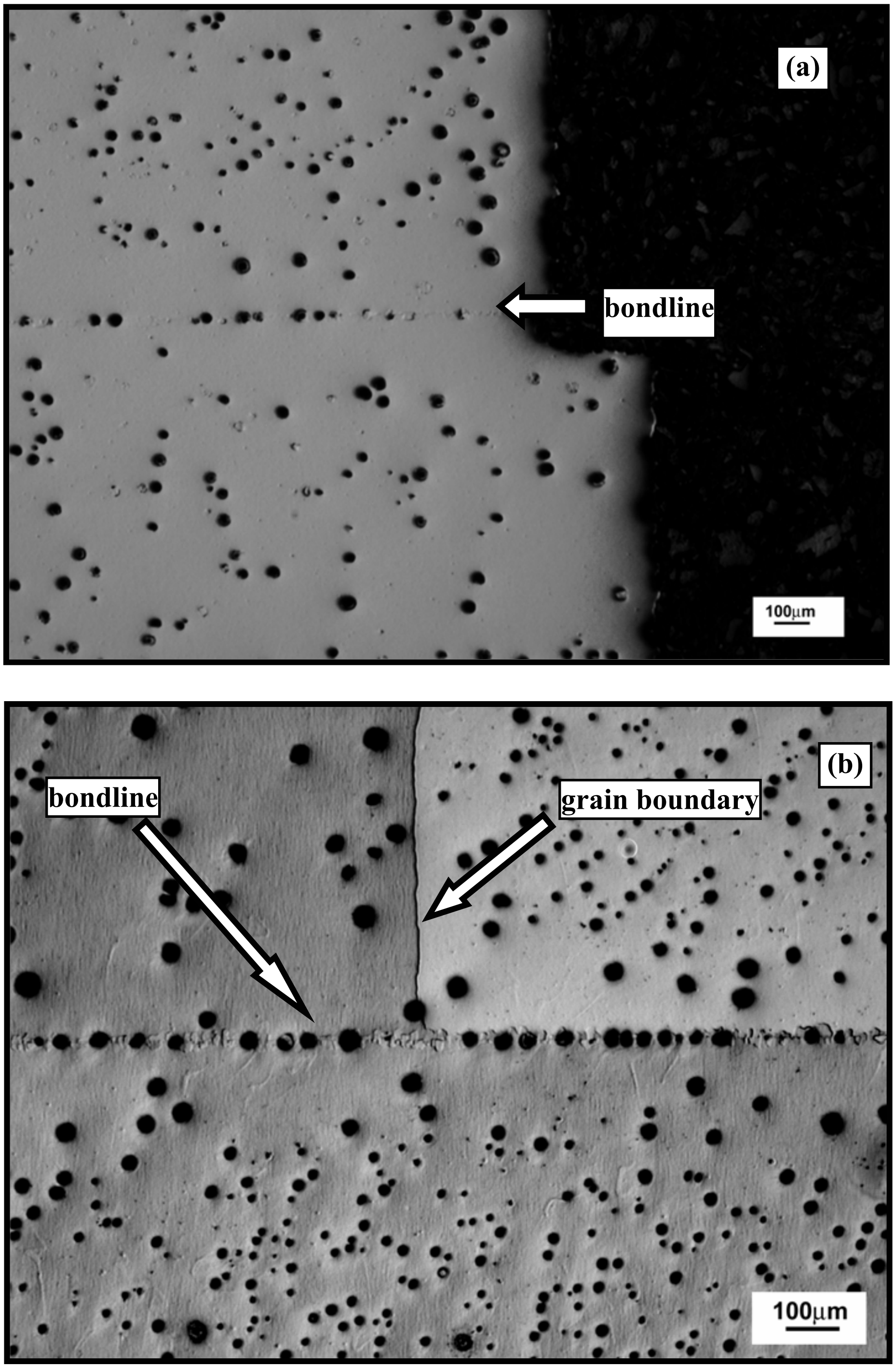

Figure 5.34 Post bond recrystallization heat treated 2 h, 1385 °C (a) L-L orientation bond, same as shown in figure 5.31 and (b) T-T orientation bond, same as shown in figure 5.32. Note: The porosity formation as a result of PBHT.

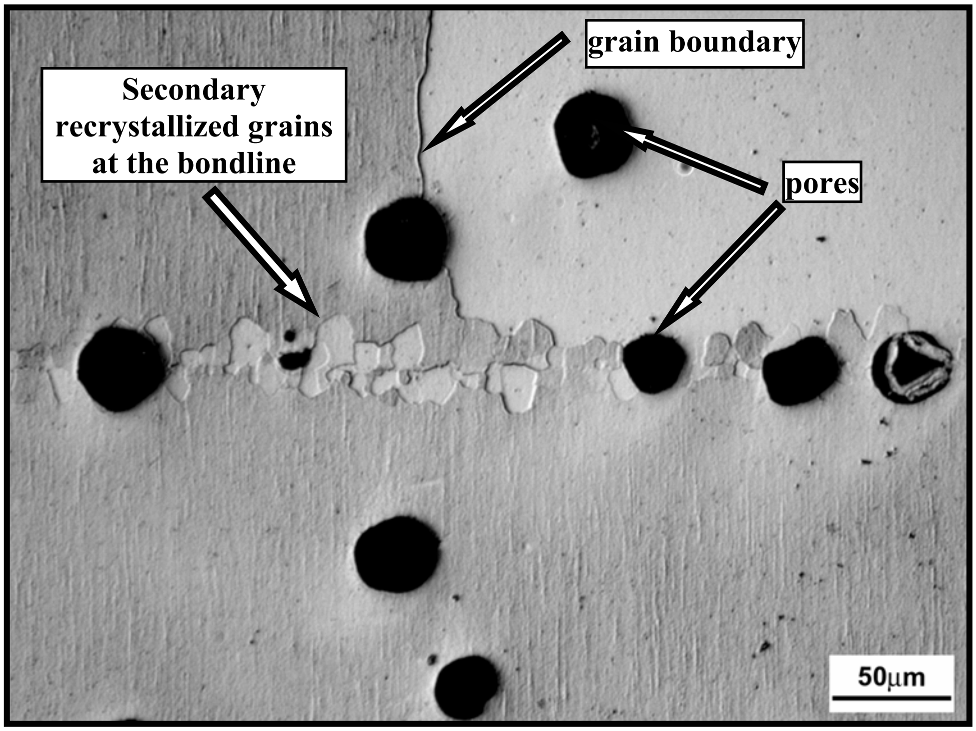

Figure 5.35 Post bond recrystallization heat treated 2 h, 1385 °C, T-T orientation bond, same as shown in figure 5.34. Note: The secondary recrystallized grains at the bondline.

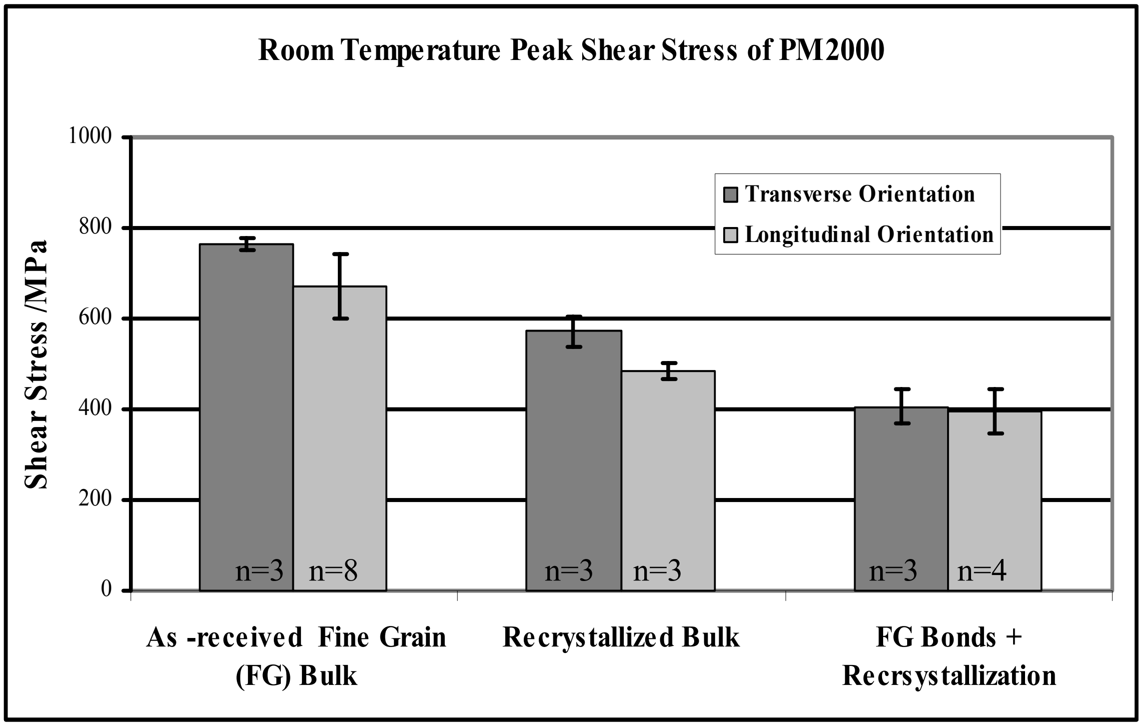

Figure 5.36 Room temperature shear tests of PM2000 in the as-received fine grain condition, recrystallized condition and bonded + recrystallized condition in both transverse and longitudinal orientations. Note the error bars represent standard deviation of the test results and n represents the number of tests conducted.

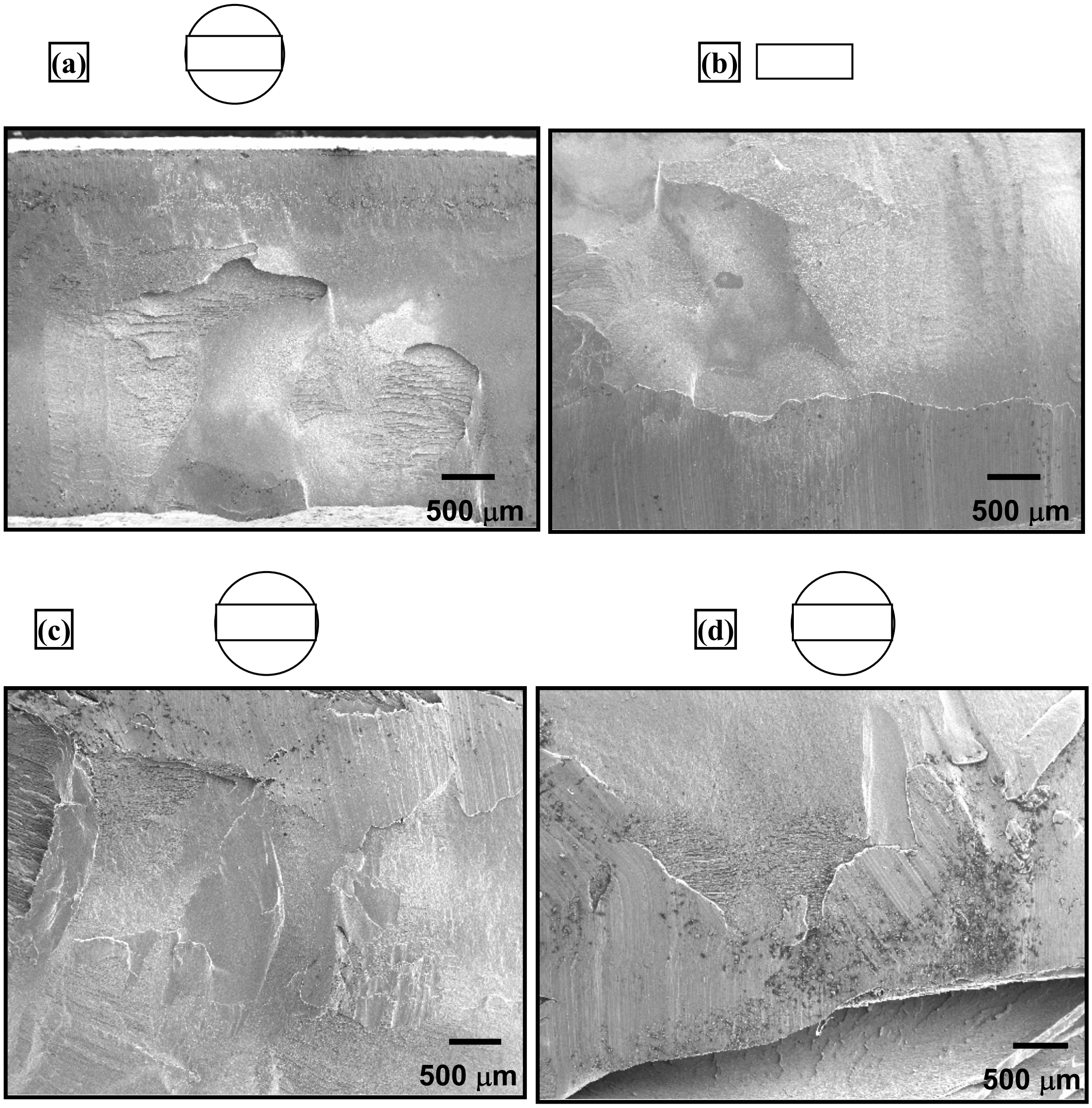

Figure 5.37 Shear test fracture surfaces of fine grain PM2000 bulk material. Schematics of the fracture specimens from which the fractographs were extracted are shown above each figure: (a) and (b) are from the two halves of a transverse sample, and (c) and (d) are from two different longitudinal samples. Notice that mostly planar shear occurred in the samples, although secondary cracking was also observed in some samples (d)

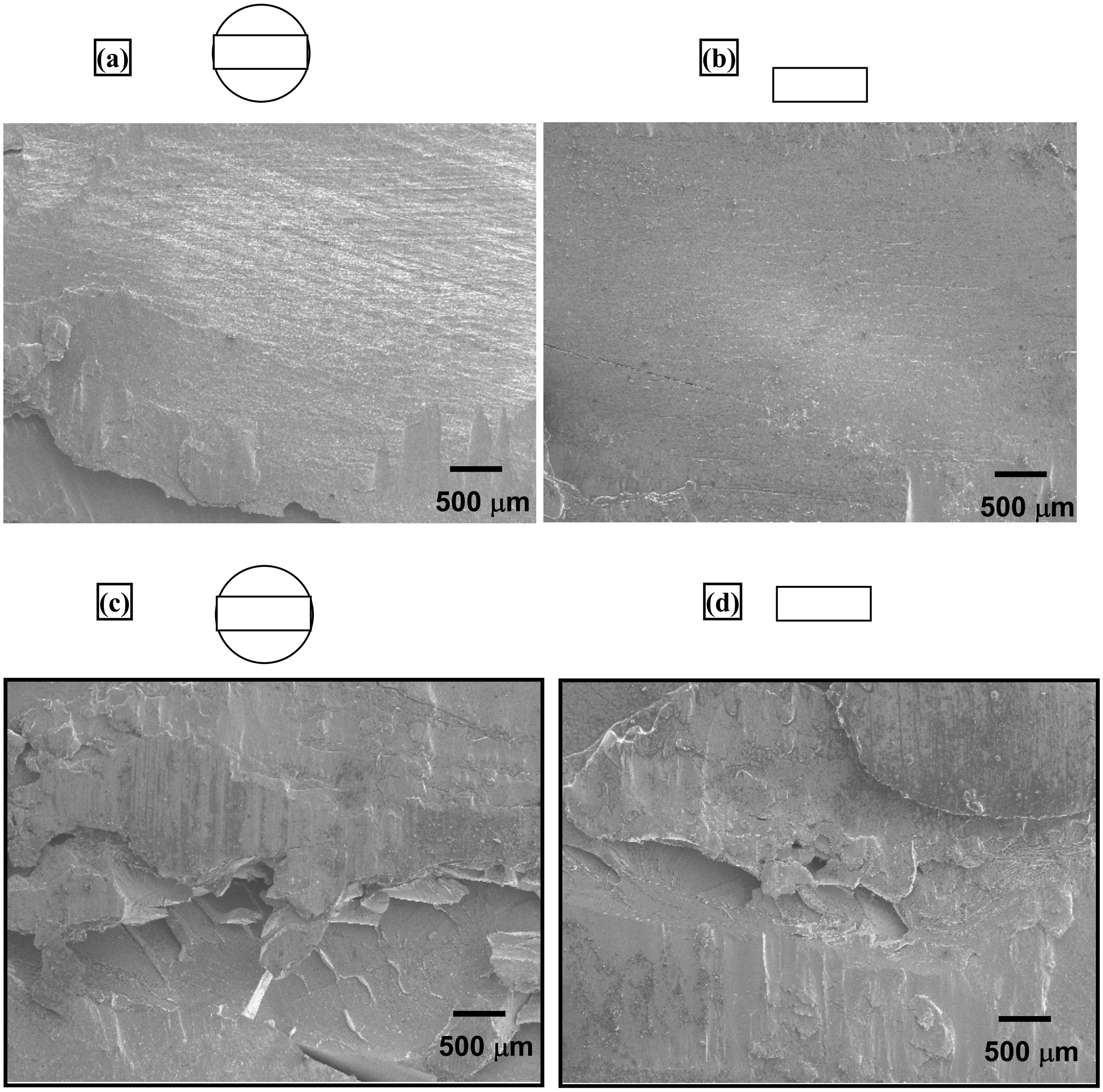

Figure 5.38 **Shear test fracture surfaces of PM2000 transverse-transverse bonds. Schematics of the fracture specimens from which the fractographs were extracted are shown above each figure: (a) and (b) 300 s, 1250 °C + PBHT 2 h, 1385 °C, mostly planar shear cracking, and (c) and (d) 309 s, 1250 °C + PBHT 2 h, 1385 °C, secondary + planar shear (mixed) cracking.**

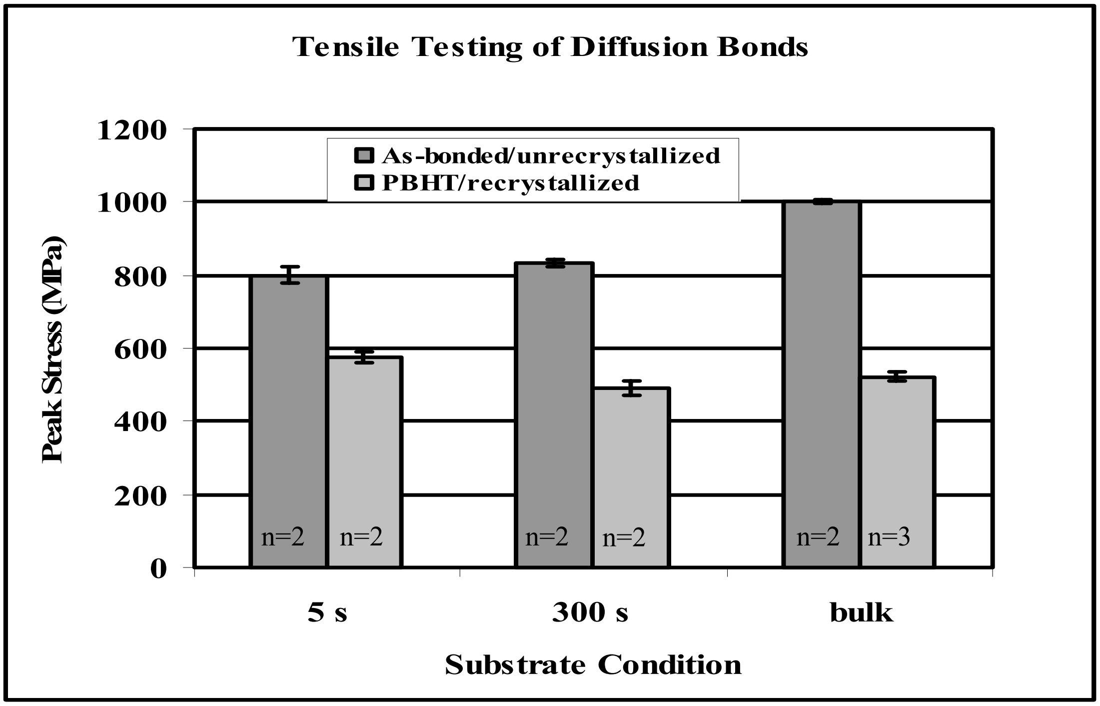

Figure 5.39 Room temperature tensile tests of PM2000 material 5 s bond, 300 s bond and bulk in the unrecrystallized (■) and recrystallized (□)conditions. Note the error bars represent standard deviation of the test results and n represents the number of samples tested.

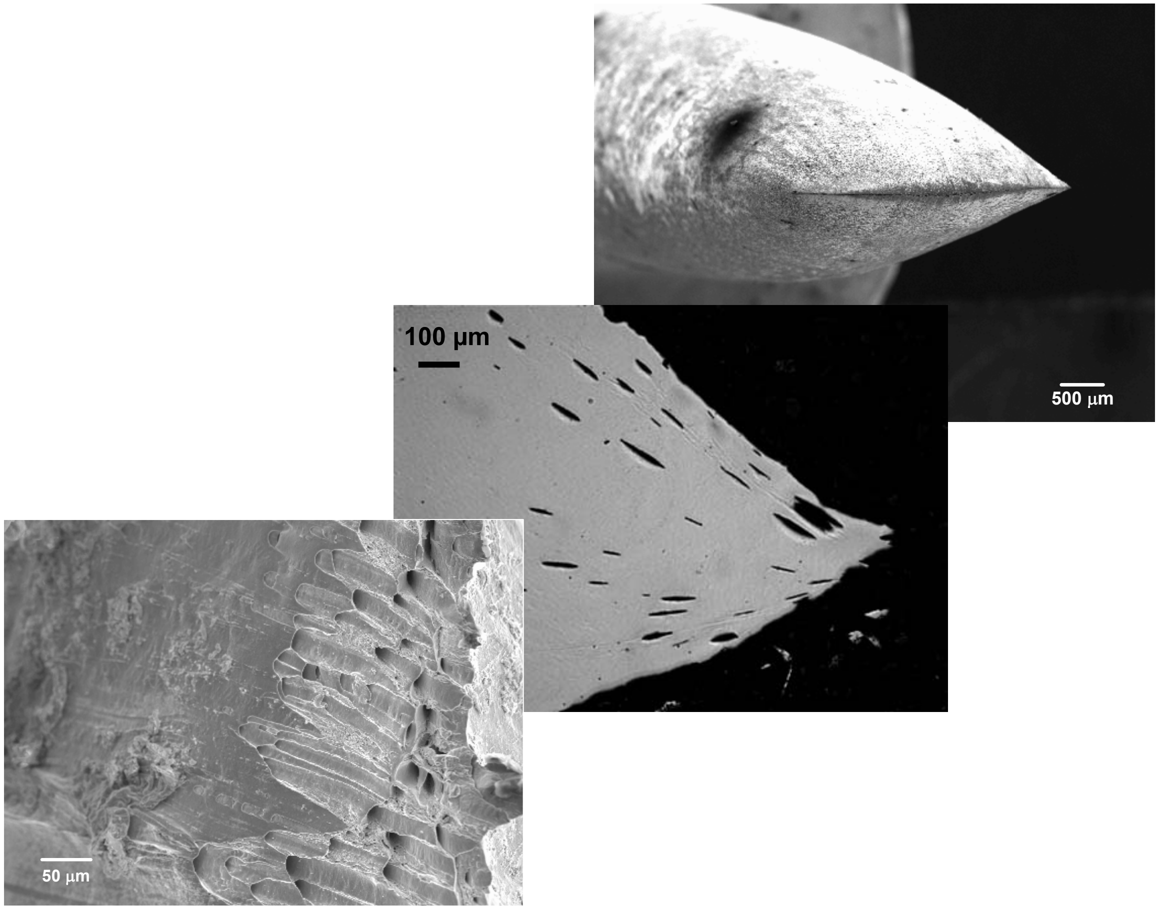

Figure 5.40 PM 2000 Creep rupture sample that failed soon after reaching 1000 ºC at a load of 85 MPa (top = fracture surface overview, middle = cross-section, bottom = fracture surface detail). Note the apparent effect of the elongated microstructure on the macroscopic shape of the fracture surface.

6. CONCLUSIONS

6.1. Transient Liquid Phase Bonding

1. TLP bonding was successfully used to join ferritic oxide dispersion strengthened alloys, MA956 and PM200, using physical vapor deposited thin film boron coatings as interlayers. The use of thin films as interlayers reduced dissolution of the substrate, yttria agglomeration and formation of second phase precipitates at the bondline.

2. Bonds joined in the longitudinal-longitudinal (L-L) orientation (i.e., both the substrates aligned parallel to the working direction) resulted in better microstructural continuity than either the transverse-transverse (T-T) or longitudinal-transverse (L-T) bond orientations. This was attributed to the number of yttria stringers cut by the bondline. In the L-L orientation, the disturbance of these stringers' alignment was less than in the L-T and T-T orientations, hence retaining the parent metal microstructure.

3. Fine grain material resulted in better microstructural continuity across the bondline than coarse grain material. Bonding conducted in the fine grain condition encouraged grain growth across the bondline, unlike when using

a coarse grain material which has already undergone recrystallization. Faster dissolution of the substrate, due to the significant contribution from the grain boundaries, occurs when using a fine grain material. Grain boundaries increase the liquid penetration and decrease the boron available at the bondline to an amount low enough that secondary recrystallization does not take place.

4. A large amount of porosity is developed during recrystallization heat treatment, both in the bulk and in the bond. This can be attributed to the release of gases trapped in the material during mechanical alloying.

6.2. Solid-State Diffusion Bonding

1. A diffusion bonding process was successfully developed for ferritic oxide dispersion strengthened alloys, MA956 and PM2000, under unusually low stresses of 1-5 MPa, at a bonding temperature of 1250 °C and for short bonding times of 6-8 minutes using unrecrystallized fine grain material.

2. Successful bonding occurred only when fine grain material was used. This was attributed to the enhanced material transfer through grain boundary diffusion, which increases the rate of bonding and the bonding area between the two faying surfaces.

3. The bonding of the longitudinal orientation specimens resulted in bonds with a higher room temperature shear stress (average of 80% bulk strength) than for transverse-transverse orientations (average of 70% bulk strength) as compared with the bulk shear stress.

4. Room temperature tensile testing of bonds found them to have strengths between 83% and 110% of that of the bulk PM2000 subjected to the same thermal cycle. Comparison of the bonds in the as-bonded and PBHT conditions was made with unrecrystallized and recrystallization heat treated bulk material, respectively. An increase in the bond tensile strength with increase in the bonding time was observed. However, a decrease in the bond strength was observed after heat treatment, which was mainly attributed to the porosity developed during post bond heat treatment.

6.3. Bulk Material

1. Large variations in the material properties were observed in the current study. Only partial recrystallization took place in MA956, even after prolonged recrystallization heat treatment (8 h, 1300 °C). This was attributed to prior thermomechanical heat treatments.

2. Porosity was developed during recrystallization heat treatment in PM2000. This was attributed to the release of the gases that were trapped in the

alloy during the mechanical alloying process. Region to region differences in composition, porosity and response to recrystallization were observed along the length of the as-received bars.

7. FUTURE WORK

a) Porosity Reduction

TLP and diffusion bonding were successfully used to join the as-received MA956 and PM2000. However, the defects in these materials, including partial recrystallization in MA956 and a large amount of porosity in PM2000, prevented any improvement in either their bulk or joint performance. It is highly desirable to reduce the porosity in these materials, and the use of a dual stage heat treatment might yield good results. Dual stage heat treatment includes annealing the material at a temperature well below the recrystallization temperature such that it promotes the release of any trapped gases from the material without influencing the recrystallization phenomena followed by recrystallization heat treatment to obtain coarse columnar grain structure.

b) Creep Testing

Mechanically alloyed oxide dispersion strengthened alloys exhibit excellent creep strength [5]. In order to evaluate the high temperature properties of the bonds, TLP and solid-state diffusion bonds should be prepared using PM2000 and the bonds should be tested for creep properties. The microstructures of samples that have undergone creep should be investigated using SEM and transmission electron microscopy (TEM).

c) Development of Novel Interlayers

The present research helped to understand the process of microstructural development and the relationship with mechanical properties. However, the use of thin interlayers of the order of μm is difficult in industrial settings. Hence, the development of wide-gap interlayers of the order of tens or hundreds of μms that melt well below the respective recrystallization temperatures of the ODS alloys would be highly beneficial in order to avoid any adverse effects of recrystallization. ODS alloy powders developed using internal oxidation technique mixed with a separate eutectic liquid former, such as, an Fe-B alloy, may be used for wide-gap interlayers. Preannealing heat treatments might reduce the large amounts of stored energy in the mechanically alloyed ODS alloys, which is required to obtain coarse columnar grain structure. Hence, the bonding temperature should be kept well below the substrate recrystallization temperature in order to reduce the influence of recrystallization phenomena on the microstructural development during the bonding cycle.

In order to reduce the base metal dissolution, Fe-B interlayers should be investigated. The Fe-B interlayer melts when heated above the eutectic temperature and forms the eutectic liquid. This minimizes the microstructural disruption of the base metal as the eutectic liquid forms without requiring to reacting with the base metal.

d) Dissimilar Metal Joining

Industrial applications, in general, require joining of a material to itself or dissimilar materials. Joining of MA ODS alloys to conventional alloys is also being considered for applications in the nuclear industry. Hence, it would be of considerable interest to investigate joining techniques for MA ODS with other nuclear grade materials such as ferritic/martensitic stainless steels, austenitic steels, Ni-base alloys or ceramic materials.

e) Boron Induced Secondary Recrystallization

Wavelength dispersive spectroscopy (WDS) may be used to conduct light weight elemental analysis. The above techniques may be used to develop boron diffusion profiles in the bonds. Boron induced secondary recrystallization may be investigated by correlating the boron diffusion profiles to the bond microstructural development.

f) Influence of Grain Size

The above mentioned characterization technique along with electron back scatter diffraction and electron channeling patterns may be used to investigate the influence of grain size on the ODS alloy bond microstructural development [102]. Detailed grain boundary dissolution in ODS alloys may be studied in order to understand the influence of grain boundary energy and texture on the planarity of the solid/liquid interface and hence, on solid/liquid interfacial area and thus diffusion of boron into the substrate.

g) Recrystallization Phenomenon in Bulk ODS Alloys

In general, mechanically alloyed ODS alloys upon recrystallization heat treatment result in coarse columnar grain structure. However, only partial recrystallization occurred in MA956 material, unlike PM2000. Differences in the recrystallization behavior were also observed in the same batch. In order to understand the recrystallization behavior in the bulk and the bonds, detailed prior thermomechanical history of the MA ODS alloys is needed. A detailed statistical analysis of the material in the unrecrystallized fine grain condition including grain size, grain orientation, yttria dispersion and the material's response to recrystallization heat treatment should be investigated.

h) Effects of Oxide Chemistry and Grain boundaries on Diffusion Bonding

In general, it is very difficult to join materials which form a continuous oxide layer, e.g. alumina, on the faying surface using diffusion bonding. In this current work, diffusion bonding occurred at low stresses, although the ferritic ODS alloys are likely to be alumina formers. In the past, Maddrell [116] observed, during diffusion bonding of aluminum alloys, that variation in the local oxide chemistry lead to the formation a discontinuous oxide layer. This results in the formation of exposed metal surfaces, which contribute to the diffusion bonding of the metals. Likewise, in the present case, a mixture of alumina and yttria should be present on the faying surfaces. In other experiments [117], Gale and Wallach observed oxide layer discontinuities, such as, shear type cracks associated with the formation of voids in the grain boundary under the oxide. It would therefore be interesting to investigate the influence of the oxide chemistry and the grain boundaries at the substrate faying surface on the diffusion bonding of the ODS alloys.

REFERENCES

1. Annual Energy Outlook 2005 with Projections to 2025, Report #: DOE/EIA-0383(2005) (http://www.eia.doe.gov/oiaf/aeo/ 07/05/2005)
2. F. L. VerSnyder: “Superalloy Technology – Today and Tomorrow”, High Temperature Alloys for Gas Turbines, Conference Proceedings, Liège, Belgium, 4-6 October, 1982. ed. R. Brunetud et al., D. Reidel Publishing Company, England, pp. 1- 49.
3. J. J. deBarbadillo: “Product Development in the 1990s – Adapting to a New Paradigm”, Heat-Resistant Materials II, Conference Proceedings of the 2nd International Conference on Heat-Resistant Materials, 11-14 September, 1995, Gatlinburg, Tennessee, ed. K. Natesan, P. Ganesan and G. Lai, ASM INTERNATIONAL, Materials Park, OH, pp. 1-10.
4. J. Stringer: “Applications of High-Temperature Materials Heat-Resistant Materials II, Conference Proceedings of the 2nd International Conference on Heat-Resistant Materials, 11-14 September, 1995, Gatlinburg, Tennessee, ed. K. Natesan, P. Ganesan and G. Lai, ASM INTERNATIONAL, Materials Park, OH, pp. 19-29.
5. J. S. Benjamin: “Dispersion Strengthened Superalloys by Mechanical Alloying”, Met. Trans., 1970, Vol. 1, pp. 2943-51.

6. D. Mukhopadhyay: “Development of Low Activation Oxide Dispersion Strengthened Ferritic Steels for Fusion Reactors”, PhD Thesis, University of Idaho, USA, December, 1996.

7. J. J. deBarbadillo and J. J. Fisher: “Dispersion-Strengthened Nickel-Base and Iron-Base Alloys”, ASM Handbook, Vol. 2, 1990, p. 943; Materials Park, OH, ASM International.

8. C. White: “Oxide Dispersion Strengthened (ODS) Alloys” in “Research and Development of High Temperature Materials for Industry”, ed. E. Bullock et al., 1989, pp. 71-78.

9. Ch. Lecomte-Mertens, A. Magnée, L. Coheur, J.J. Heut, and C. Driesen: “O.D.S. Ferritic Steels with high Damping Capacity”, High Temperature Alloys for Gas Turbines, Conference Proceedings, Liège, Belgium, 4-6 October, 1982. ed. R. Brunetud et al., D. Reidel Publishing Company, England, pp. 737-45.

10. “Dispersion-Strengthened-High-Temperature Materials: Material Properties and Applications”, Information Brochure, Plansee, Metallwerk Plansee GmbH/ Lechbruck, Germany, 2005.

11. S. Yamashita, S. Watanabe, S. Ohnuki, H. Takahashi, N. Akasaka, and S. Ukai: “Effect of mechanical alloying parameters on irradiation damage in oxide dispersion strengthened ferritic steels”, J. Nucl. Mater., 2000, Vol. 283-287 (1), pp. 647-51.

12. W. G. Johnston, J. H. Rosolowski, A. M. Turkalo, and T. Lauritzen: “An Experimental Survey of Swelling in Commercial Fe-Cr-Ni Alloys Bombarded with 5Mev Ni ions”, J. Nucl. Mater., 1974, Vol. 54, pp. 24-40.

13. J. J. Fischer: “Dispersion Strengthened Ferritic Alloy for Use in Liquid-Metal Fast Breeder Reactors (LMFBRS)”, US Patent No. 4,075,010, February 21, 1978.

14. M. L. Hamilton, D. S. Gelles, R. J. Lobsinger, G. D. Johnson, W. F. Brown, M. M. Paxton, R. J. Puigh, C. R. Eiholzer, C. Martinez, and M. A. Blotter: “Fabrication Technological Development of the Oxide Dispersion Strengthened Alloy MA957 for Fast Reactor Applications”, Report, DOE-ER-7552/2, February, 2000.

15. D. S. Gelles: “Microstructural Evolution of Commercial Ferritic Alloys at 200 DPA”, Conf. Proc. “Fusion Reactor Materials 7th International Conference”, November 1995, Russia, U.S. DOE under Contract No. DE-AC06-76RLO 1830.

16. D. O’ Donnell: “Joining of Oxide-Dispersion- Strengthened Materials”, ASM Handbook, Vol. 6, 1990, ASM INTERNATIONAL, Materials Park, OH, pp. 1037-1040.

17. T. J. Kelly: “Welding of Mechanically Alloyed ODS Materials”, in Trends in Welding Research in the United States, proceedings, ed. S.A. David, ASM, Materials Park, OH, 1982, pp. 471-78.

18. L. E. Shoemaker: “Joining Techniques for a Ferritic Oxide Dispersion Strenghtened Alloy”, Proceedings of the International Conference on Trends in Welding Research”, ed. S. A. David, ASM, Materials Park, OH, 1986, pp. 371-77.

19. C. Y. Kang, T.H. North, and D.D. Perovic: “Microstructural Features of Friction Welded MA956 Superalloy Material”, Metall. Mater. Trans. A, 1996, Vol. 27A, pp. 4019-29.

20. J. R. Stringer: “Alloys for Advanced Power Systems”, Heat-Resistant Materials, Proceedings of the First International Conference, 23-26 September, 1991, Fontana, Wisconsin, USA, ed. K. Natesan and D. J. Tillack.,ASM INTERNATIONAL, Materials Park, OH, pp. 9-23

21. M. H. Van de Voorde: “Advanced High Temperature Materials” in “Research and Development of High Temperature Materials For Industry”, ed. E. Bullock et.al., Elsevier Applied Science, pp. 1-9.

22. P. S. Gilman, and J. S. Benjamin: “ Nickel- and Iron-Based Dispersion Strengthened Alloys” in Dispersion-Strengthened Materials, Metals Handbook, 1984, 9th edn., vol. 7, ASM International, Metals Park, OH, pp.722-727.

23. W. D. Coolidge, US Patent No. 1082933, 1913.

24. M. Rühle, T. Steffens, and K. Zöltzer, “Structural Characterization of Mechanically Alloying Process” in “High Temperature Materials For Power Engineering”, Proceedings of a Conference, Liège, Belgium, 24-27 September, 1990, pp. 1431-1442.

25. C. Suryanarayana, E. Ivanov, and V.V. Boldyrev: “The Science and Technology of Mechanical Alloying”, Materials Science and Engineering A, 2001, Vol. 304-306, pp. 151-58.

26. J. S. Benjamin, and T. E. Volin: "The Mechanism of Mechanical Alloying", Met. Trans.,1974, Vol. 5, pp. 1929-34.

27. J.S. Benjamin: "Mechanical Alloying", Sci. Am., 1975, Vol. 234 (5), pp. 40-48.

28. P. S. Gilman, and J. S. Benjamin: "Mechanical Alloying", Ann. Rev. Mat. Sci., 1983, Vol. 13, 279-300.

29. C. C. Koch: “Materials Synthesis by Mechanical Alloying”, Ann. Rev. Mat. Sci., 1989, Vol. 19, pp. 121-43.

30. M. Sherif El-Eskandarany: Mechanical Alloying for Fabrication of Advanced Engineering Materials, William Andrew Publishing, NY, USA

31. C. Suryanarayana: ASM Handbook, 10th edn., Vol. 7, p 80; Materials Park, OH, ASM International.

32. Y. L. Chen and A. R. Jones: “Reduction of Porosity in Oxide Dispersion-Strengthened Alloys Produced by Powder Metallurgy”, Metall. Mater. Trans. A, 2001, Vol. 32A, pp. 2077-2084.

33. Y. L. Chen, A. R. Jones, and U. Miller: “Origin of Porosity in Oxide-Dispersion-Strengthened Alloys Produced by Mechanical Alloying”, Metall. Mater. Trans. A, 2002, Vol. 33A, pp. 2713-2718.

34. J. L. González-Carrasco, V. Guttmann, and H. Fattori: “Void Formation during Oxidation of the ODS Alloy MA 6000”, Metall. Mater. Trans. A, 1995, Vol. 26A, pp. 915-924.

35. M. Turker: “Formation of Porosity in Ferritic ODS Alloys on High Temperature Exposure”, J. Mater. Sci., 2005, Vol. 40, pp. 1201-1208.

36. D. Haussler, B. Reppich, M. Bartsch, and U. Messerschmidt: “Interaction Processes between Dislocations and Particles in the ODS Nickel-base Superalloy INCONEL MA 754 Studied by means of In-situ Straining in an HVEM”, Mater. Sci. Eng., 2001, Vol. A 309-310, pp. 500-04.

37. H. K. D. H. Bhadeshia: “Recrystallization of Practical Mechanically Alloyed Iron-Base and Nickel-Base Superalloys”, Mater. Sci. Eng., 1997, Vol. A 223, pp. 64-77.

38. G. Korb and D. Sporer: “Recrystallization Behaviour of PM 2000 Oxide Dispersion Strengthened Iron-Base Superalloy” in “High Temperature Materials For Power Engineering”, Proceedings of a Conference, Liège, Belgium, 24-27 September, 1990, pp. 1417-1430.

39. R. S. Herrick: “Dislocation/Particle Interactions as a Function of Temperature in Oxide Dispersion Strengthened Alloys”, PhD Thesis, Northwestern University, 1991.

40. J. Markham: “The Diffusion Brazing of Nickel-Based Oxide Dispersion Strengthened Alloys”, PhD Thesis, University of Cambridge, 1998.

41. Capdevila, Y. L. Chen, A. R. Jones and H. K. D. H. Bhadeshia: “Grain Boundary Mobility in Fe-Base Oxide Dispersion Strengthened PM2000 Alloy”, ISIJ International, 2003, Vol. 43, No. 5, pp. 777-83.

42. T. Grosdidier, E. Suzon, and F. Wagner: “Primary Recrystallization in an ODS FeAl alloy: an effective way to modify Texture and Microstructure”, Intermetallics, 2004, Vol. 12, pp. 645-654.

43. T. J. Kelly: Personal communication, “7th International Conference on Trends in Welding Research”, Pine Mountain, Georgia, USA, May 16-20, 2005

44. J. W. Martin: “Discussion of the “Distribution of Dispersoid Phases in the Extruded ODS Superalloy MA-957”, Metall. Mater. Trans. A, 1994, Vol. 25A, pp. 651-652.

45. IncoMAP Datasheet: “Forming of Incoloy alloy MA 956”.

46. Wasilkowska, M. Bartsch, U. Messerschmidt, R. Herzog, and A. Czyrska-Filemonowicz: “Creep Mechanisms of Ferritic Oxide Dispersion Strengthened Alloys”, J. Mater. Process. Tech., 2003, Vol. 133, pp. 218-24.

47. M. F. Hupalo, M. Terada, A. M. Kliauga, and A. F. Padilha: “Microstructural Characterization of INCOLOY alloy MA956”, Mat-wiss. U. Werkstofftech., 2003, Vol. 34, pp. 505-08.

48. P. Krautwasser, A. Czyrska-Filemonowicz, M. Widera, and F. Carsughi: “Thermal Stability of Dispersoids in Ferritic Oxide-Dispersion Strengthened Alloys”, Mater. Sci. Eng., 1994, Vol. A 177, pp. 199-208.

49. Czyrska-Filemonowicz, and B. Dubiel: “Mechanically Alloyed, Ferritic Oxide Dispersion Strengthened Alloys: Structure and Properties”, J. Mater. Process. Technol., 1997, Vol. 64, pp. 53-64.

50. M. M. Baloch: “Directional Recrystallization in Dispersion Strengthened Alloys”, PhD Thesis, University of Cambridge, October, 1989.

51. Czyrska-Filemonowicz, and B. Dubiel: “ Mechanically Alloyed, Ferritic Oxide Dispersion Strengthened Alloys: Structure and Properties”, J. Mater. Process. Technol., 1997, Vol. 64, pp. 53-64.

52. P. Lours, J. Alexis , and G. Bernhart: “Oxidation resistance of ODS alloy PM2000 from 880 °C to 1400 °C”, J. Mater. Sci. Lett., 1998, Vol. 17, pp. 1089-93.

53. Czyrska-Filemonowicz, D. Clemens, and W. J. Quadakkers: “The Effect of High Temperature Exposure on the Structure and Oxidation Behavior of Mechanically

Alloyed Ferritic ODS Alloys", J. Mater. Process. Technol., 1995, Vol. 53, pp. 93-100.

54. Oxide Dispersion Strengthened Alloys: Publication No. SMC-004, Special Metals Corporation, Huntington, WV, USA.

55. M. Debata and G.S. Upadhyaya: "Corrosion Behavior of Powder Metallurgy Y2O3 Dispersed Iron- and Nickel-base Superalloys", J. Mater. Eng. Perform., 2001, Vol. 10 (5), pp. 602-07.

56. J. W. Brooks and P. J. Bridges: "Metallurgical Stability of Inconel Alloy 718", Conf. Proc. "Superalloys 1988", Proceedings of the Sixth International Symposium on Superalloys, ed. D. N. Duhl et al., The Metallurgical Society, September 18-22, 1988, Pennsylvania, pp. 33 – 42.

57. INCONEL® alloy MA754: Publication No. SMC-040, Special Metals Corporation, Huntington, WV, USA.

58. INCONEL® alloy MA758: Publication No. SMC-075, Special Metals Corporation, Huntington, WV, USA.

59. INCOLOY® alloy MA956: Publication No. SMC-008, Special Metals Corporation, Huntington, WV, USA.

60. PM2000: Material Data sheet ODS-Superlloy, Plansee, Metallwerk Plansee GmbH/ Lechbruck, Germany.

61. J. O. Stiegler and L. K. Mansur: "Radiation Effects in Structural Materials", Ann. Rev. Mater. Sci., 1979, Vol. 9, pp. 405-54.

62. D. Brailsford and R. Bullough: "The Rate Theory of Swelling due to Void Growth in Irradiated Metals", J. Nucl. Mater., 1972, Vol. 44, pp. 121-35.

63. H. Kinoshita, N. Akasaka, H. Takahashi, I. Shibahara, and S. Onose: “Microstructural Change on Electron Irradiated Oxide Dispersion Strengthened Ferritic Steels”, J. Nucl. Mater., 1992, Vol. 191-194(2), pp. 874-78.

64. R. S. Barnes: “A Theory of Swelling and Gas Release for Reactor Materials”, J. Nucl. Mater., 1964, Vol. 2, pp. 135-48.

65. C. Capdevila: “Oxide Coarsening and its Influence on Recrystallization in a Mechanically Alloyed Fe-Base Oxide Dispersion Strengthened Alloy”, Metall. Mater. Trans. A, 2005, Vol. 36A, pp. 1547.

66. T. W. Eager: "Challenges in Joining Emerging Materials," in Proceedings of Advances in Joining Newer Structural Materials, Proceedings, International Conference, Montreal, Canada; 23 - 25 July 1990, Pergamon Press, Oxford, pp. 3 - 14 (p. 4) (English) and pp. 15 - 29 (French), 1990.

67. P. A. Molian, Y.M. Yang, and P.C. Patnaik: “Laser Welding of Oxide Dispersion-Strengthened Alloy MA754”, J. Mater. Sci., 1992, Vol. 27, pp. 2687-94.

68. Welding and Brazing: Metals Handbook, 8th ed., ASM International, Materials Park, OH, p. 401, 451.

69. T. J. Moore, and T.K. Glasgow: “Diffusion Welding of MA6000 and a Conventional Nickel-Base Superalloy”, Weld. J., 1985. Vol. 64, pp. 219-226.

70. A. Bucklow: “Diffusion Bonding a Creep Resistant Fe-ODS Alloy”, conf. proc., Advances in Joining Newer Structural Materials, Proceedings of the International Conference, Montreal, Canada: Elmsford, NY: Pergamon. (1990), pp. 299-304.

71. G. Zhang, R. S. Chandel, H. P. Seow and H. H. Hng: “Microstructural Features of Solid-State Diffusion Bonded Incoloy MA 956”, Mater. Manuf. Processes, 2003, vol. 18: pp. 599-608.

72. Welding, Brazing, and Soldering: ASM Handbook, Vol. 6, 10th edn., ASM International, Materials Park, OH.

73. “Mechanically Alloyed Superalloys”, in Heat-Resistant Materials, ed. J. R. Davis, ASM Specialty Handbook, 1997, ASM International, Materials Park, OH, pp. 279-89.

74. D. S. Duvall, W.A. Owczarski, and D.F. Paulonis: “TLP Bonding: A New Method for Joining Heat Resistant Alloys”, Weld. J., 1974. vol. 53, pp. 203-14.

75. T. I. Khan: “The Diffusion Bonding of Oxide Dispersion Strengthened Ferritic Superalloys”, PhD Thesis, University of Cambridge, UK, 1992.

76. Y. Nakao and K. Shinozaki: “Transient Liquid Phase Diffusion Bonding of Iron Base Oxide Dispersion Strengthened Alloy MA956”, Mat. Sci. Tech., 1995, Vol. 11, pp. 304-311.

77. S. Wei: “Diffusion brazing of mechanically alloyed Oxide Dispersion Strengthened Materials”, Rare Metals, 1996, Vol. 15(1), pp. 16-22.

78. Hill and E. R. Wallach: “Modelling Solid-State Diffusion Bonding”, Acta Metall.¸ 1989, Vol. 37(9), pp. 2425-37.

79. M. G. Nicholas: “Joining Processes”. Kluwer Academic Publishers, The Netherlands, 1988.

80. T. W. Eager: “Processes of Joining Materials”, http://web.mit.edu/ 3.37/www/ chapter.shtml (06/09/2005).

81. J. T. Niemann and R. A. Garret: "Eutectic Bonding of Boron-Aluminum Structural Components", Weld. J., 1974, pp. 175 s - 183 s.

82. W. A. Owczarski: "Eutectic Brazing of Zircalloy 2 to Type 304 Stainless Steel", Weld. J. 1962, pp. 78 s – 83 s.

83. Tuah-poku, M. Dollar, and T. B. Massalski: "A Study of the Transient Liquid Phase Bonding Process Applied to a Ag/Cu/Ag Sandwich Joint", Metall. Mater. Trans. A, 1998, Vol. 19A(3), pp. 675-86.

84. H. Nakagawa, C. H. Lee, and T. H. North, "Modelling of Base Metal Dissolution Behavior During Transient Liquid Phase Brazing", Metall. Mater. Trans. A, 1991, Vol. 22A, pp. 543-55.

85. Y. Zhou, W.F. Gale, and T.H. North: "Modelling of Transient Liquid Phase Bonding", Int. Mater. Rev., 1995, 40(5), pp. 181-96.

86. S. R. Cain, J. R. Wilcox, and R. Venkataraman: "A Diffusional Model for Transient Liquid Phase Bonding", Acta Mater., 1997, Vol. 45, pp. 701-07.

87. W. D. MacDonald and T. W. Eagar: "Transient Liquid Phase Bonding", Ann. Rev. Mater. Sci., 1992, Vol. 22, pp. 23-46.

88. C. W. Sinclair, G. R. Purdy, and J. E. Morral: "Transient Liquid-Phase Bonding in Two-Phase Ternary Systems", Metall. Mater. Trans. A, 2000, Vol. 31A, pp. 1187-92.

89. A. A. Shirzadi and E. R. Wallach: "Analytical Modelling of Transient Liquid Phase (TLP) Bonding when a Temperature Gradient is Imposed", Acta Mater., 1999, Vol. 47(13), pp. 3551-60.

90. W. F. Gale and D. A. Butts: “Transient Liquid Phase Bonding”, Sci. Technol. Weld. Join., 2004, Vol. 9(4), pp.283-300.

91. M. J. Alinger, G. R. Odette, and G. E. Lucas: “Tensile and Fracture Toughness Properties of MA957: Implications to the Development of Nanocomposited Ferritic Alloys”, J. Nucl. Mater., 2002, Vol. 307–311, pp. 484–489.

92. S. Weinbruch, A. Anastassiadis, H. M. Ortner, H. P. Martinz, and P. Wilhartitz: "On the Mechanism of High Temperature Oxidation of ODS Alloys: Significance of Yttrium Depletion within the Oxide Scales”, Oxid. Met., 1999, Vol. 51, No. 112, pp. 111-128.

93. http://www.chaindustries.com/mark50.html

94. ASM Binary Alloy Phase Diagram Collection, ASM International, Materials Park, OH

95. P. Yan and E. R. Wallach: “Diffusion Bonding of TiAl”. Intermetallics, 1993, Vol. 1, pp. 83-97.

96. T. S. Chou: “Recrystallization Behavior and Grain Structure in Mechanically Alloyed Oxide Dispersion Strengthened MA956 Steel”, Mat. Sci. Eng., Vol. A223, 1997, 78-90.

97. T. S. Chou and H. K. D. H. Bhadeshia: “Crystallographic Texture in Mechanically Alloyed Oxide Dispersion Strengthened MA956 and MA957 Steels”, Met. Trans. A, Vol. 24A, 1993, pp. 773-79.

98. A.Ekrami, T. I. Khan, and H. Malik: “Effect of transient liquid phase diffusion bonding on properties of ODS nickel alloy MA758”, Mat. Sci. Technol., Vol. 19 (1), 2003, pp. 132-136.

99. W. F. Gale and E. R. Wallach: “Microstructural Development in Transient Liquid Phase Bonding”, Metall. Trans. A, 1991, Vol. 22A, pp. 2451-57.

100. P. E. Busby and C. Walls: Journal of Metals, 1953, pp. 1463-68.

101. W. Wang, S. Zhang and X. He: Acta. Metall. Mater., Vol. 43(4), 1995, pp. 1693-99.

102. H. Kokawa, C. H. Lee and T. H. North: “Effect of Grain Boundaries on Isothermal Solidification during Transient Liquid Phase Brazing”, Met. Trans. A, Vol. 22A, 1991, pp. 1627-31.

103. A.Y. Badmos: “Some Properties of Mechanically Alloyed Oxide Dispersion Strengthened Metals”, Ph.D. Thesis, University of Cambridge, October 1997.

104. G. Gottstein and L. S. Shvindlerman: “Grain Boundary Migration in Metals : Thermodynamics, Kinetics, Applications”, Ed. B. Ralph, CRC Press, 1999, pp. 339, Boca Raton, Florida, USA.

105. W. Sha and H. K. D. H. Bhadeshia: “Modelling of Recrystallization in Mechanically Alloyed Materials”, Mat. Sci. Eng. A, Vol. 223 (1-2), 1997, pp. 91-98.

106. C. Capdevila and H. K. D. H. Bhadeshia: “Manufacturing and Microstructural Evolution of Mechanically Alloyed Oxide Dispersion Strengthened Superalloys”, Adv. Eng. Mater., Vol. 3(9), 2001, pp. 647-56.

107. C. Capdevila and H. K. D. H. Bhadeshia: “Influence of Deformation on Recrystallization of an Yttrium Oxide Dispersion Strengthened Iron Alloy (PM2000)”, Adv. Eng. Mater., Vol. 5(4), 2003, pp. 232-37.

108. C. Capdevila and H. K. D. H. Bhadeshia: “Deformation and Recrystallization of a Yttria Disperion-Strengthened Mechanically Alloyed Iron (MA957)”, Conf. Proc. “Proceedings of the 21st Risø International Symposium on Materials Science: Recrystallization – Fundamental Aspects and Relations to Deformation Microstructure”, ed. N. Hansen et al., Denmark, 2000.

109. C. Capdevila, Y. L. Chen, N. C. K. Lassen, A. R. Jones and H. K. D. H. Bhadeshia: “Heterogeneous Deformation and Recrystallization of Iron Base Oxide Dispersion Strengthened PM2000 Alloy”, Mater. Sci. Technol., 2001, Vol. 17, pp. 693 – 699.

110. Ekrami and T. I. Khan: “Transient liquid phase diffusion bonding of oxide dispersion strengthened nickel alloy MA758”, Mat. Sci. Technol., Vol. 15 (8), 1999, pp. 946-50.

111. H. D. Hedrich and H. G. Mayer, G. Haufler, and M. Kopf: “Joining of ODS-Superalloys”, Conf. Proc. “High Temperature Materials for Power Engineering 1990”, Liège, Belgium, 24-27 September, 1990, pp.789-98.

112. D. Nobili, F. Mezzetti and E. Susi De Maria: “Study of the Kinetics of Recrystallization of Dispersions-Strengthened (A/Al2O3) Alloys”, J. Mater. Sci., Vol. 3, 1968, pp. 282-87.

113. J. M. Pénisson and T. Vystavel: “Wetting of Molybdenum Grain Boundary by Nickel: Effect of the Boundary Structure and Energy”, Acta. Mater., Vol. 48, 2000, pp. 3303-3310.

114. B.S. Bokstein, V.S. Gostomelskii, V.A. Ivanov, A.L. Petelin, and S.A. Petelin: “Kinetics of Diffusion Pores Dissolving at Intercrystalline Boundary under

Coinfluence of Compressive Stresses and Capillary Forces", Mater. Lett., Vol. 39(1), 1999, pp. 77-79.

115. N. Orhan, M. Aksoy, and M. Eroglu: "A New Model for Diffusion Bonding and its Application to Duplex Alloys", Mater. Sci. Eng., Vol. A271, 1999, pp. 458-68.

116. E. R. Maddrell: "Diffusion Bonding of Aluminium Alloys", Ph.D. Thesis, University of Cambridge, 1989.

117. W. F. Gale and E. R. Wallach: "Reinitiation of Substrate Oxide Undermining by Ni-P Filler Metals during Wetting of Nickel-base Alloy", J. Mater. Sci., Vol. 28, 1993, pp. 243-248.

118. L. N. Payton, S. V. Chitti, D. R. Taarea, N. I. Sofyan, W. F. Gale, D. A. Butts, R. Aluru, and V. G. Krishnardula: "Hot-Stage Light Microscopy Studies of the Wettability of Nickel-BaseSuperalloys during Transient Liquid Phase Bonding" Proc. Intl. Conf. Join. Adv. Spl.Matl. VI, Pittsburgh, PA, In Press, October 2003.

APPENDIX

Porosity and composition survey of PM2000 bars: Surveys were conducted on 25 mm (1 in) diameter x 1.52 m (60 in) long PM2000 and 51 mm (2 in) diameter x 419 mm (19.5 in) long bars to check for the presence of inhomogeneities or defects, such as fine grain formation on recrystallization, and to verify any variations in the composition along the length of the bar. The survey was conducted by extracting 18 mm x 12.5 mm (longitudinal x transverse) samples from six different regions spread uniformly along the length of the 25 mm (1 in) bar, along with 16 mm x 24.5 mm (longitudinal x transverse) samples from the two ends and center of the 51 mm (2 in) bar. To see the effects of bonding thermal cycle on the recrystallization of the PM2000 fine grain condition material, two different heat treatments were conducted. A heat treatment denoted here as HT-bR involved the bonding thermal cycle (15 min at 1250ºC) followed by recrystallization treatment (2 hrs at 1385ºC), while another heat treatment indicated here by HT-R involved only the standard recrystallization treatment (2 hrs at 1385ºC). One set of samples from each region were exposed to heat treatment HT-bR and a second set of samples from each region were exposed to heat treatment HT-R. The samples were mounted and were polished using the procedure shown in table 5.3. Etching was conducted using a solution of 2 gms $CuCl_2$, 40 ml HCl and 40-80 ml methanol. Light microscopy and scanning electron microscopy (SEM), the latter employing a JEOL JSM-840 instrument operated at 20 kV, were used to investigate the microstructural features of the material. Energy dispersive x-ray spectroscopy (EDS) analysis was also performed to observe the compositional profile of the bars. See figure A.1 for the locations from which the samples were taken from the 25 mm diameter bar. For reference, and also to confirm the accuracy of the EDS, compositional analysis was also performed on IN939 and CMSX-4 alloys.

Results:

Microstructure: The microstructures of all the samples (for both bars and sets of heat treatments) were similar and did not contain any fine grains, figures A.2 and A.3. No significant effect of the bonding thermal cycle on the recrystallization of the fine grain PM2000 material was observed. However, porosity was observed in all the regions of both 25 mm (1 in) and 51 mm (2 in) bars. Variations in the porosity level were also observed for different regions of the 25 mm (1 in) bar for the same standard heat treatment of 2 hrs at 1385ºC, figure A.2 (a).

Composition:

25 mm (1 in) bar: The composition of the 25 mm (1 in) diameter PM2000 material varied significantly along the length of the bar. The chromium content in some regions of the material was 12 wt %, which is significantly lower than the standard of 19 wt %, figure A.4 and table A.1. However, the concentrations of the variations of other elements (titanium, aluminum, oxygen and yttrium) were within the experimental uncertainty of the measurements.

51 mm (2 in) bar: The composition of the 51 mm (2 in) diameter PM2000 did not vary significantly along the length of the bar. However, the chromium content of the bar was 10 wt %, which is significantly lower than the standard 19 wt %, figure A.5 and table A.2.

IN939 and CMSX-4: Compositional analysis performed on IN939 and CMSX-4 alloys (used to verify the accuracy of the system) agreed with the specifications [116], table 3.

PM2000 Analysis for compositional inhomogeneities

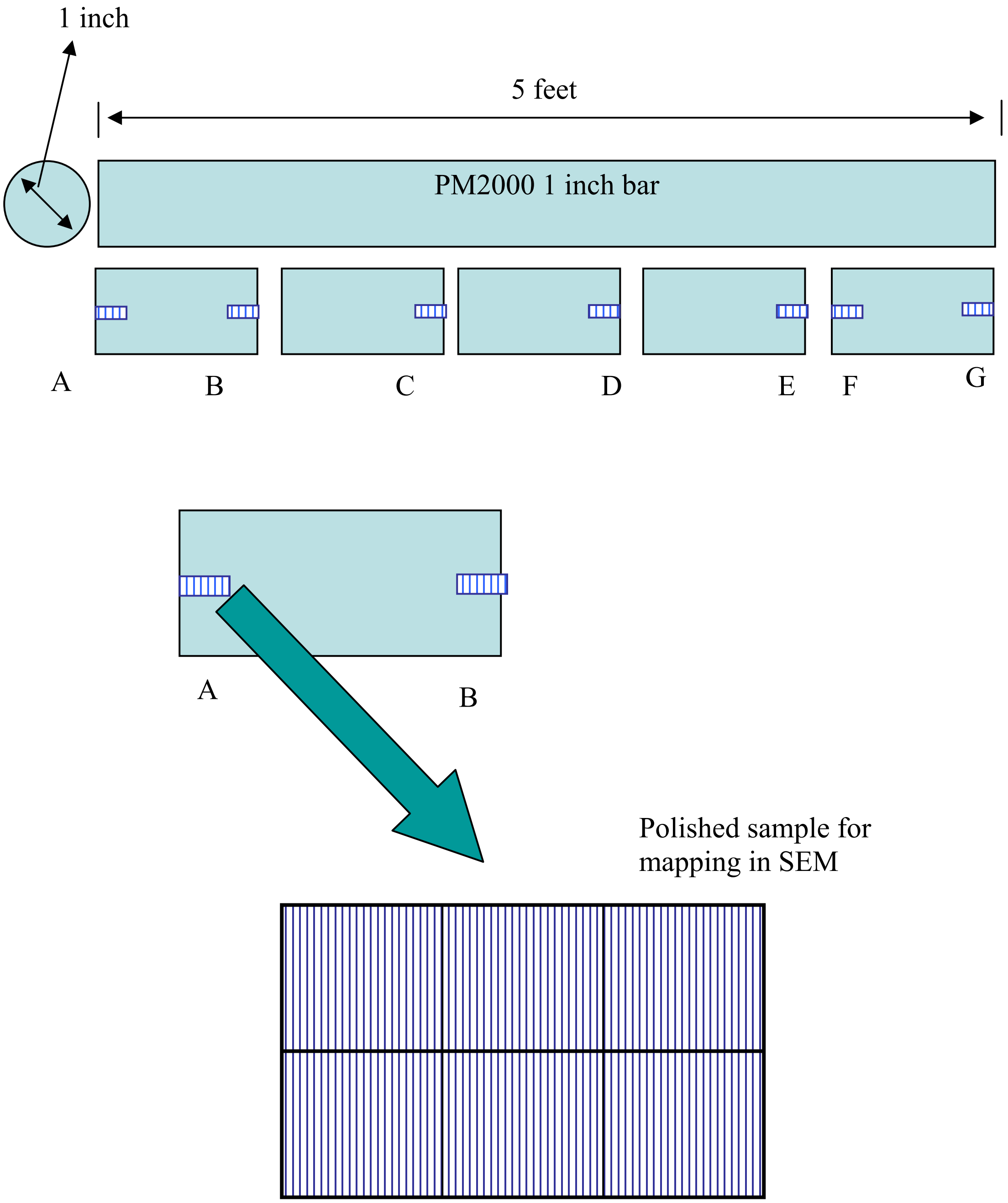

Figure A.1 Sample preparation for EDS and microstructural analysis.

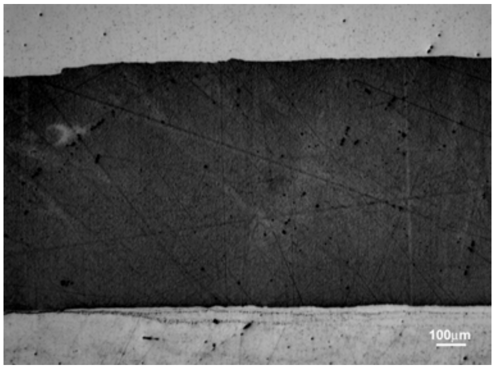

Region A

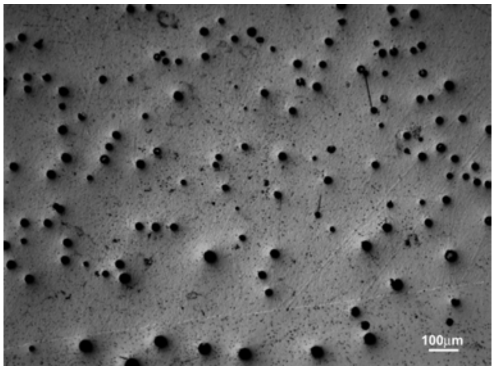

Region B

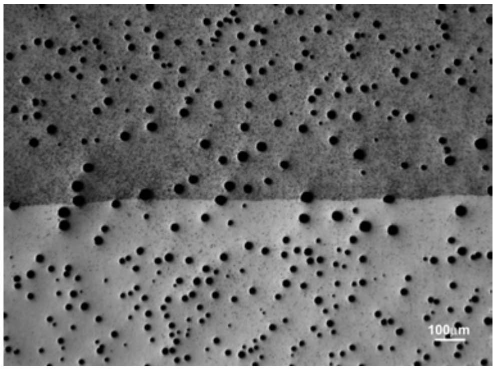

Region C

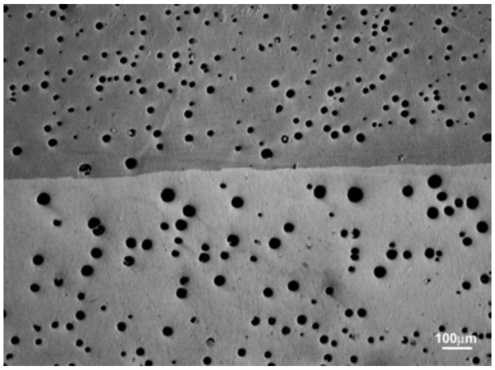

Region D

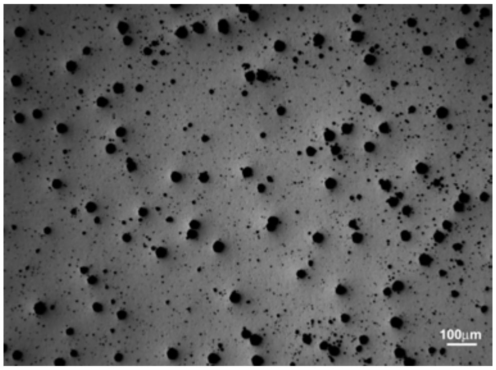

Region E

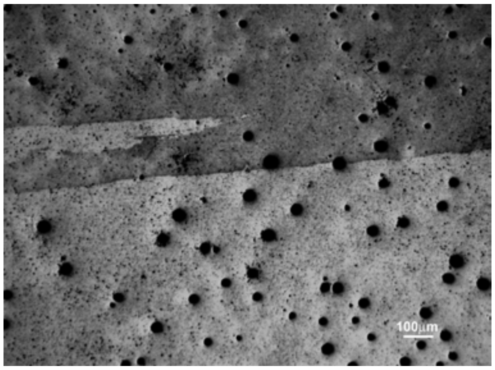

Region F

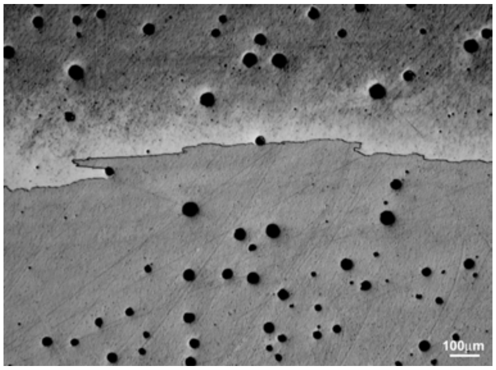

Region G

Figure A.2.a
A-G Regions of PM2000 bar
1 inch
2 hrs, 1385 °C

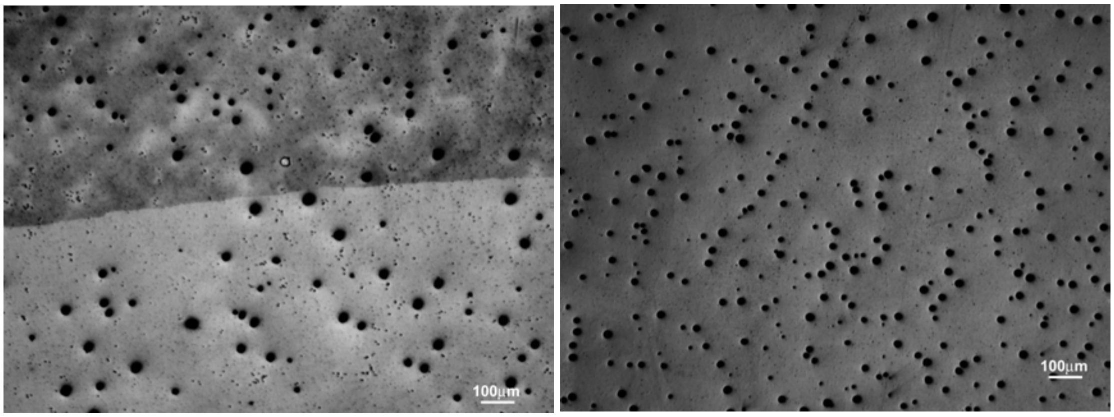

Region A

Region B

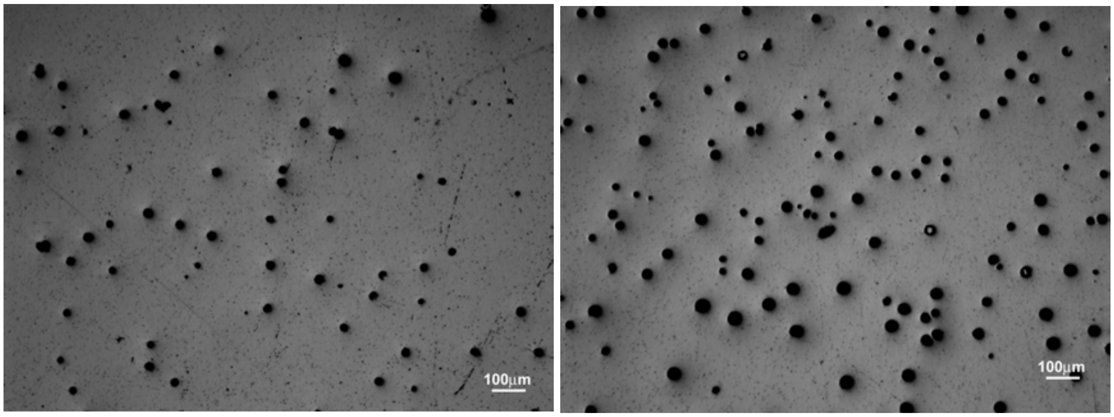

Region C

Region D

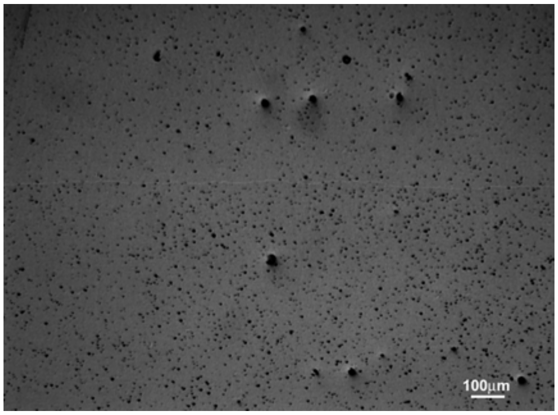

Region E

Figure A.2.b
A-E Regions of PM2000 bar
1 inch
15 min, 1250 °C + 2 hrs, 1385 °C

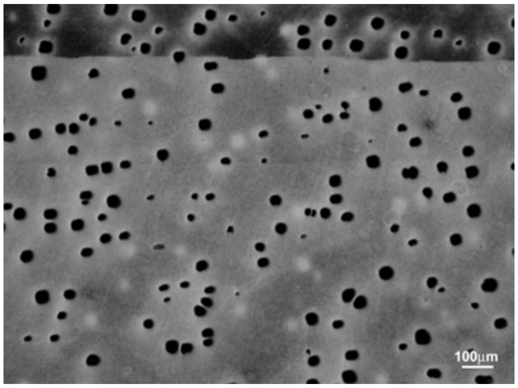

Region A

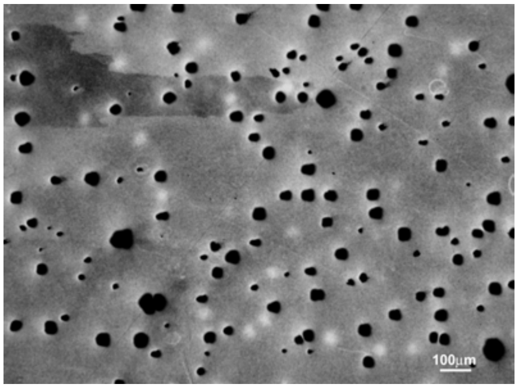

Region B

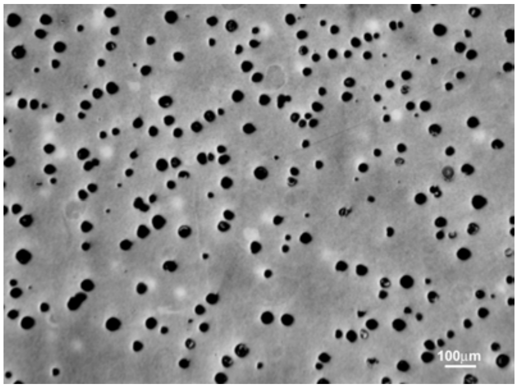

Region C

Figure A.3.a
A-C regions of PM2000 bar
2 inch
2 hrs, 1385 °C

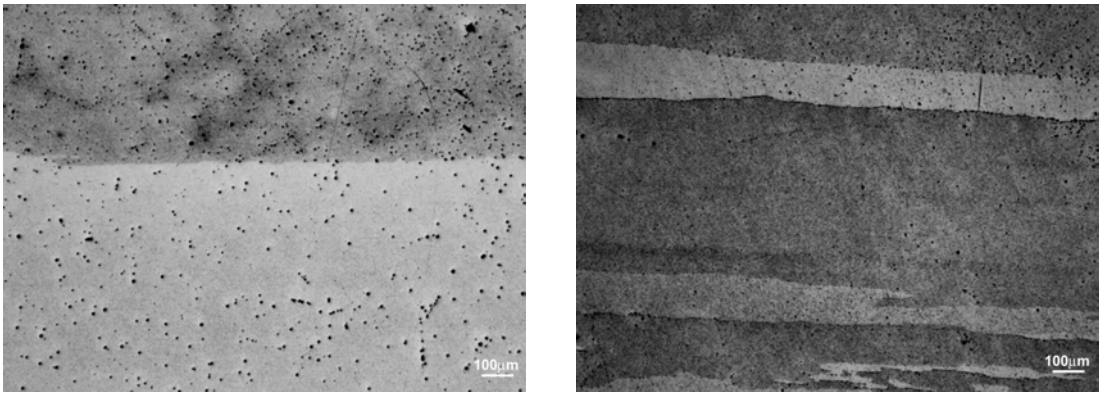

Region A

Region B

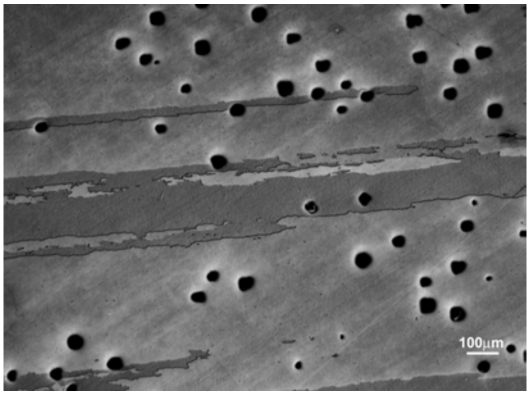

Region C

Figure A.3.b
A-C Regions of PM2000 bar
2 inch
15 min, 1250 °C + 2 hrs, 1385°C

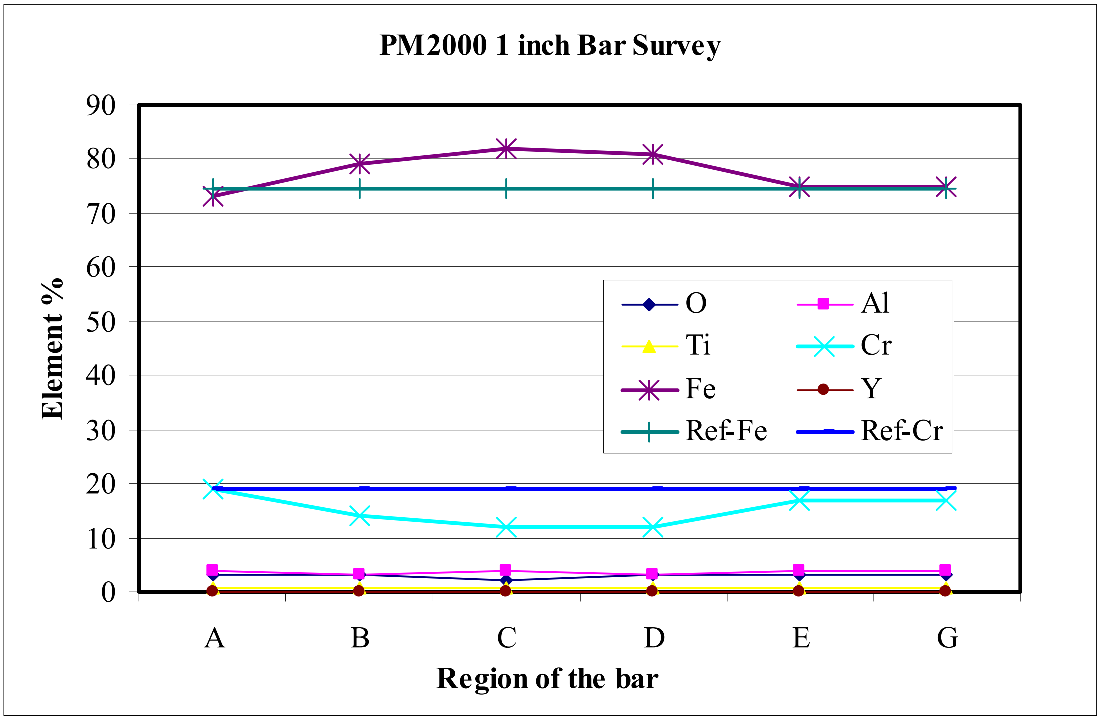

Figure A.4. Compositional profile along the 1 inch PM2000 bar.

Region / Element%	A	B	C	D	E	G	Reference PM2000
O	3	3	2	3	3	3	
Al	4	3	4	3	4	4	5.5
Ti	0.6	0.7	0.7	0.7	0.6	0.6	0.5
Cr	19	14	12	12	17	17	19
Fe	73	79	82	81	75	75	74.5
Y	< 1	< 1	< 1	< 1	< 1	< 1	< 1

Table A.1. Compositions at regions A-G of the 1 inch PM2000 bar.

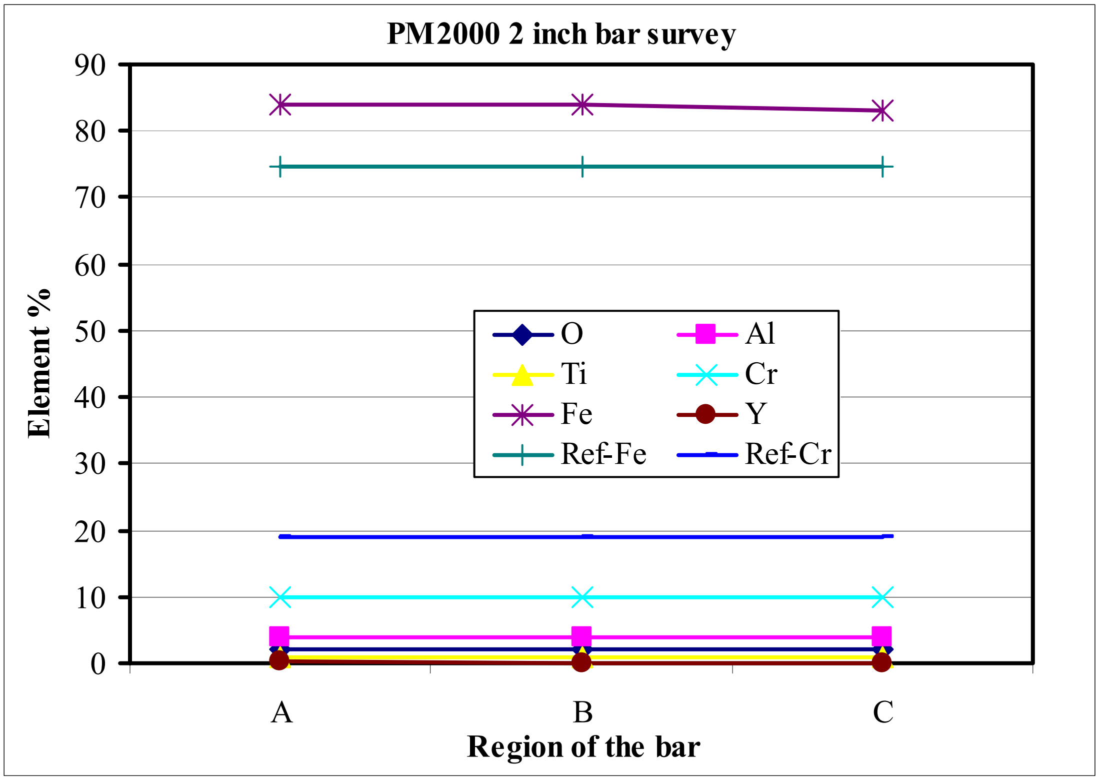

Figure A.5. Compositional profile along the 2 inch PM2000 bar.

Region / Element%	**A**	**B**	**C**	**Reference PM2000**
O	2	2	2	
Al	4	4	4	5.5
Ti	0.8	0.8	0.8	0.5
Cr	10	10	10	19
Fe	84	84	83	74.5
Y	< 1	< 1	< 1	< 1

Table A.2. Compositions at regions A-C of the 2 inch PM2000 bar.

Alloy/Element%	**IN939 Spec**	**IN939 SEM**	**CMSX-4 spec**	**CMSX-4 SEM**
Cr	22.5	23	6.5	6.4
Al	1.9	1.5	5.5	4.6
Ti	3.7	3.9	1	1.
Co	19	19	10	10.
Ni	48	47	60	63
Zr	0.09	<1	0	0
Nb	1	1	3.5	0
Mo	0	0	0.5	<1
Ta	1.4	2	6.3	6.9
W	2	2.6	6.5	8

Table A.3. Nominal compositions of IN939 and CMSX-4 alloys [118].